Designed Biodegradable and Osteoconductive Porous Scaffolds for Human Trabecular Bone

by

Eiji Saito

A dissertation submitted in partial fulfillment
of the requirements for the degree of
Doctor of Philosophy
(Biomedical Engineering)
in The University of Michigan
2011

Doctoral Committee:

Professor Scott J. Hollister, Chair
Professor Paul H. Krebsbach
Professor Shuichi Takayama
Associate Professor William L. Murphy, University of Wisconsin-Madison

2011

To my family, especially my grand mother who suffered from rheumatoid arthritis

ACKNOWLEDGEMENTS

Many people have supported me throughout my time as a graduate student at the University of Michigan, and without them I would not have made it to where I am today. I would like to thank all of my committee members for the opportunity to work with them and for their dedication to my research project. First of all, I would like to acknowledge my advisor, Professor Scott Hollister, for his kind and significant support, and the mentoring he provided to help me achieve my research goals and Ph.D. Under Professor Hollister's guidance, I was able to work on a wide range of tissue engineering research, from scaffold fabrication to scaffold implantation, enabling me to always keep the clinical applications of our work in sight. I would also like to thank Professor Paul Krebsbach who was also a mentor to me throughout most of my graduate studies. I appreciate his patience with me, always taking the time to listen and offer advice. His advice helped me to thoroughly plan, design and execute my *in vivo* experiments.

I am also thankful for the advice and help of Professor Shuichi Takayama with regard to all of my projects. Professor Takayama was instrumental in my pursuit of a Ph.D. in biomedical engineering at the University of Michigan. His advice was often unique and he pushed me to think about the research from different perspectives and with more of a global view. Professor William Murphy's guidance was instrumental in helping me to accomplish the project which combined our scaffold with biomineral coating. Although

he was in Madison, Wisconsin, he responded to my emails very quickly and offered thoughtful, detailed advice. By collaborating with Professor Murphy and his group members I was able to improve my project to develop advanced scaffolds. Again, it was truly great honor to work with my committee members, and I believe that our research will contribute to future tissue engineering research to improve patients' lives.

I would also like to express my sincere gratitude to all current and former lab members of Professor Hollister's lab and Professor Krebsbach's lab including Juan Taboas, Rachel Schek, Catherine Kuo, Chia-Ying Lin, Cheng-Yu Lin, Colleen Flanagan, Darice Wong, Elly Liao, Jessica Kemppainen, Erin Morffitt, Alisha Diggs, Sara Mantilla, Claire Jeong, Annie Mitsak, Huina Zhang, Heesuk Kang, Shelly Brown, Erica Scheller, William King, Frank Winterroth, Auresa Thomas, Wei-Wen Hu, Zhou Wang, Jun-Hui Song, Francesco Migneco, Leena Jongpaiboonkit, Felix Liu, Kaitlin Harrington, Danielle Wurth, Wei-Ju Tseng, Michael Pressler, Wilbur Tong, Yaseen Elkasabi, Ying Zhang, Luis Vila Diaz, Hongli Sun and Premjit Arpornmaeklong. It was a pleasure working with and spending time with each of them, both at the lab and outside of it. I appreciate their help and support not only during regular work hours but also at later hours and often at my urgent request. Their critiques were vital to the improvement of my research plan, my papers, and my presentations. Not only did my lab mates critique my research and attend conferences with me, they also made sure we had fun at lab lunches and happy hours.

I would also like to acknowledge Darilis Suarez from Professor Murphy's group at the University of Wisconsin, who I worked with to develop biomineral coatings for scaffolds. The development of novel scaffolds with Darilis was very productive, and we made significant achievements to the project.

I would also like to express my appreciation to Professor Hollister's collaborators. Especially, Professor William Giannoblie and his group members, James Sugai, Qiming Jin, Chan-Ho Park, Dr. Hector Rios, Po-Chun Chung, Zhao Lin, and Andrei Taut, provided important advice on biological experiments for scaffold evaluations. In addition, I would like to thank the members of the orthopaedics research laboratory (ORL), including Professor Steven Goldstein, Jeff Meganck, Ben Sinder and Jon Baker, who provided valuable assistance with micro-CT imaging and histology. Chris Strayhorn at the dental school histology core was very patient with my requests and helped me to obtain high quality sectioning and histological staining of many of my samples.

I would like to thank many people from the School of Dentistry, the College of Engineering, the University of Michigan 3D Lab and the Chemistry Instrument Shop, including Professor John Halloran, Dr.Tien-Min Gabriel Chu, Dr. Junro Yamashita, Dr. Kenichi Kuroda, Dr. Shin Mineishi, Dr. Shinichiro Kuroshima, Dr. Akira Abe, Dr. Yasuhiro Tsume, Dr.Toshiki Matsuoka and Dr. Akira Saito, for generous donation of their time to discuss my research and offer advice. I also greatly appreciate the support of our fellow LBME inhabitants, especially Professor Stegemann's and Professor El-Sayed's groups, who kindly helped me with my experiments and offered use of their equipment. The advice from and discussions with these colleagues afforded me a great opportunity to learn and experiment with ideas outside of my area of expertise.

I have also been supported by many people outside of the research world. The administrative staff of the BME department, especially Maria Steele, supported my academic endeavors and was always there to guide me at each step of the way. My

fellow BME classmates were more than just colleagues and many of them became mentors and great friends.

Lastly, I am deeply grateful to many of my significant friends and family whose kindness and support were critical as I transitioned into life in the United States. They patiently listened to me, supported me and gave me advice. They also invited me into their family and included me in family events on many occasions. My running friends helped to keep me in shape and provided stress relief from research. Their kindness and generosity played a huge role in the achievement of my goals. All of them are very important not only my Ph.D life but also in my future life. Again, to all of my family and friends, I thank you for your endless support along the way to achieving my Ph.D.

TABLE OF CONTENTS

LIST OF FIGURES

Figure

LIST OF TABLES

Table

LIST OF APPENDICES

Appendix

CHAPTER 1

Overview and Rational

1.1 Overview of Dissertation

Major bone losses due to cancer trauma and other diseases have been treated with autografts, allografts and other bone graft substitutes. However, these techniques have their limitations, such as the availability of grafts, immune responses, and stress shielding. As an alternative approach, porous bone scaffolds using FDA approved synthetic biodegradable polymers, such as poly (L-lactic acid) (PLLA), Poly (lactic-co-glycolic acid) (PLGA), Poly (glycolic acid) (PGA) and Poly (ε-caprolactone) (PCL), have been developed and examined both *in vitro* and *in vivo*. The ideal scaffolds are required to support physiological loads at the defect sites, to be favorable for bone formation and degrade in concert with the rate of bone formation.

The current efforts combining computer aided design and solid freeform fabrication (SFF) techniques enable the fabrication of porous scaffolds with controlled architectures for bone tissue applications using both biodegradable and non-degradable materials. Furthermore, biomineral coatings have been studied to improve bone tissue generation on and into non-osteoconductive implants, such as polyester biodegradable scaffolds.

The goal of this study was to design and fabricate osteoconductive porous biodegradable scaffolds with controlled 3D architectures, to enhance bone generation as well as control scaffold degradation, for human trabecular bone

applications. First, scaffolds with controlled architectures and mechanical properties within the range of human trabecular bone were designed with an image based design (IBD) technique and fabricated with SFF techniques. Second, the effects of the scaffold architectures and materials on *in vivo* bone formation were determined. Third, scaffolds *in vivo* degradation ratio depending on the pore sized were determined. Last, the effects of the biomineral coating he polymer scaffolds was evaluated to improve *in vivo* bone formation.

In the dissertation, goal of the study and rational are presented in chapter one. Chapter two describes important backgrounds, including bone grafts and current scaffold fabrication techniques. There are four individual studies (aims) in the thesis, and they are described in chapter three through six. Lastly, the thesis was summarized, and the potential future directions were discussed in chapter seven.

1.2 Experimental and Computational Characterization of Designed and Fabricated 50:50PLGA Porous Scaffolds for Human Trabecular Bone (Chapter Three)

Rationale: Ideal scaffolds for bone application are should provide mechanical properties which are similar to native bone tissue and have controlled structures for tissue formation. Porous biodegradable scaffolds have been developed using several techniques, such as particle leaching, gas forming and phase separation. However, due to their high porosity and thin walls between pores, they do not have sufficient mechanical strength to support bone defect loading. Furthermore, the pores are randomly located, and their interconnectivity is not well controlled. The goal of this study was to fabricate scaffolds

with designed architectures and control their mechanical properties within the range of the trabecular bone.

Summary: 50:50PLGA porous scaffolds with two porosities (50% and 70%) were designed and fabricated using the IBD and indirect SFF techniques, and characterized using micro-computed tomography (μ-CT) and mechanical testing. Scaffolds' compressive moduli and yield stress were controlled by scaffold designs and within the range of human trabecular bone and. μ-CT data was successfully implemented in a voxel-based finite element (FE) method to predict compressive moduli and yield stress and match to those of the experiment. This technique can be applied for scaffold quality control.

1.3 Effects of designed PLLA and 50:50PLGA scaffold architectures on bone formation *in vivo* (Chapter Four)

Rationale: Engineered scaffolds should have an architecture that is favorable for bone formation and mechanical properties. Conventional scaffolds have been used to determine the effect of scaffolds architectures on bone formation. However, in this case, scaffold architecture is controlled only in terms of average pore sizes and global porosities, with wide variations in each. These scaffolds furthermore have uncontrollable internal architectures, and limited pore interconnectivity. The scaffolds with random structures may prevent body fluid infiltration, cell migration and tissue ingrowth into a scaffold. As shown in chapter three, the fabricated 50:50PLGA scaffolds using the indirect SFF technique had orthogonally interconnected pores and mechanical properties within the human trabecular bone range. SFF scaffolds were used to investigate the

effect of scaffold architectures and material choice on bone formation using designed and controlled architectures.

Summary: Three types of porous scaffold architecture from two biodegradable materials, PLLA and 50:50PLGA, were designed and fabricated using image based design and indirect solid freeform fabrication techniques. The fabricated scaffolds were seeded them with bone morphogenic protein-7 (BMP-7) transduced human gingival fibroblasts and implanted them subcutaneously into mice for 4 and 8 weeks. The PLLA scaffolds maintained their architecture at both time points and showed improved bone ingrowth which followed the internal architecture of the scaffolds. The 50:50PLGA scaffolds, however, degraded and did not maintain their architecture after 4 weeks. PLLA scaffolds maintained greater mechanical properties than 50:50PLGA after implantation. The results indicated the importance of choice of scaffold materials and computationally designed scaffolds to control tissue formation and mechanical properties for desired bone tissue regeneration.

1.4 Architecture Effects on Long Term *In Vivo* Degradation in 3D Designed PLLA Porous Scaffolds (Chapter Five)

Rationale: Scaffold architectures may significantly influence *in vivo* degradation due to the geometric influences on polymer hydrolysis and the significant variations (cell populations, local fluid conditions) of the *in vivo* environment. However, the previous studies used scaffolds with random pore architectures fabricated by conventional techniques such as salt leaching and phase separation. In addition, many of degradation studies were performed *in vitro* which shows different profiles than *in vivo* degradation.

Therefore, it is important to determine the *in vivo* degradation dependence on designed scaffold architectures. As examined in chapter four, PLLA scaffolds may be suitable for bone application compared with 50:50PLGA scaffolds due to their slower degradation. Therefore, the influence of initial PLLA scaffold architecture on degradation was examined.

Summary: The effect of controlled scaffold initial architectures on *in vivo* degradation were examined regarding pore size, strut size, porosity and surface area. Three types of computer designed and solid freeform fabricated porous PLLA scaffolds in addition to PLLA bulk cylinders were implanted into mice subcutaneously for 6, 12 and 21 weeks. The cylinders lost weight faster as a percentage of initial weight than all porous scaffolds. Of the scaffolds, the group with the largest strut size lost weight percentage the fastest, and strong correlations between the surface area and weight loss were found. Scaffold porosity, however, was not significantly correlated with degradation rate. Scaffold mechanical properties decreased with degradation and maintained modulus in the lower range of the human trabecular bone even after 21 weeks. This study suggests that computer design and fabrication, within a given material, control scaffold degradation profiles.

1.5 Effect of hydroxyapatite-coated PLLA and PCL porous scaffolds on bone formation *in vivo* (Chapter Six)

Rationale: Through chapter three to five, the effect of scaffolds architectures and materials were examined using PLLA and 50:50PLGA. One of the limitations of poly ester biodegradable scaffolds is their poor osteoconductivity. To enhance bone formation

on these non-osteoconductive substrate, biomineral coating using simulated body fluid has been developed. Although varieties of biodegradable scaffolds have been successfully coated with biomineral coating, the effects of biomineral coated biodegradable scaffolds on *in vivo* bone formation are not well studied, especially scaffolds with different degradation profiles, such and PLLA and PCL. In addition, the combination of SFF scaffolds with biomineral coated has also not well investigated. PLLA and PCL scaffolds with the same architecture were mineralized in the same condition to study the effect of mineralization on bone formation.

Summary: PLLA and PCL scaffolds with the same design were fabricated using SFF and coated with biomineral layers using modified simulated body fluid which were done by Darilis Suarez-Gonzalez in Dr. Murphy's lab at the University of Wisconsin. μ-CT, XRD and SEM data showed that both PLLA and PCL scaffolds had the identical structures with orthogonally interconnected pores, and their surfaces were successfully coated with biomineral layers. The scaffolds were seeded with either BMP-7 or green fluorescent protein (GFP) tranduced human gingival fibroblasts, and then, implanted into mice subcutaneous sites for 3 and 10 weeks. From μ-CT and histological data at 3 weeks, there is no significant difference between the coated scaffolds and uncoated scaffolds for both PLLA and PCL. At 10 weeks, however, the coated scaffolds had significantly advanced bone ingrowth compared with the uncoated scaffolds. The bone ingrowth improved the mechanical properties of PLLA scaffolds. This study concluded that combination of SFF technique and biomineral coatings improve bone ingrowth of both PLLA and PCL scaffolds, and advanced bone ingrowth improve mechanical properties of PLLA scaffolds.

CHAPTER 2

Background and Motivation

2.1 Bone structure, composition and mechanical property

Bone is a complex tissue and plays many significant roles to maintain the body, such as providing structural support, protecting organs, and storing cells and mineral ions [1,2]. Bone tissue is composed of about 30% organic matrix, 60% inorganic mineral matrix, and 10% water by weight [3,4]. Type I collagen occupies 90% of the organic component, and the other 10% contains non collagenous proteins, such as proteoglycans and glycoproteins. Structurally, bone is largely composed of two parts, compact (cortical) bone and cancellous (trabecular) bone (Fig 2.1) [1,4,5]. In the adult skeleton, the ratio of compact bone and the cancellous bone are 80 and 20%, respectively [6]. These bones contain the same microstructural elements, including cells, organic matrix, inorganic mineral matrix and soluble factors.

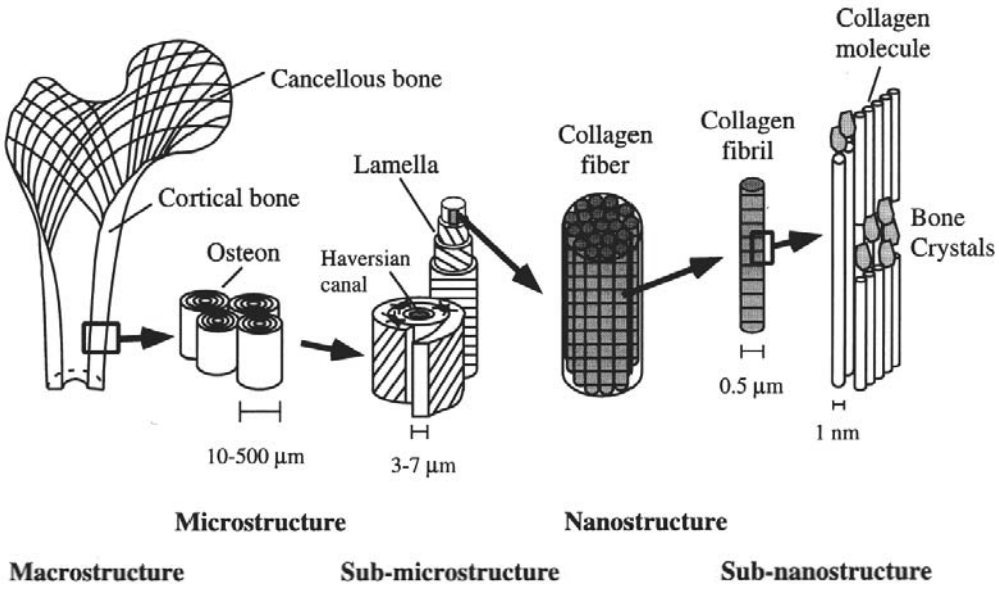

Fig 2.1 Bone Structure. Cited from [1]

As reviewed in previous papers [2,6], compact bone has about 10% porosity, is composed of organized structures, and contains osteon which is a cylindrical shape of bone units 200-250 µm in diameter and oriented in longitudinal directions. The osteon is also called the Harversian system and contain Haversian canals in their center which has blood vessels and supplies nutrients to mature bone cells (osteocytes). The osteon consists of the mineralized sheets called lamellae 3-7 µm in thickness. The collagen fibers are present and oriented parallel in each lamella. Each collagen fiber is composed of a collagen fibril where collagen molecule and mineral crystals are arranged regularly [1]. Due to the highly dense structures, compact bone has high mechanical properties with 12-18GPa [7].

In contrast to compact bone, cancellous bone has active turn over and less organized structures [8]. It is found at the end of long bones and within some other bones including the spinal vertebrae, sternum and pelvis [9]. It has three dimensional highly porous structure with 50 -95% porosity and is filled with bone marrow and bone cells, and the

trabeculae have 100-300 μm thickness and 300-1,500 μm spacing [2,4,6,9]. Elastic moduli of cancellous bone is range from 100 to 500MPa which is much lower than that of compact bone [7].

2.2 Bone cells and bone formation

Bone is an active tissue which constantly turns over to adapt to mechanical stimuli and repair damaged area. Bone formation and resorption are regulated by the major bone cells, osteoblast, osteocyte and osteoclast [10]. Osteoblasts are derived from mesenchymal cells, have a rounded, oval or polyhedral shape and reside on the surface of bone to form new bone tissue, lamellar bone and woven bone[6]. They synthesize and secrete mostly type I collagen and other organic components including osteopontin, osteocalcin, cytokines and growth factors, and also produce and regulate calcium phosphate minerals [3]. After these activities, osteoblasts undergo transformation into osteocytes, remaining less active as bone-lining cell, and undergoing apoptosis [5,6].

Osteocytes are matured cells of osteoblasts, which make up more than 90% of bone cells in adult human bone and are embedded in the mineralized matrix [6]. A single osteocyte resides in small lacunae and is connected with neighboring cells through canaliculi to communicate each other. In the lacunae and canaliculi system, osteocytes sense and respond to fluid flow change or mechanical stimuli and produce signaling molecules which regulate osteoblasts and osteoclasts to adjust bone formation and resorption [5,10-12].

In contrast to the other bone cells, osteoclasts are derived from hematopoietic stem cells and large multinucleated cells with from 3 to 30 nuclei. Their main function is to

resorb mineralized bone by acidification and enzymatically degrade demineralized bone [5].

Bone formation and development occur by two distinct pathways, intramembraneous and endochondral bone ossification. The intramembraneous bone formation occurs at flat bones in the cranium and facial bones, and some parts in the mandible [13,14]. It starts from the invasion of capillaries into mesenchymal zone which leads mesenchymal cells to turn into osteoblasts. The osteoblasts deposits bone spicules and form trabeculae which become interconnected forming woven bone. The woven bone is eventually replaced with lamellar bone. During the process, some osteoblasts are caught within the bone matrix and become osteocytes.

Endochondral bone formation occurs at the long, short bones and during bone regeneration due to bone fracture, and the process has been reported in several reviews [14-16]. Briefly, mesenchymal cells become condense and differentiate into chondrocytes as the process called precartilage condensation, and chondrocyte become hypertrophic at the center of the condensation. Perichondral cells around the hypertrophic chondrocyte differentiate into osteoblasts which form a bone collar. The hypertrophic chondrocytes continue to proliferate, are involved by blood vessels and eventually replaced by bone and marrow.

2.3 Autografts, allografts, xenografts, and bone graft substitutes

Over 500,000 bone graft procedures are performed annually in the US and the market size was about $1.5 billion in 2009, estimated to reach $3 billion by 2015 [17-19]. The definition of a bone graft is, “Any implanted material that, alone or in combination with

other materials, promotes a bone healing response by providing osteogenic, osteoconductive, or osteoinductive activity to a local site" [20]. Bone graft materials can be categorized as an autograft, allograft, xeonograft, and synthetic materials.

Autografts, which are obtained and implanted into the same patient, are recognized as the gold standard for most procedures [20-22]. For example, cancellous bone autograft contains hydroxyapaptite and collagen as osteoconductive material, stromal cells as osteogenic cells and growth factors as for osteoinduction [23]. However, the major disadvantages of autografts are limited availability of tissues, second surgery, donor site morbidity and increased blood loss [24].

Allografts, which are harvested from one individual and implanted into another individual of the same species, comprise about one third of the bone grafts used in North America [20,25]. They are more available than the autografts and do not require the second surgery to patients. However, host immune reactions or disease transmissions including HIV, hepatitis B and C, are major problems, and supply of cadaveric bone is not abundant [23,26]. To lower the risk of immune reaction, allograft processing and sterilization are used such as freeze-drying, demineralization, irradiation and ethylene oxide. These techniques also sacrifice oseoinductivity and osteogenic capability of allografts, and furthermore, the mechanical properties of the graft are also altered.

Xenografts are harvested from one species (animal) and implanted into another individual of different species [20,27]. The grafts have significant immune response, and therefore are not favorable. Although the immune response can be reduced using deproteinization and deffatting, osteoinductive proteins are also terminated.

Due to the limitations of the aforementioned grafts, metal and ceramics have been used as bone grafts. Metal implants, including stainless steel, titanium and cobalt, are applied to fracture healing and spine fusion [28,29]. However, they are neither osteoinductive nor osteoconductive. Their mechanical properties far stronger than the bone tissues which causes stress shielding. Ceramics are inorganic materials with crystalline structures produced by high temperatures, and include calcium phosphate, calcium sulfate and hydroxyapatite [20,30]. Their osteoconductivity is favorable for bone formation. However, the mechanical properties due to brittleness as well as their resorption rate do not satisfy load bearing applications. For example, tricalcium phosphate with Ca:P ratio of 1.5 absorbed too fast, while hydroxyapaptite with a Ca:P raito of 1.67 has too long degradation[30].

2.4 Biodegradable synthetic polymers

Biodegradable materials have been applied to orthopaedic and spine products towing to the ability to degrade and thereby avoid surgery for implant removal, proper mechanical properties and their radiolucency. Many biodegradable polymers belong to the polyester family and are available including poly orthoester, poly dioxanoe (PDS), poly (ε-caprolactone) (PCL), polyhydroxybutyrate (PHB), polylactide (PLA) and polyglycolide (PGA) [28,31,32]. Especially PLA, PGA and their co-polymer (PLGA) have been widely used as orthopaedics products, such as pins, fixations, and screws, and tissue engineering applications over the past two decades. Their chemical properties and degradation in animal tissues have been widely investigated [31,33-36]. Therefore, PLLA and PLGA were mostly used as scaffold materials in this thesis. PGA was also

used for preliminary purpose to find the bulk property and manufacturability of such scaffolds.

PLA, PGA and PLGA belong to poly (α-hydroxy acid) group and degrade in the body by hydrolysis of ester bonds and forms lactic acid and/or glycolic acid [31,35,36]. Lactic acid and glycolic acid are further broken down to pyruvate by lactate dehydrogenase, and enter the citric acid cycle, where they are converted and removed from the body as carbon dioxide and water. Glycolic acid is also removed through urine.

PLA and PGA can be obtained from the ring opening polymerization of lactide or glycolide (Fig 2.2 (a, b)), and PLGA can be formed via copolymerization of lactide and glycolide (Fig 2.2 (c)). PLA has two optical stereo-isomers, d(-) and l(+) and racimid (d,l), and l- isomer, and Poly (l-lactic acid) (PLLA) is commonly used [31,33,34]. PLLA is a semi-crystalline polymer with about 37% crystalline, and has a 175-178°C melting point and 60-65°C glass transition temperature. It has higher crystallinity about 45-55%, melting point (220-225°C) and glass transition temperature (35-40°C) than PLA. It is also more hydrophilic than PLA, which causes faster degradation. Degradation of PLGA can be adjusted by varying the ratio of lactide and glycolide with non-linear relations. Generally, PLGA with the copolymer ratio of 50:50 shows the fastest degradation.

PCL is more likely used for tissue engineering scaffolds and drug delivery due to its long degradation time [31,37]. It is synthesized through the ring opening polymerization of cyclic monomer ε-caprolactone (Fig 2.2 (d)). This polymer has low melting point about 59-64 °C and a glass transition temperature of -60°C [31,33].

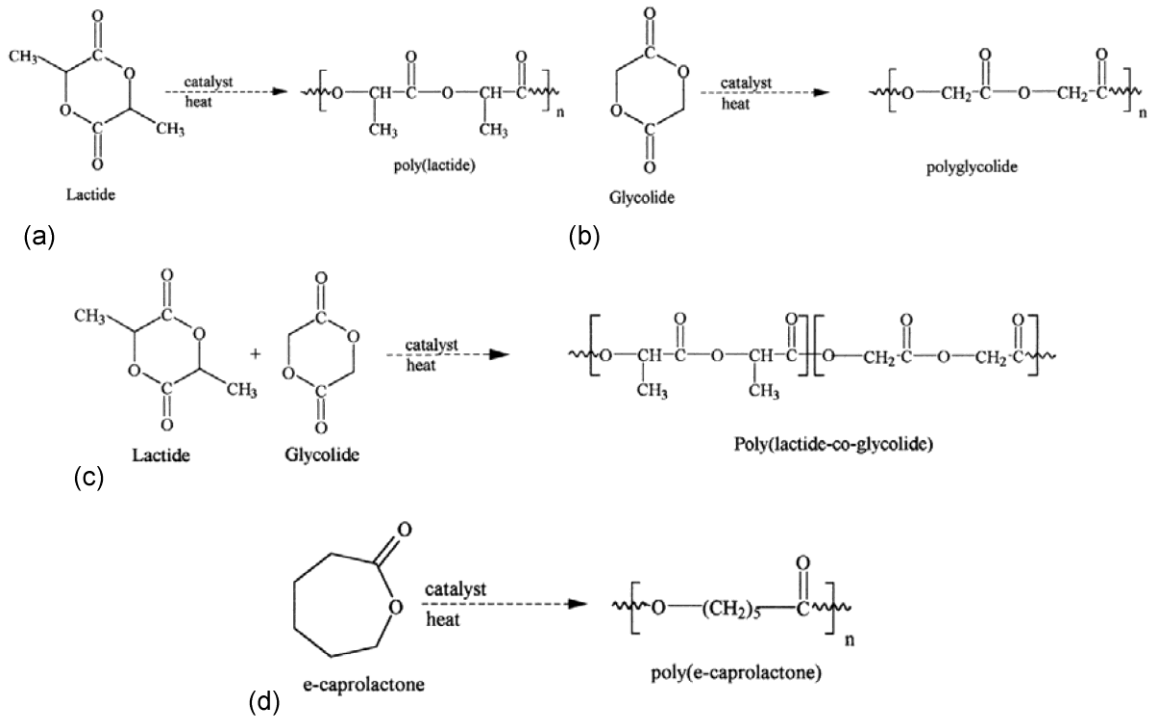

Fig 2.2 Chemical Structures of PLLA (a), PGA (b), PLGA (c) and PCL (d). Cited and modified from [33] .

Mechanical properties of PLLA, PGA, PLGA, and PCL vary depending on polymer types and their molecular weights. We have preliminary fabricated cubes of PLLA, 50:50PLGA and PGA using melt casting to test their compressive moduli and yield stress, and also compared these with PCL cubes fabricated using a SLS system (PCL data provided by Colleen Flanagan). As shown in Fig 2.3, PGA cubes show the highest compressive modulus and yield strength. PLLA and 50:50 PLGA cubes have lower mechanical properties than those of PGA cubes, however, the bulk moduli are higher than those of trabecular bone. In contrast, the reported bulk mechanical properties of PCL are significantly lower than the others.

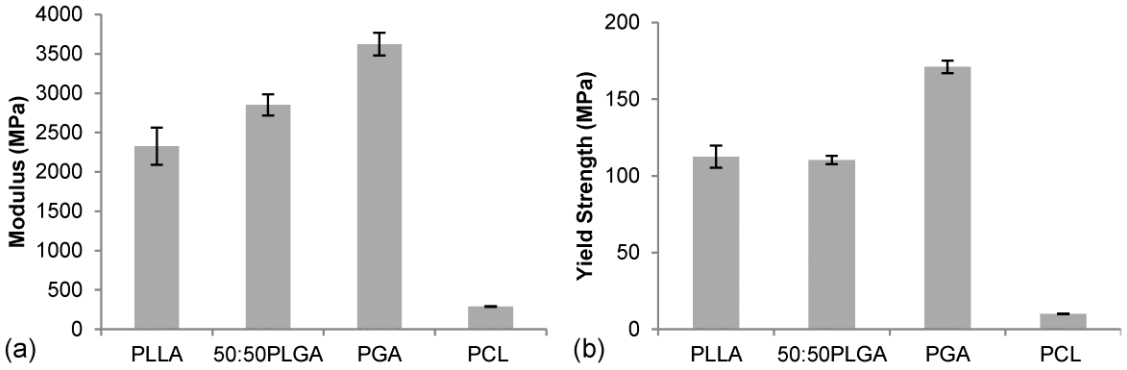

Fig 2.3 Compressive moduli (a) and yield stress (b) of bulk polymers, PLLA, 50:50PLGA, PGA and PCL. PCL cubes were fabricated using a SLS system (PCL data provided by Colleen Flanagan).

2.5 Computational design and solid freeform fabrication

Tissue engineered scaffolds have been developed as an alternative methods of the current bone grafts using varieties of biodegradable materials. Scaffolds should have interconnected porous architectures for tissue integration, and furthermore have sufficient mechanical properties to match and support physiological loading, then degrade in a favorable manner to transfer load support to tissues during healing [35,38-40]. In attempting to achieve these requirements, biodegradable porous bone scaffolds have conventionally been fabricated using several methods, including phase separation [41-43], particle leaching [44-46], gas foaming [47] and electrospining [48-51]. All of these techniques are relatively easy to access and able to use a variety of materials including PLLA, PLGA and PCL. Furthermore, the fabricated scaffolds can achieve high porosity (~90%) and high surface area to support cell migration and proliferation. However, they do not have sufficient mechanical strength to support loading in bone defect sites [7] due to their high porosity and thin walls between pores. In addition, uncontrolled architectures including, poor pore interconnectivities, prevent cell infiltration and tissue ingrowth or further surface modification since these scaffolds are controlled their pore

diameters and overall scaffold porosities with changing variables, such as porogen diameter, [52-54].

Computer aided tissue engineering is a proven method to achieve desired engineering scaffolds and to characterize fabricated scaffolds using computer aided design (CAD), computed tomography(CT) and Finite element analysis (FEA) [55,56]. In addition, the image based design technique has been used to design scaffolds to mimic anatomical and physical properties of human bone [57-59]. Then, computer designed scaffolds can be fabricated using solid freeform fabrication (SFF) methods or rapid prototyping (RP) techniques, where 3D scaffolds are built in a layer-by-layer manner [39,60-62]. Various SFF techniques have been developed, such as stereolithography (SLA) [54,63,64], selective laser sintering (SLS) [55,65-67], fused deposition molding (FDM) [68,69], 3D printing [70-72] and 3D-plotting [73,74].

Each technique is run with unique system and fabricates scaffolds with different biodegradable materials as shown in Fig 2.4. Utilizing ultraviolet photo-curable monomer (Fig 2.4 (a)), SLA technique create designed scaffolds using poly (D,L-lactide) and poly (propylene fumarate) (PPF)-diethyl fumarate (DEF), and good cell behaviors were shown in the fully interconnected architectures [54,64]. In SLS system (Fig 2.4 (b)), powdered materials are fused by a laser beam, and various shapes of PCL scaffolds fabricated to apply *in vivo*. For example, mandibular condyle scaffolds based on CT data were fabricated and implanted to pig models [75]. In FDM system (Fig 2.4 (c)), material is melted and extruded from a nozzle. FDM techniques are extensively developed to fabricate PCL scaffolds and PCL-HA composite scaffolds for human clinical trials, and the scaffolds were approved by FDA [61]. 3D printing technique utilizes a liquid binder

ejected from a printer head to bind powdered material (Fig 2.4 (d)). This technique has been used to create calcium phosphate scaffolds and calcium phosphate-PLGA composite scaffolds, and the scaffolds for bone or osteochondral applications [70-72]. Compared with the previous techniques, 3D bioplotter have unique feature to fabricate hydrogel scaffolds by dispensing a material into liquid medium (Fig 2.4 (e)). This system is operated in a sterile laminar flow and able to incorporate live cells for soft tissue applications [73].

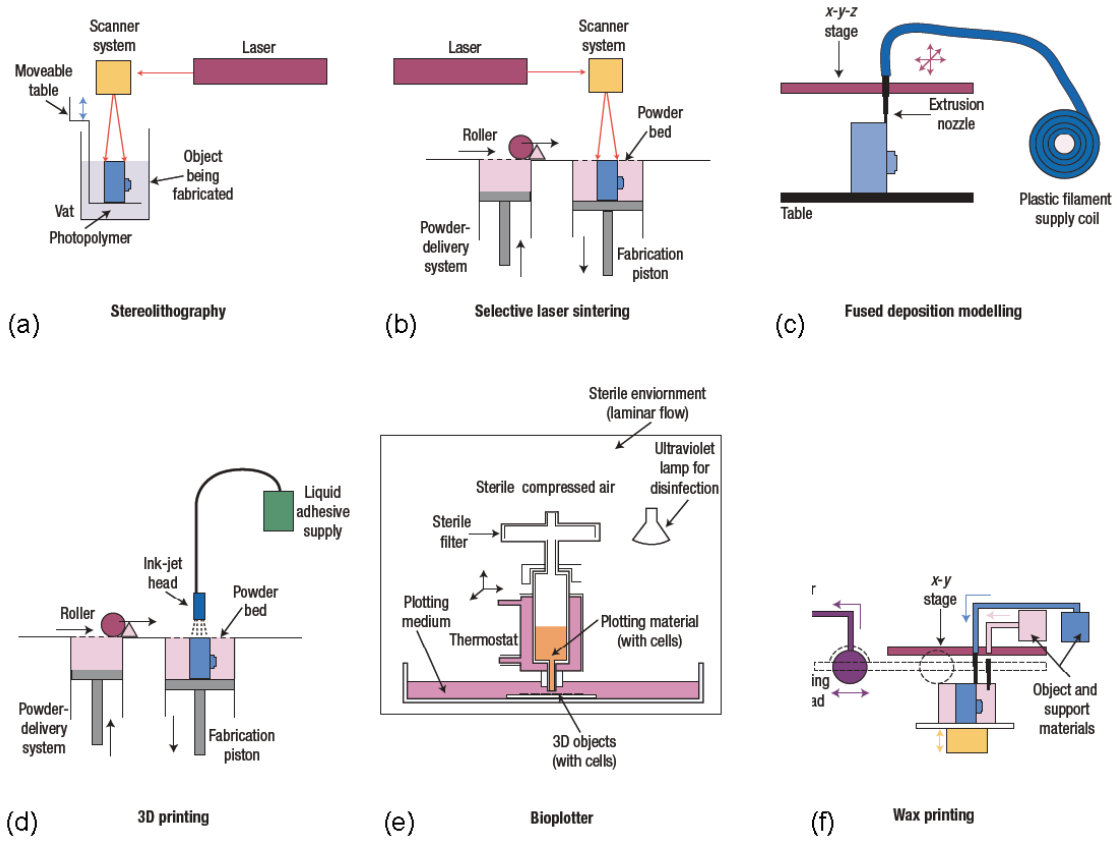

Fig 2.4 Schematics of various SFF systems. Stereolithography (SLA) (a), Selective laser sintering (SLS) (b), Fused deposition modeling (c), 3D printing (d), Bioplotter (f), and Wax printing (f) cited from [55].

Although the aforementioned SFF techniques have been widely accepted for tissue engineering scaffold fabrication, the techniques has not been fully applicable to fabricate

PLLA, PLGA, and PGA scaffolds with complex architectures due to their high melting temperatures and viscosities. We chose the indirect SFF method, which developed by Taboas et al [76] using wax printing system (Fig 2.4 (f)), to fabricate our scaffolds. Briefly, designed scaffolds image representations were converted to stereolithography (STL) formats and sliced in Modelworks software (Solidscape, Inc., Merrimack, NH) to fabricate wax molds using a ModelMaker II or PatternMaster™ 3D printer (Solidscape, Inc., Merrimack, NH). The wax molds were cast into hydroxyapatite ceramic (HA) secondary molds. Polymer pellets were heated at required temperature of each polymer and melted in a Teflon mold. The HA molds were then placed into the Teflon mold containing molten polymer, in order to force the polymer through the open pore network. The HA molds were then removed from the porous polymer scaffolds using RDO Rapid Decalcifier (APEX Engineering Products Corp, Plainfield, IL). The fabricated scaffolds were rinsed with 100% ethanol for further experiments. We preliminary fabricated designed PLLA and PGA scaffolds which have high melting temperature as mentioned earlier (Fig 2.5).

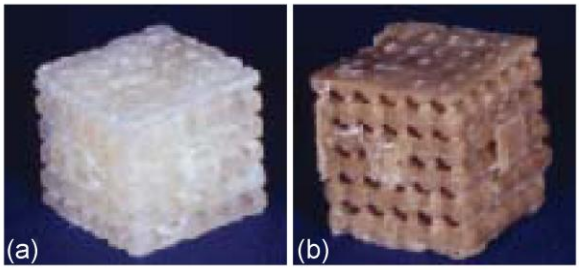

Fig 2.5 PLLA scaffold (a) and PGA scaffold fabricated by indirect SFF technique

2.6 Biomineral coating

One of the disadvantages of many polymeric and metallic biomaterials is their non-osteoconductive property compared with hydroxyapatite (HA) and tricalcium phosphate

(TCP) scaffolds. To improve ostoconductivity of biomaterials, a biomineral coating of substrate surfaces using simulated body fluid (SBF) is a unique technique and was developed by Kokubo et al [77]. Many researchers have shown mineralization with various substrates to compensate for their non-osteoconductivities. In this technique, the negatively charged surfaces of substrates are created using various techniques, such as hydrolysis. The substrates are immersed SBF which has similar ion contents as human blood plasma. Carbonate apatite minerals which are similar to the mineral component of bone tissue are deposit with less than 30μm thickness on the substrates [78,79]. This technique has successfully been applied to various biomaterials including metals [80-82], polymers [78,83-86], and the composites of polymers and hydroxyapatite [84,87] to enhance bone cell function and bone tissue regeneration.

However, the effects of mineral coatings on bone formation in 3D designed porous polymer scaffolds have not been thoroughly studied. Some studies showed that there was no significant effect on mineral coating of biodegradable polymers on bone formation [84,85]. Another study demonstrated that mineral coated salt leaching scaffolds tend to have less open pore structures which terminate effectively coat at the center of the scaffolds and have undeveloped bone ingrowth towards the center of the scaffolds [53]. Therefore, we developed biomineral coated biodegradable SFF scaffolds with interconnected pores to enhance *in vivo* bone formation. As mentioned in chapter one, SFF scaffolds were fabricated by our group and then, coated with biomineral layers by Prof. Willam Murphy's group in the University of Wisconsin.

2.7 Ectopic bone formation using *ex vivo* gene therapy

We used mice ectopic sites to test our scaffolds for chapter four, five and six. *Ex vivo* gene therapy was used to induce bone formation on and into the scaffolds (chapter four and six) [88,89]. This regenerative gene therapy strategy using adenoviral vectors can be applied to transduce various cells, such as bone marrow stromal cells [90], and fibroblasts [91,92]. The tranceduced cells secrete proteins, such as BMP-7 and BMP-2, to recruit and induce host cells towards osteogenesis. Additionally, this approach has been studied to induce endochondral-like bone tissue formation by transduced HGFs [91,93]. We have been seeding BMP-7 transduced human gingival fibroblasts and seeding them to porous SFF scaffolds to facilitate bone generation in mice ectopic sites [66,94-96]. All of our previous studies showed that good bone formation in and on to the scaffolds. Therefore, *ex vivo* gene therapy is a good technique to form bone tissues to test our scaffolds.

Ectopic site has been used to test biodegradable bone scaffolds including PLLA and PLGA. The major advantages of this model are relatively easy to implant and harvest scaffolds, and achieve large numbers of replicates for preliminary study. Some surgical complication may need to be considered to implant scaffolds into orthotopic sites due to removing or cutting existing bone tissues surrounded by blood vessels and nerve tissues. However, the limitation of the ectopic model is not identical to the orthotopic sites and there are some study compared ectopic models with orthotopic models for the sake of bone tissue engineering research. For example, in ectopic model, there are delays of vascularization causing delay of bone ingrowth into porous constructs as well as lack of fracture healing response [97,98]. Furthermore, there is lack of mechanical signal in

ectopic sites which would affect bone formation and scaffolds degradation. [99-101]. In spite of some limitations, ectopic model is still useful to evaluate our scaffolds to perform preliminary studies. This model allows easily implanting and harvesting scaffolds without further complications.

References

[1] Rho JY, Kuhn-Spearing L, Zioupos P. Mechanical properties and the hierarchical structure of bone. Med Eng Phys 1998;20:92-102.

[2] Sikavitsas VI, Temenoff JS, Mikos AG. Biomaterials and bone mechanotransduction. Biomaterials 2001;22:2581-2593.

[3] Barrere F, Mahmood TA, de Groot K, van Blitterswijk CA. Advanced biomaterials for skeletal tissue regeneration: Instructive and smart functions. Mater Sci Eng R-Rep 2008;59:38-71.

[4] Athanasiou KA, Zhu C, Lanctot DR, Agrawal CM, Wang X. Fundamentals of biomechanics in tissue engineering of bone. Tissue Eng 2000;6:361-381.

[5] Gruber R, Pietschmann P, Peterlik M. Introduction to Bone Development, Remodelling and Repair. 2008:1-23.

[6] Buckwalter JA, Glimcher MJ, Cooper RR, Recker R. Bone Biology .1. Structure, Blood-Supply, Cells, Matrix, and Mineralization. J Bone Joint Surg -Am vol 1995;77A:1256-1275.

[7] Rezwan K, Chen QZ, Blaker JJ, Boccaccini AR. Biodegradable and bioactive porous polymer/inorganic composite scaffolds for bone tissue engineering. Biomaterials 2006;27:3413-3431.

[8] Rodan GA. Introduction to bone biology. Bone 1992;13 Suppl 1:S3-6.

[9] Keaveny TM, Morgan EF, Niebur GL, Yeh OC. Biomechanics of trabecular bone. Annu Rev Biomed Eng 2001;3:307-333.

[10] Robling AG, Castillo AB, Turner CH. Biomechanical and molecular regulation of bone remodeling. Annu Rev Biomed Eng 2006;8:455-498.

[11] Klein-Nulend J, Bacabac RG, Mullender MG. Mechanobiology of bone tissue. Pathol Biol (Paris) 2005;53:576-580.

[12] Zaidi M. Skeletal remodeling in health and disease. Nat Med 2007;13:791-801.

[13] Buckwalter JA, Glimcher MJ, Cooper RR, Recker R. Bone Biology .2. Formation, Form, Modeling, Remodeling, and Regulation of Cell-Function. J Bone Joint Surg -Am vol 1995;77A:1276-1289.

[14] Kanczler JM, Oreffo RO. Osteogenesis and angiogenesis: the potential for engineering bone. Eur Cell Mater 2008;15:100-114.

[15] Kronenberg HM. Developmental regulation of the growth plate. Nature 2003;423:332-336.

[16] Kelly DJ, Jacobs CR. The role of mechanical signals in regulating chondrogenesis and osteogenesis of mesenchymal stem cells. Birth Defects Res C Embryo Today 2010;90:75-85.

[17] Greenwald AS, Boden SD, Goldberg VM, Khan Y, Laurencin CT, Rosier RN, et al. Bone-graft substitutes: facts, fictions, and applications. J Bone Joint Surg Am 2001;83-A Suppl 2 Pt 2:98-103.

[18] Inc Global Industry Analysts. 200920118/11/2011http://www.prweb.com/releases/bone_grafts/standard_allografts/prweb2296804.htm.

[19] Greenwald AS, Boden SD, Barrack RL, Bostrom M, Goldberg VM, Heim CS. THE EVEOLVING ROLE OF BONE-GRAFT SUBSTITUTES.

[20] Bauer TW, Muschler GF. Bone graft materials. An overview of the basic science. Clin Orthop Relat Res 2000;(371):10-27.
[21] Giannoudis PV, Dinopoulos H, Tsiridis E. Bone substitutes: an update. Injury 2005;36 Suppl 3:S20-7.
[22] Hing KA. Bone repair in the twenty-first century: biology, chemistry or engineering? Philos Transact A Math Phys Eng Sci 2004;362:2821-2850.
[23] Sutherland D, Bostrom M. Grafts and bone graft substitues. In: Lieberman JR, Friedlaender GE, editors. Bone Regeneration and Repair Biology and Clinical Applications: Humana Press, 2005. p. 133.
[24] Chau AM, Mobbs RJ. Bone graft substitutes in anterior cervical discectomy and fusion. Eur Spine J 2009;18:449-464.
[25] De Long WG,Jr, Einhorn TA, Koval K, McKee M, Smith W, Sanders R, et al. Bone grafts and bone graft substitutes in orthopaedic trauma surgery. A critical analysis. J Bone Joint Surg Am 2007;89:649-658.
[26] Carson JS, Bostrom MP. Synthetic bone scaffolds and fracture repair. Injury 2007;38 Suppl 1:S33-7.
[27] Damien CJ, Parsons JR. Bone graft and bone graft substitutes: a review of current technology and applications. J Appl Biomater 1991;2:187-208.
[28] Navarro M, Michiardi A, Castano O, Planell JA. Biomaterials in orthopaedics. J R Soc Interface 2008;5:1137-1158.
[29] Niinomi M. Metallic biomaterials. J Artif Organs 2008;11:105-110.
[30] Chau AM, Mobbs RJ. Bone graft substitutes in anterior cervical discectomy and fusion. Eur Spine J 2009;18:449-464.
[31] Gunatillake PA, Adhikari R. Biodegradable synthetic polymers for tissue engineering. Eur Cell Mater 2003;5:1-16; discussion 16.
[32] Kontakis GM, Pagkalos JE, Tosounidis TI, Melissas J, Katonis P. Bioabsorbable materials in orthopaedics. Acta Orthop Belg 2007;73:159-169.
[33] Middleton JC, Tipton AJ. Synthetic biodegradable polymers as orthopedic devices. Biomaterials 2000;21:2335-2346.
[34] Ambrose CG, Clanton TO. Bioabsorbable implants: review of clinical experience in orthopedic surgery. Ann Biomed Eng 2004;32:171-177.
[35] Athanasiou KA, Agrawal CM, Barber FA, Burkhart SS. Orthopaedic applications for PLA-PGA biodegradable polymers. Arthroscopy 1998;14:726-737.
[36] Peltoniemi H, Ashammakhi N, Kontio R, Waris T, Salo A, Lindqvist C, et al. The use of bioabsorbable osteofixation devices in craniomaxillofacial surgery. Oral Surg Oral Med Oral Pathol Oral Radiol Endod 2002;94:5-14.
[37] Labet M, Thielemans W. Synthesis of polycaprolactone: a review. Chem Soc Rev 2009;38:3484-3504.
[38] Hutmacher DW. Scaffold design and fabrication technologies for engineering tissues--state of the art and future perspectives. J Biomater Sci Polym Ed 2001;12:107-124.
[39] Hollister SJ. Porous scaffold design for tissue engineering. Nat Mater 2005;4:518-524.
[40] Karageorgiou V, Kaplan D. Porosity of 3D biomaterial scaffolds and osteogenesis. Biomaterials 2005;26:5474-5491.

[41] Guan L, Davies JE. Preparation and characterization of a highly macroporous biodegradable composite tissue engineering scaffold. J Biomed Mater Res A 2004;71:480-487.
[42] Huang YX, Ren J, Chen C, Ren TB, Zhou XY. Preparation and properties of poly(lactide-co-glycolide) (PLGA)/ nano-hydroxyapatite (NHA) scaffolds by thermally induced phase separation and rabbit MSCs culture on scaffolds. J Biomater Appl 2008;22:409-432.
[43] Hu Y, Grainger DW, Winn SR, Hollinger JO. Fabrication of poly(alpha-hydroxy acid) foam scaffolds using multiple solvent systems. J Biomed Mater Res 2002;59:563-572.
[44] Ma PX, Choi JW. Biodegradable polymer scaffolds with well-defined interconnected spherical pore network. Tissue Eng 2001;7:23-33.
[45] Thomson RC, Yaszemski MJ, Powers JM, Mikos AG. Fabrication of biodegradable polymer scaffolds to engineer trabecular bone. J Biomater Sci Polym Ed 1995;7:23-38.
[46] Wu L, Zhang H, Zhang J, Ding J. Fabrication of three-dimensional porous scaffolds of complicated shape for tissue engineering. I. Compression molding based on flexible-rigid combined mold. Tissue Eng 2005;11:1105-1114.
[47] Harris LD, Kim BS, Mooney DJ. Open pore biodegradable matrices formed with gas foaming. J Biomed Mater Res 1998;42:396-402.
[48] Fujihara K, Kotaki M, Ramakrishna S. Guided bone regeneration membrane made of polycaprolactone/calcium carbonate composite nano-fibers. Biomaterials 2005;26:4139-4147.
[49] Li C, Vepari C, Jin HJ, Kim HJ, Kaplan DL. Electrospun silk-BMP-2 scaffolds for bone tissue engineering. Biomaterials 2006;27:3115-3124.
[50] Shin M, Yoshimoto H, Vacanti JP. In vivo bone tissue engineering using mesenchymal stem cells on a novel electrospun nanofibrous scaffold. Tissue Eng 2004;10:33-41.
[51] Yoshimoto H, Shin YM, Terai H, Vacanti JP. A biodegradable nanofiber scaffold by electrospinning and its potential for bone tissue engineering. Biomaterials 2003;24:2077-2082.
[52] Karande TS, Ong JL, Agrawal CM. Diffusion in musculoskeletal tissue engineering scaffolds: design issues related to porosity, permeability, architecture, and nutrient mixing. Ann Biomed Eng 2004;32:1728-1743.
[53] Du C, Meijer GJ, van de Valk C, Haan RE, Bezemer JM, Hesseling SC, et al. Bone growth in biomimetic apatite coated porous Polyactive 1000PEGT70PBT30 implants. Biomaterials 2002;23:4649-4656.
[54] Melchels FP, Barradas AM, van Blitterswijk CA, de Boer J, Feijen J, Grijpma DW. Effects of the architecture of tissue engineering scaffolds on cell seeding and culturing. Acta Biomater 2010;6:4208-4217.
[55] Hollister SJ, Lin CY, Saito E, Lin CY, Schek RD, Taboas JM, et al. Engineering craniofacial scaffolds. Orthod Craniofac Res 2005;8:162-173.
[56] Sun W, Starly B, Darling A, Gomez C. Computer-aided tissue engineering: application to biomimetic modelling and design of tissue scaffolds. Biotechnol Appl Biochem 2004;39:49-58.

[57] Hollister SJ, Levy RA, Chu TM, Halloran JW, Feinberg SE. An image-based approach for designing and manufacturing craniofacial scaffolds. Int J Oral Maxillofac Surg 2000;29:67-71.
[58] Hollister SJ, Maddox RD, Taboas JM. Optimal design and fabrication of scaffolds to mimic tissue properties and satisfy biological constraints. Biomaterials 2002;23:4095-4103.
[59] Lin CY, Kikuchi N, Hollister SJ. A novel method for biomaterial scaffold internal architecture design to match bone elastic properties with desired porosity. J Biomech 2004;37:623-636.
[60] Butscher A, Bohner M, Hofmann S, Gauckler L, Muller R. Structural and material approaches to bone tissue engineering in powder-based three-dimensional printing. Acta Biomater 2011;7:907-920.
[61] Hutmacher DW, Cool S. Concepts of scaffold-based tissue engineering--the rationale to use solid free-form fabrication techniques. J Cell Mol Med 2007;11:654-669.
[62] Peltola SM, Melchels FP, Grijpma DW, Kellomaki M. A review of rapid prototyping techniques for tissue engineering purposes. Ann Med 2008;40:268-280.
[63] Lee KW, Wang S, Fox BC, Ritman EL, Yaszemski MJ, Lu L. Poly(propylene fumarate) bone tissue engineering scaffold fabrication using stereolithography: effects of resin formulations and laser parameters. Biomacromolecules 2007;8:1077-1084.
[64] Kim K, Dean D, Wallace J, Breithaupt R, Mikos AG, Fisher JP. The influence of stereolithographic scaffold architecture and composition on osteogenic signal expression with rat bone marrow stromal cells. Biomaterials 2011;32:3750-3763.
[65] Hollister SJ, Lin CY, Lin CY, Schek RD, Taboas JM, Flanagan CL, et al. Design and fabrication of scaffolds for anatomic bone reconstruction. Med J Malaysia 2004;59 Suppl B:131-132.
[66] Williams JM, Adewunmi A, Schek RM, Flanagan CL, Krebsbach PH, Feinberg SE, et al. Bone tissue engineering using polycaprolactone scaffolds fabricated via selective laser sintering. Biomaterials 2005;26:4817-4827.
[67] Lin LL, Tong AL, Zhang HC, Hu QX, Fang ML. The mechanical properties of bone tissue engineering scaffold fabricating via selective laser sintering. Life System Modeling and Simulation, Proceedings 2007;4689:146-152.
[68] Hutmacher DW, Schantz T, Zein I, Ng KW, Teoh SH, Tan KC. Mechanical properties and cell cultural response of polycaprolactone scaffolds designed and fabricated via fused deposition modeling. J Biomed Mater Res 2001;55:203-216.
[69] Hsu SH, Yen HJ, Tseng CS, Cheng CS, Tsai CL. Evaluation of the growth of chondrocytes and osteoblasts seeded into precision scaffolds fabricated by fused deposition manufacturing. J Biomed Mater Res B Appl Biomater 2007;80:519-527.
[70] Sherwood JK, Riley SL, Palazzolo R, Brown SC, Monkhouse DC, Coates M, et al. A three-dimensional osteochondral composite scaffold for articular cartilage repair. Biomaterials 2002;23:4739-4751.
[71] Roy TD, Simon JL, Ricci JL, Rekow ED, Thompson VP, Parsons JR. Performance of degradable composite bone repair products made via three-dimensional fabrication techniques. J Biomed Mater Res A 2003;66:283-291.

[72] Khalyfa A, Vogt S, Weisser J, Grimm G, Rechtenbach A, Meyer W, et al. Development of a new calcium phosphate powder-binder system for the 3D printing of patient specific implants. J Mater Sci Mater Med 2007;18:909-916.
[73] Mironov V, Boland T, Trusk T, Forgacs G, Markwald RR. Organ printing: computer-aided jet-based 3D tissue engineering. Trends Biotechnol 2003;21:157-161.
[74] Yousefi AM, Gauvin C, Sun L, DiRaddo RW, Fernandes J. Design and fabrication of 3D-plotted polymeric scaffolds in functional tissue engineering. Polym Eng Sci 2007;47:608-618.
[75] Smith MH, Flanagan CL, Kemppainen JM, Sack JA, Chung H, Das S, et al. Computed tomography-based tissue-engineered scaffolds in craniomaxillofacial surgery. Int J Med Robot 2007;3:207-216.
[76] Taboas JM, Maddox RD, Krebsbach PH, Hollister SJ. Indirect solid free form fabrication of local and global porous, biomimetic and composite 3D polymer-ceramic scaffolds. Biomaterials 2003;24:181-194.
[77] Chou YF, Huang W, Dunn JC, Miller TA, Wu BM. The effect of biomimetic apatite structure on osteoblast viability, proliferation, and gene expression. Biomaterials 2005;26:285-295.
[78] Murphy WL, Mooney DJ. Bioinspired growth of crystalline carbonate apatite on biodegradable polymer substrata. J Am Chem Soc 2002;124:1910-1917.
[79] Dorozhkin SV. Bioceramics of calcium orthophosphates. Biomaterials 2010;31:1465-1485.
[80] Barrere F, van der Valk CM, Dalmeijer RA, Meijer G, van Blitterswijk CA, de Groot K, et al. Osteogenecity of octacalcium phosphate coatings applied on porous metal implants. J Biomed Mater Res A 2003;66:779-788.
[81] Barrere F, van der Valk CM, Meijer G, Dalmeijer RA, de Groot K, Layrolle P. Osteointegration of biomimetic apatite coating applied onto dense and porous metal implants in femurs of goats. J Biomed Mater Res B Appl Biomater 2003;67:655-665.
[82] Li P. Biomimetic nano-apatite coating capable of promoting bone ingrowth. J Biomed Mater Res A 2003;66:79-85.
[83] Murphy WL, Kohn DH, Mooney DJ. Growth of continuous bonelike mineral within porous poly(lactide-co-glycolide) scaffolds in vitro. J Biomed Mater Res 2000;50:50-58.
[84] Chim H, Hutmacher DW, Chou AM, Oliveira AL, Reis RL, Lim TC, et al. A comparative analysis of scaffold material modifications for load-bearing applications in bone tissue engineering. Int J Oral Maxillofac Surg 2006;35:928-934.
[85] Holmbom J, Sodergard A, Ekholm E, Martson M, Kuusilehto A, Saukko P, et al. Long-term evaluation of porous poly(epsilon-caprolactone-co-L-lactide) as a bone-filling material. J Biomed Mater Res A 2005;75:308-315.
[86] Gorna K, Gogolewski S. Preparation, degradation, and calcification of biodegradable polyurethane foams for bone graft substitutes. J Biomed Mater Res A 2003;67:813-827.
[87] Kim SS, Park MS, Gwak SJ, Choi CY, Kim BS. Accelerated bonelike apatite growth on porous polymer/ceramic composite scaffolds in vitro. Tissue Eng 2006;12:2997-3006.
[88] Franceschi RT, Yang S, Rutherford RB, Krebsbach PH, Zhao M, Wang D. Gene therapy approaches for bone regeneration. Cells Tissues Organs 2004;176:95-108.

[89] Hutmacher DW, Garcia AJ. Scaffold-based bone engineering by using genetically modified cells. Gene 2005;347:1-10.
[90] Chang SC, Chuang HL, Chen YR, Chen JK, Chung HY, Lu YL, et al. Ex vivo gene therapy in autologous bone marrow stromal stem cells for tissue-engineered maxillofacial bone regeneration. Gene Ther 2003;10:2013-2019.
[91] Krebsbach PH, Gu K, Franceschi RT, Rutherford RB. Gene therapy-directed osteogenesis: BMP-7-transduced human fibroblasts form bone in vivo. Hum Gene Ther 2000;11:1201-1210.
[92] Hirata K, Tsukazaki T, Kadowaki A, Furukawa K, Shibata Y, Moriishi T, et al. Transplantation of skin fibroblasts expressing BMP-2 promotes bone repair more effectively than those expressing Runx2. Bone 2003;32:502-512.
[93] Rutherford RB, Moalli M, Franceschi RT, Wang D, Gu K, Krebsbach PH. Bone morphogenetic protein-transduced human fibroblasts convert to osteoblasts and form bone in vivo. Tissue Eng 2002;8:441-452.
[94] Schek RM, Wilke EN, Hollister SJ, Krebsbach PH. Combined use of designed scaffolds and adenoviral gene therapy for skeletal tissue engineering. Biomaterials 2006;27:1160-1166.
[95] Lin CY, Schek RM, Mistry AS, Shi X, Mikos AG, Krebsbach PH, et al. Functional bone engineering using ex vivo gene therapy and topology-optimized, biodegradable polymer composite scaffolds. Tissue Eng 2005;11:1589-1598.
[96] Roosa SM, Kemppainen JM, Moffitt EN, Krebsbach PH, Hollister SJ. The pore size of polycaprolactone scaffolds has limited influence on bone regeneration in an in vivo model. J Biomed Mater Res A 2010;92:359-368.
[97] Kruyt MC, Dhert WJ, Oner FC, van Blitterswijk CA, Verbout AJ, de Bruijn JD. Analysis of ectopic and orthotopic bone formation in cell-based tissue-engineered constructs in goats. Biomaterials 2007;28:1798-1805.
[98] Kruyt MC, Dhert WJ, Yuan H, Wilson CE, van Blitterswijk CA, Verbout AJ, et al. Bone tissue engineering in a critical size defect compared to ectopic implantations in the goat. J Orthop Res 2004;22:544-551.
[99] Duty AO, Oest ME, Guldberg RE. Cyclic mechanical compression increases mineralization of cell-seeded polymer scaffolds in vivo. J Biomech Eng 2007;129:531-539.
[100] Kang Y, Yao Y, Yin G, Huang Z, Liao X, Xu X, et al. A study on the in vitro degradation properties of poly(L-lactic acid)/beta-tricalcuim phosphate (PLLA/beta-TCP) scaffold under dynamic loading. Med Eng Phys 2009;31:589-594.
[101] Yang Y, Tang G, Zhao Y, Yuan X, Fan Y. Effect of cyclic loading on in vitro degradation of poly(L-lactide-co-glycolide) scaffolds. J Biomater Sci Polym Ed 2010;21:53-66.

CHAPTER 3

Experimental and Computational Characterization of Designed and Fabricated 50:50 PLGA Porous Scaffolds for Human Trabecular Bone Applications

3.1 Abstract

The present study utilizes image-based computational methods and indirect solid freeform fabrication (SFF) technique to design and fabricate porous scaffolds, and then computationally estimates their elastic modulus and yield stress with experimental validation. 50:50 Poly (lactide-*co*-glycolide acid) (50:50 PLGA) porous scaffolds were designed using an image-based design technique, fabricated using indirect SFF technique, and characterized using micro-computed tomography (μ-CT) and mechanical testing. μ-CT data was further used to non-destructively predict the scaffold elastic moduli and yield stress using a voxel-based finite element (FE) method, a technique that could find application in eventual scaffold quality control. μ-CT data analysis confirmed that the fabricated scaffolds had controlled pore sizes, orthogonally interconnected pores and porosities which were identical to those of the designed files. Mechanical tests revealed that the compressive modulus and yield stresses were in the range of human trabecular bone. The results of FE analysis showed that potential stress concentrations inside of the fabricated scaffold due to fabrication defects. Furthermore, the predicted moduli and yield stresses of the FE analysis showed strong correlations with those of the experiments.

In the present study, we successfully fabricated scaffolds with designed architectures as well as predicted their mechanical properties in a nondestructive manner.

3.2 Introduction

Tissue engineering scaffolds have been studied as temporary templates for defects in the body to support loads, cell attachment and tissue regeneration. To enhance bone tissue integration into the constructs, scaffolds should have interconnected porous architectures for cell migration and blood vessel infiltration [1]. It is also necessary to have sufficient mechanical properties to match and support physiological loading, which degrade in a favorable manner to transfer load support to tissues during healing [2-4]. To fulfill these requirements, it is necessary to design and fabricate scaffolds with controlled porous architectures [5,6].

Biodegradable porous bone scaffolds have been fabricated using several methods, including phase separation [7-10], particle leaching [5,11,12] and gas foaming [13]. These techniques can achieve high porosities (~90%) and large surface area for cell adhesion and tissue regeneration. These techniques further incorporate hydroxyapatite or bioactive glass to increase the scaffolds mechanical properties [14,15]. However, due to their high porosity and thin walls between pores, they do not have sufficient mechanical strength to support bone defect loading [16]. Furthermore, the pores are randomly located, and their interconnectivities are not well controlled. Although the mean pore diameter and overall scaffold porosity can be controlled by changing fabrication parameters like porogen diameters, it is impossible to precisely control pore location,

pore diameter, pore interconnectivity, wall thickness, and wall location [17]. Therefore, the internal pore architectures of those scaffolds cannot be designed.

To fabricate designed scaffolds with higher mechanical properties and interconnected pores, researchers have studied solid freeform fabrication (SFF) methods with various rapid prototyping (RP) machines, such as stereolithography (SLA) [18], selective laser sintering (SLS) [19,20], fused deposition molding (FDM) [21,22] and 3D printing [23]. These techniques enable fabrication of scaffolds with a high mechanical modulus and well interconnected pore structures compared to the aforementioned techniques of porogen leaching, gas foaming and phase separation. Although SFF techniques expand the capability of fabrication of designed scaffolds, only a limited numbers of materials can be used due to their temperature limitation, or chemical cross linking methods [24].

To address these limitations, indirect SFF technique is another unique and versatile technique using inverse molding to cast custom scaffolds [25]. In this technique, the inverse molds of the desired scaffold shapes are fabricated using rapid prototyping machines, such as SLA or other 3D printing machines. These secondary molds are then cast into the desired polymer or polymer solution. This technique has increased the material choices of scaffolds with various synthetic biodegradable polymers, including poly lactic acid (PLA) [26], poly glycolic acid (PGA) [25], poly propylene fumerate (PPF) [27,28], poly ε-carprolactone (PCL) [29] and a composite of poly (propylene fumerate) /tricalcium phosphate (PPF/TCP) [30,31].

Poly (lactide-*co*-glycolide acid) (PLGA) is a FDA approved biodegradable material [32] and has been widely studied both *in vitro* and *in vivo*. Many previous studies have shown low mechanical properties for load bearing purposes [5,6,13,33-36]. Although

some researchers achieved high compressive moduli, about 40MPa to 400MPa, their scaffolds are still not well controlled for pore size and porosity [11,37,38]. We postulate that PLGA porous scaffolds can be fabricated using indirect SFF technique with controlled internal architectures and compressive modulus for load bearing sites.

A critical need for scaffold engineering is the ability to a priori design scaffolds for desired effective properties, to non-destructively assess how closely the fabricated scaffold compares to its design and to investigate if differences between designed and fabricated properties can be determined from fabrication artifacts using computer aided design (CAD), computed tomography (CT) and finite element analysis (FEA) [19,39]. Image-based design (IBD) techniques have been utilized to design scaffolds that mimic anatomical and physical properties of human bone [40-42], and readily interface with indirect SFF technique to fabricate designed scaffolds. In addition, micro-computed tomography (μ-CT) has been utilized to assess the fabricated scaffolds architecture in a nondestructive manner [43,44]. Subsequently, the μ-CT techniques have been combined with voxel-based FEA to estimate scaffold mechanical properties and compare with experimental mechanical properties [20,45-48].

In this study, the porous scaffolds were designed by IBD and fabricated by indirect SFF technique to evaluate the ability to control scaffold architecture and mechanical properties. We hypothesized that designed 50:50 PLGA porous scaffolds could be fabricated using indirect SFF technique whose compressive moduli and yield stresses were within the range of the human trabecular bone. In addition, those mechanical properties could be computationally predicted from non-destructive μ-CT scans using voxel-based finite element method. To assess this hypothesis, we designed three

porosities, 0, 50, and 70%, of porous scaffolds with orthogonally interconnected pores using IBD and fabricated these scaffolds from 50:50 PLGA scaffolds using indirect SFF technique. We then measured the porosities, pore size and strut diameter of the fabricated scaffolds using μ-CT. Compressive moduli and strength of three orthogonal directions were measured by mechanical testing. Voxel-based FE methods were used to simulate both the designed and the fabricated scaffolds in order to computationally obtain elastic moduli and yield stresses. These values were compared to the experimental elastic moduli and yield stresses.

3.3 Methods

3.3.1 Material

50:50 PLGA (lot D#01080, Inherent Viscosity = 0.61dL/g) was purchased from Birmingham Polymers, Inc. (Birmingham, AL) and preserved in a container with desiccants at -20˚C to prevent moisture buildup. The polymer was left at room temperature for 30 minutes before further processing.

3.3.2 50:50 PLGA Solid Cube Fabrications

50:50 PLGA solid cubes with 0% porosity were fabricated in a customized polytetrafluoroethylene (PTFE) mold with 7x7mm square holes. The Teflon mold was preheated in the oven for 30 minutes, and the polymer pellets were periodically added to the mold until the desired volume was achieved and heated in a vacuum oven at 170°C for 3.5hours. The cubes were cooled to 100°C for 0.5 hours, and then to room temperature. After removing the Teflon mold, 50:50 PLGA cubes were trimmed to

become 7mm height. X, Y, Z orientations of the solid cubes were determined as shown in Fig 3.1 (e).

3.3.3 50:50 PLGA Porous Scaffold Fabrication

Porous scaffolds with interconnected pores were fabricated using the indirect SFF technique as previously described [25]. An image of each step is shown in Fig 3.1 (a - d). First, two porous scaffold designs with 50 % and 70% porosities were designed by IBD method using the interactive data language (IDL) software (Research Systems, Inc., Boulder, CO) [40]. The orthogonally interconnecting pores were generated as a unit cell and replicated to fill the cubic volume. The external shapes of scaffolds were designed into 7mm cubic shapes which were filled with the designed unit cells containing pore and struts. The pore and strut sizes of each scaffold were 664μm and 464μm respectively for the 50% porous scaffold, and 878μm and 228μm respectively for the 70% porous scaffold. The IDL generated image-based designs of the scaffolds were converted into stereolithography (STL) format, then, sliced using Modelworks software (Solidscape, Inc., Merrimack, NH), and finally read by PatternMaster™ 3D printer (Solidscape, Inc., Merrimack, NH) to fabricate wax molds.

Our fabrication method for the HA molds have been reported previously [49,50]. From our previous research, HA has been known to shrink during the sintering process, and we designed the HA secondary molds to account for this, by a scaling factor of 1.37 [25]. HA slurry was casted into the wax molds, cured in a nitrogen atmosphere overnight under a fume hood for one day, and immersed in acetone to remove the wax molds. The

HA molds were cyclically burned out in the furnace to remove the polymer binding the HA particles and then, sintered at 1350˚C.

The 50:50PLGA polymer pellets were added to the PTFE molds with a square hole to fit the HA secondary mold. The HA molds were then placed into the PTFE mold containing the molten PLGA polymer, and pushed through until the HA molds reached the bottom of the PTFE mold in order to force the polymer to penetrate into the open pore networks of the HA molds. The remainder of the casting protocol is identical to the solid cube fabrication. The polymer scaffolds containing HA molds were ground with a hand-milling machine to expose the HA on the surface of the scaffolds and submersed in RDO (APEX Engineering Products Corp, Plainfield, IL) under fluid agitation to remove HA from the porous polymer scaffold. Every 1 to 1.5 hours, the scaffold was blown with air to clean out residual HA. X, Y and Z directions of scaffolds were determined and marked (Fig 3.1). After the HA was removed from the scaffolds, polymer scaffolds were washed with ethanol, dried and returned to the freezer.

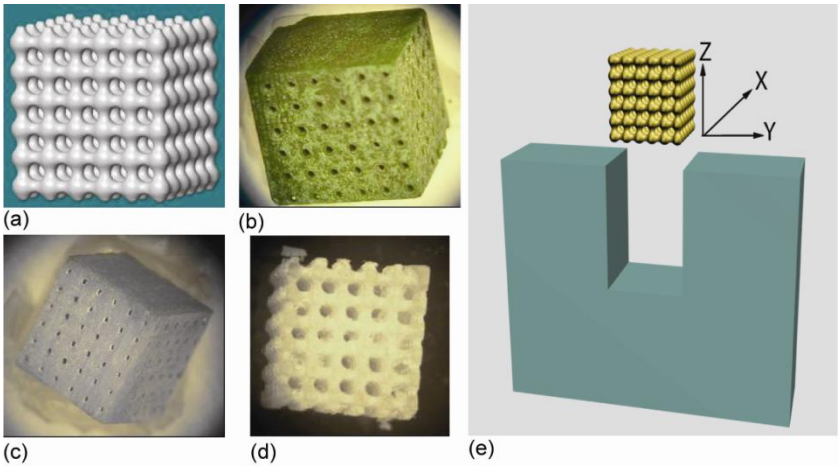

Fig 3.1 Images of the scaffold fabrication process. (a) A porous scaffold was designed using IBD techniques and converted into stil file format. (b) A thermoplastic mold was fabricated using PatternMaster rapid prototyping machine. (c) A hydroxyapatite secondary mold was cast into the thermoplastic mold followed by burning and sintering process. (d) 50:50 PLGA porous scaffold was cast into the HA secondary mold and the HA mold was removed by RDO. (e) Orientation of the fabricated scaffolds. The orientations of the scaffolds were defined along to the casting directions. Green color represents one of the Teflon molds, and there are two Teflon plates attached both size in X direction.

3.3.4 Characterization of Fabricated Scaffold Morphology and Volume Fraction

Determination of the fabricated scaffold morphology, pore sizes, pore interconnectivity and volume fraction was done using a MS-130 high resolution Micro-CT Scanner (GE Medical Systems, Toronto, CAN). All of the solid cubic, 50% and 70% porous scaffolds were scanned at a resolution of 16μm. The source volume was 75kV and 75 mA and an aluminum filter was used. The scanned images were reconstructed using Microview software (GE Healthcare) and stored as .vff files. To determine the volume fraction of the scaffolds, the vff files were reoriented and output as .jpg files using Microview software. Finally, regions of interest (ROI) from the .jpg images were determined and converted to raw files, and the raw files were used to automatically calculate the fraction of volume using IDL software. The ROI was chosen to contain the entire scaffold, but not any area outside of the scaffold.

3.3.5 Mechanical Testing

Compression tests were performed at a rate of 1mm/min after a preload of 0.454kg (1lb) using a MTS Alliance RT30 Electromechanical test frame (MTS Systems Corp., MN). After scanning, all scaffolds were compressed to failure in one of three orthogonal directions (X, Y, Z) defined in the scaffold fabrication section. TestWorks4 software (MTS Systems Corp., MN) was used to record load and displacement data, and stress-strain curves were calculated from the initial dimensions of the specimens. The compressive modulus was defined by the slope at the initial linear section of the stress-strain curve. The yield stresses were calculated using the 0.2% offset method. One-Way ANOVA was performed using SPSS (SPSS, Inc., Chicago, IL USA), with significance defined as $p < 0.05$.

3.3.6 Finite Element (FE) Analysis of Fabricated Scaffold

The μ-CT scanned scaffolds were simulated using a voxel-based FE method to compare the compressive moduli with those of the experiments. The 3D .vff files were converted to Analyze.hdr format using the Microview software, and then imported into the ScanIP^{TM} software (Simpleware Ltd. UK.). The imported files were processed and exported into .stl formats. The stl files were imported into the voxel-based homogenization software, VOXELCON (Quint Corp, Tokyo, Japan), to create voxel, or equivalently 8-node hexahedral elements. The input moduli (Ex = 2706.5MPa, Ey = 2845.5MPa, Ez = 2986.9MPa) were determined from the compressive tests of the solid cubes and Poisson's ratio of 0.3 was assumed for all models. The voxel size with 30μm was applied to 50% and 70% porous scaffolds, and the voxel size with 50 μm was

applied to the solid cubes. The uniaxial loads in z direction are applied to one side of the models, and the other sides were confined in z direction. One voxel (not one node) of the constrained side was constrained with X and Y direction to prevent the rotation of the model. Convergence was achieved when the force and displacement residuals were less than 1×10^{-4}.

3.3.6.1 Prediction of modulus and yield stress of the designed porous scaffolds

Two loads were applied to the structure within the linear region of scaffold deformation. One was applied at the lower end of the linear region and one was applied at the upper end of the linear region. Since elastic modulus is linear, it could be determined from either applied load. The effective scaffold modulus was calculated as the slope of the applied stress (applied load/cross-sectional area) versus average strain (maximum displacement/initial length). To determine the yield stress of the designed scaffolds, the maximum stress of the voxels under each applied stress of the designed scaffold was calculated. Then, the relation between the applied stress and the maximum stress were plotted. Finally, the yield stress was determined at the point where the maximum stress reached value of the bulk yield stress.

3.3.6.2 Prediction of modulus and yield stress of the fabricated porous scaffolds

The effective moduli of the fabricated porous scaffold (n = 9) were calculated in the same way as the porous scaffold designs. For yield stress calculation (n = 8), cumulative histograms of von Mises stress distributions were plotted. Then, the histograms were fit to a modified cumulative Weibull function (eq.1) which includes two exponential terms.

$$f(x) = 1 - \left(p e^{-(x/\lambda)^{k_1}} + (1-p) e^{-(x/(r\lambda))^{k_2}} \right) \quad \text{(Eq. 1)}$$

Where p is a weighting value for the exponential terms, k_1 and k_2 are the shape parameters, and λ and r are scale parameters of the fitting curve. The modified Weibull function was fit using the FMINCON optimization routine in MATLAB. After several tests, p values clustered around 0.1. Therefore, p was chosen as 0.1 in this study. k_1, k_2 and r were found to be constant over the analyses for a scaffold regardless of the applied loads. It was also found that λ was proportional to the applied loads. Here, we introduced ε, a fraction of voxels having von Mises stress higher than the bulk yield stress (110MPa from our experiments). For given p, k_1, k_2 and r, λ at yield was determined for a given ε by eq 1. Also we calculated λ from bulk yield for given ε by direct relation in eq 1. Then, by interpolating two applied loads (high applied load (larger λ) and lower applied load (smaller λ)), we obtained the yield stress of the scaffold (Fig 3.7 (b)). Prediction was performed with various ε values (0.0001, 0.0003, 0.0005, 0.001, 0.002, and 0.003) and correlated to the experimental yield stresses.

3.4 Result

3.4.1 Assay of Scaffold Morphology

We designed and fabricated 18 of the 70% porous scaffolds, 16 of the 50% porous scaffolds and 25 solid cubes. As shown in Fig 3.2 (a) and (d), the designs of porous scaffolds were composed of repeating unit cells with orthogonally interconnected pores in three directions and fitted to the desired outer dimensions of the porous scaffolds using the IBD technique. The three dimensional renderings of the fabricated scaffolds were obtained from the μ-CT data. The images revealed that the fabricated scaffolds (Fig 3.2

(b) and (e)) matched well with the designed architectures (Fig 3.2 (a) and (d)) and were composed of the repeated unit cells. Some cracks and undesired pores in the struts from the fabrication process were observed (Fig 3.2 (c) and (e)). Also, some residual hydroxyapatite was found inside of the scaffolds (data is not shown).

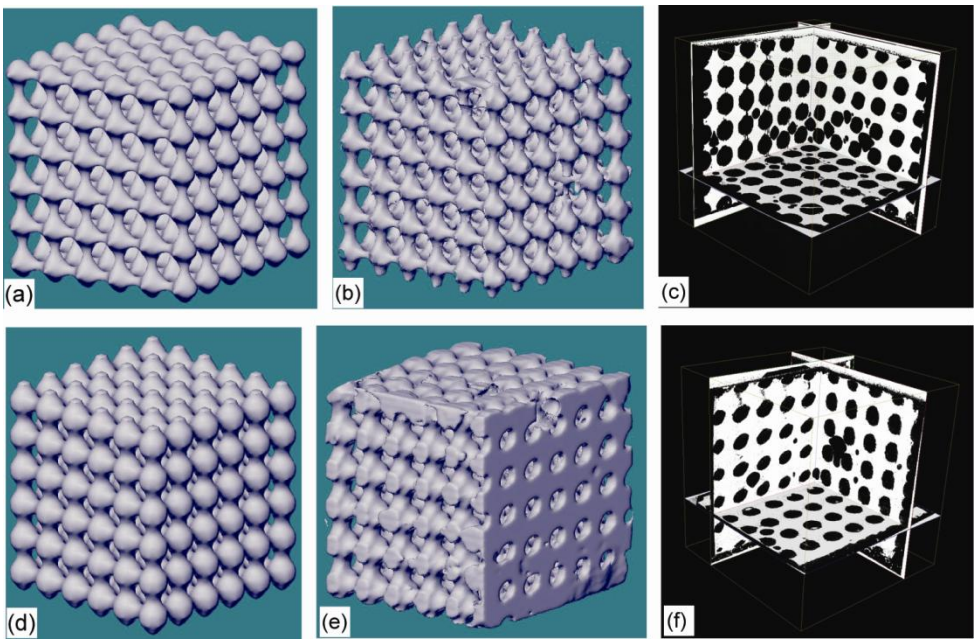

Fig 3.2 Images of 50% porous 50:50PLGA scaffold (a, b, c) and 70% porous scaffold (d, e, f). stl image of the designed scaffold (a, d). 3D rendering images of the fabricated scaffolds (b, e). µ-CT images of fabricated scaffolds shows pore interconnectivity of fabricated scaffold and some defects inside of the scaffolds (c, f)

The volume fraction (inverse of porosity) was determined by taking the volume of polymer divided by total scaffold volume. The targeted volume fractions of 70% and 50% porous scaffolds and solid cubes were 30%, 50% and 100% while the measured volume fractions were 23.6 ± 5.018 %, 41.7 ± 4.558 %, and 99.7 ± 0.789 % respectively. The interconnected pore diameters and strut sizes adjacent to the pores were measured from the µ-CT images. The average measured pore and strut sizes [Designed pore and strut sizes are in brackets] were 807 ± 49µm [878µm] and 296 ± 48µm [228µm] for the

70% porous scaffolds, and 652 ± 44μm [664μm] and 444 ± 51μm [464μm] for the 50% porous scaffolds.

3.4.2 Mechanical Properties of the fabricated Porous Scaffolds

The results of mechanical testing revealed that the compressive modulus and the yield stress varied depending on porosity of the scaffolds. The average modulus of the solid cube was obtained as 2851.9 ± 133.5 MPa. 70% porous scaffolds and 50% porous scaffolds had achieved an average modulus of 89.5 ± 36.8 MPa and 321.6 ± 140.9 MPa, respectively. The average offset yield stress also changed depending on the porosity of the scaffolds. The values were 2.1 ± 1.2 MPa, 10.3 ± 4.3 MPa and 110.4 ± 2.7 MPa for 70% porous, 50% porous and solid cubes respectively.

The anisotropy of the scaffold moduli and yield stresses were further examined (Fig 3.3 and Table 3.1). The results from the solid cube compressive modului revealed that anisotropy was determined by casting orientation. The anisotropy of solid cubes showed the highest modulus in order of Z (2986.9 ± 35.8 MPa), Y (2845.5 ± 34.7 MPa) then, X (2706.5 ± 103.9 MPa) direction, and these were significantly different ($p < 0.05$). The results of the yield stresses showed only Y direction was significantly lower that Z direction. Although both compressive modulus and yield stress were slightly higher in Z direction of 70% porous scaffold and Y direction of 50% porous scaffold, the statistical results did not show any significant difference.

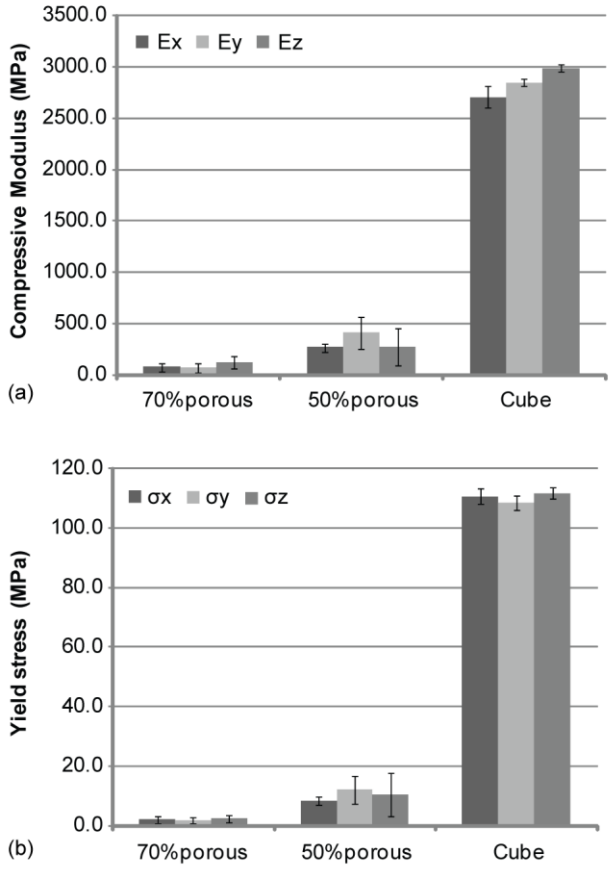

Fig 3.3 Scaffold anisotropy in terms of compressive modulus (a) and yield stress (b). The value of compressive modulus and yield stress are shown in table 3.1.

Table 3.1 Compressive modulus and Yield stress of the scaffolds with 3 orthogonal directions.

		X	Y	Z
70% Porous Scaffold	N	6	6	6
	E (MPa)	77.6 ± 40.7	69.5 ± 41.5	121.6 ± 58.4
	σ (MPa)	2.1 ± 1.3	1.7 ± 1.0	2.5 ± 1.2
50% Porous Scaffold	N	6	6	4
	E (MPa)	267.7 ± 39.5	407.7 ± 156.9	273.2 ± 178.4
	σ (MPa)	8.4 ± 1.5	12.1 ± 4.6	10.5 ± 7.3 (N = 3)
Solid cube	N	8	8	9
	E (MPa)	2706.5 ± 103.9	2845.5 ± 34.7	2986.9 ± 35.8
	σ (MPa)	110.7 ± 2.6	108.4 ± 2.4	111.8 ± 2.0

The mechanical test data of the 70% and 50% porous scaffolds were used to calculate the correlation between scaffold volume fraction and compressive modulus or yield stress depending on the scaffold test directions (Fig 3.4). The compressive modulus result shows their linear relations and the regression values were 0.9061, 0.9002 and 0.8248 in all directions. These results show the porous scaffold modulus range could be varied from 50 to 500 MPa depending on the scaffold porosities. In addition, the yield stress showed a significant correlation in σx (R^2 = 0.8397) and σy (R^2 = 0.8929), but there is a weak relation in σz (R^2 = 0.3327).

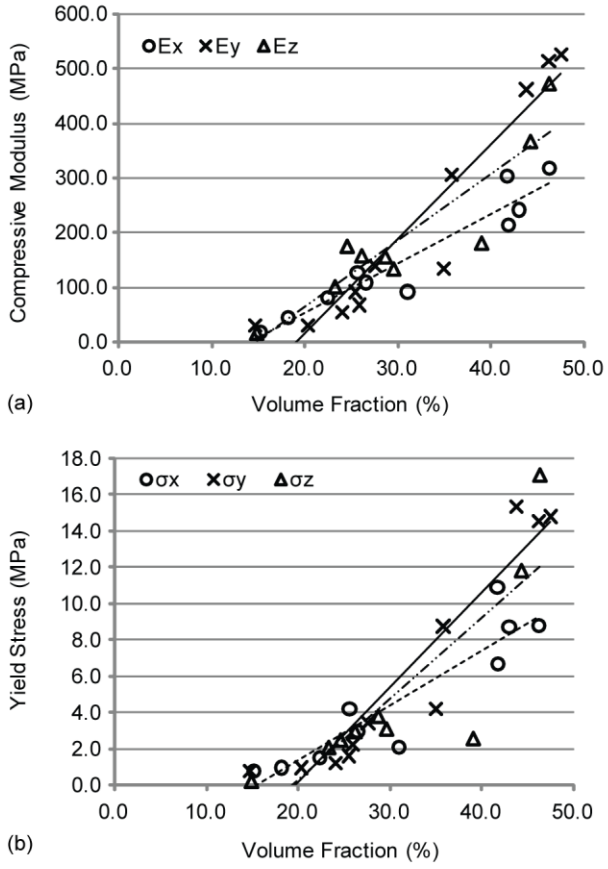

Fig 3.4 Correlation of scaffold volume fraction with compressive modulus (a) and yield stress (b). The linear fitting curves are; - - - · (Ex and σx), —— (Ey and σy), — · · - (Ez and σz).

3.4.3 Computational Simulation of solid cubes and Porous Scaffolds

3.4.3.1 Stress distribution of the designed and fabricated scaffolds

Fig 3.5 shows that stress distributions in Z direction from the FE simulation within the range of linear elastic region of the scaffolds (1~2% strain). The different color shows the different stress levels where red indicates the highest tensile stress (50MPa), blue indicates the highest compressive stress (-110MPa) and yellow indicates zero stress (0MPa). The designed porous scaffolds showed homogeneous stress in the Z direction (Fig 3.5 (b, c)), and higher stress concentrations appeared on the small struts on both designed porous scaffolds. The fabricated scaffolds demonstrated sporadic local compressive stress and tensile stress concentrations due to some casting defects in the scaffolds (Fig 3.5 (e, f)). Although there were minor stress concentrations on the fabricated scaffolds, the stress was distributed homogenously on the entire model as the designed cube. The distributions of the stresses of the fabricated porous scaffolds were similar in both designed and the fabricated scaffolds.

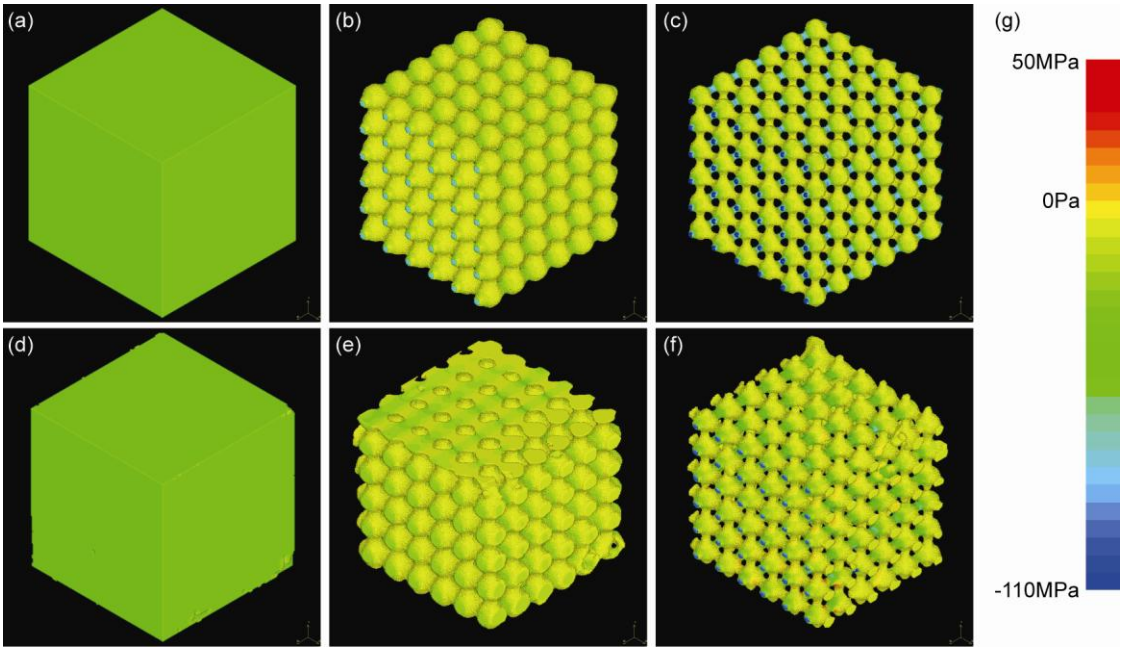

Fig 3.5 The Z-stress distributions of simulated scaffolds in the linear elastic regions (1~2% strain): (a) designed cube, (b) designed 50% porous scaffold, (c) designed 70% porous scaffold, (d) fabricated cube, (e) fabricated 50% porous scaffold, and (f) fabricated 70% porous scaffold. (g) Scale bar of the stress ranges are -110 MPa (blue) to 50 MPa (red), and the yellow shows around 0MPa stress.

Potential high stress concentrations in the fabricated scaffolds were also discovered using the FE simulation. Fig 3.6 shows an example to find the heterogeneous stress distribution of fabricated scaffolds. The scaffold was simulated with 50N of loading which caused 1.85% strain deformation. Although this strain was within the elastic region and lower than the 0.2% offset yield strain from the experiment of this scaffold (2.53%), the stress on some struts were equal to that of the yield value. In addition, there are some red color regions which indicate tensile stresses on the areas.

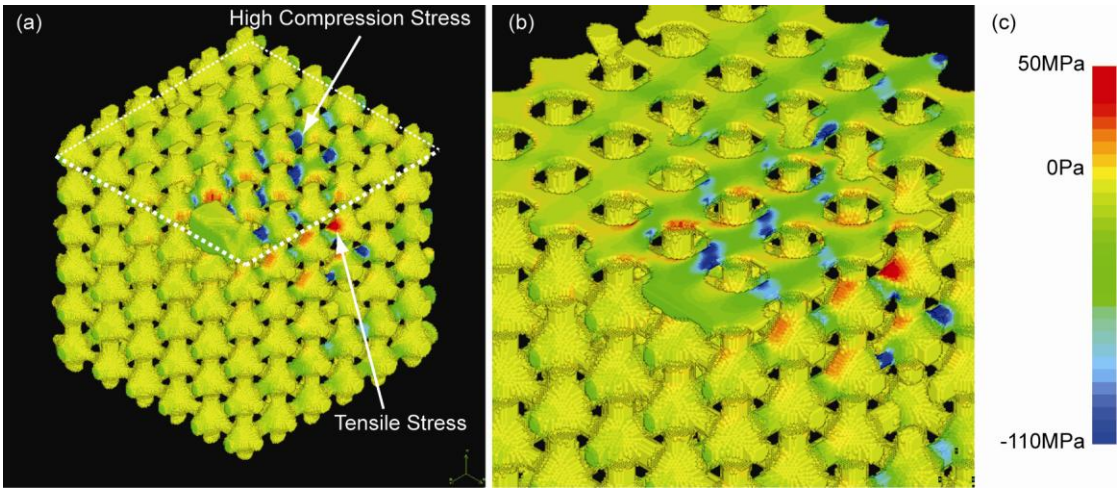

Fig 3.6 The stress distribution of fabricated 70% porous scaffolds under 50N loading which caused 1.85% strain. (a) The stress distribution of the entire scaffold. .(b) The stress distribution of the cross section of the white dot line The blue colors show the high stress region which may cause yield of the scaffold. (c) Scale bar of the stress ranges are -110 MPa (blue) to 50 MPa (red), and the yellow shows around 0MPa stress.

3.4.3.2 Prediction of compressive moduli and yield stresses of designed scaffolds

The predicted compressive moduli of the 50% and 70% porous scaffold designs determined from FE results were 553MPa and 173MPa, respectively. Further prediction of the yield stress can be performed using the relation between applied stress and scaffolds maximum stress (Fig 3.7 (a)). The predictions of the yield stresses were determined at the point where the maximum stress of a voxel reaches 110 MPa (bulk yield stress from the experiment). The 50% and 70% porous scaffold designs reached the yield stress level when 10.76MPa and 2.94MPa were applied, respectively.

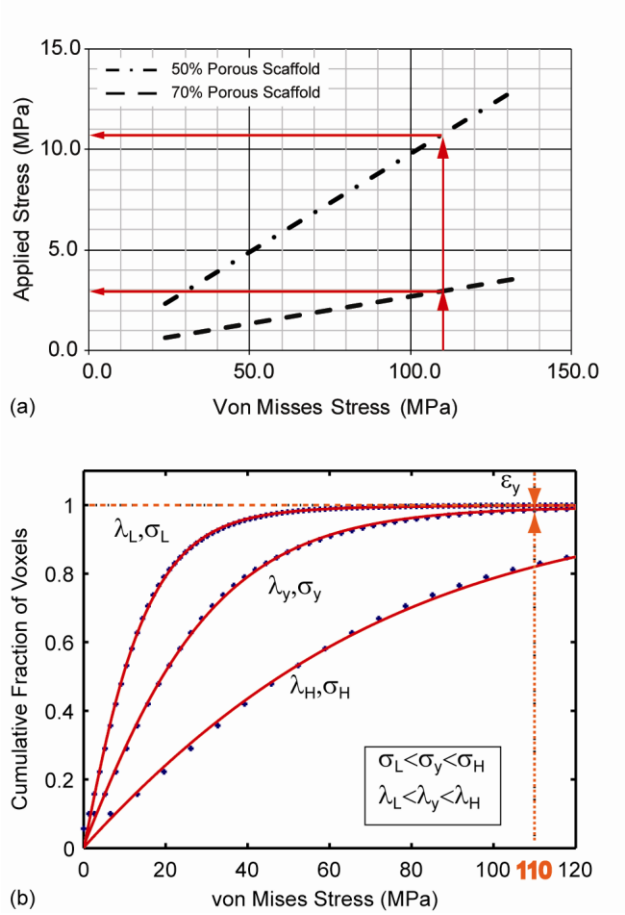

Fig 3.7 The prediction of the yield stress from the simulation of the scaffold designs, 50% porous scaffold and 70% porous scaffold (a). The relation among Weibull fittings, σ and λ (b). When the scaffold does not yield, σ and λ are smaller than the σ_y and λ_y. ε is smaller than ε_y or equal to 0. When the scaffold yields, σ and λ are larger than the σ_y and λ_y. ε is bigger than ε_y.

3.4.3.3 Prediction of moduli and stresses of fabricated scaffolds

The simulation results show the average modulus of the solid cubes were 2646 ± 36 MPa (n = 4) and similar to that of the designed cube (2707MPa) and approximately 90% of the modulus of compression tests. The moduli of the fabricated scaffolds were also calculated from the FE results and compared with the experimental data (Fig 3.8 (a)). Although the simulated values were generally lower than those of the experiments, there was a significant correlation between the simulation and the experiments of fabricated porous scaffolds (R^2 = 0.951, y = 1.6557x -44.076).

Yield stress of actual fabricated scaffolds was estimated using the modified Weibull function fitting. The Fig 3.7 (b) shows that the relation between the fraction of the voxels and their stress levels. The cumulative fraction of voxels at a given von Mises stress was fit well with the modified Weibull distribution. As applied loads increase, λ, σ and ε increase. When λ is smaller than λ_y ($\lambda = \lambda_L$), σ is smaller than σ_y($\sigma = \sigma_l$), and the scaffold does not yield. When λ is bigger than λ_y ($\lambda = \lambda_H$), σ is bigger than σ_y($\sigma = \sigma_H$), and the scaffold already yields. ε for yield stress was determined for a von Mises stress of 110MPa. Under the yield strain, more than 99% of voxels have a stress level lower than the material yield stress (110MPa). However, the simulation of the higher stress levels shows that the curves shift towards a lower fraction and indicate that more voxels are exposed to higher stress. Although various values of ε were applied, plots and linear fittings for only the minimum and maximum of ε are shown in Fig 3.8 (b). For the tested ε range, the R^2 changed from 0.941 ($y = 0.7755x + 0.154$) to 0.946 ($y = 0.9062x + 0.4012$) with $\varepsilon = 0.001$ the highest which is also shown in Fig 3.8 (b).

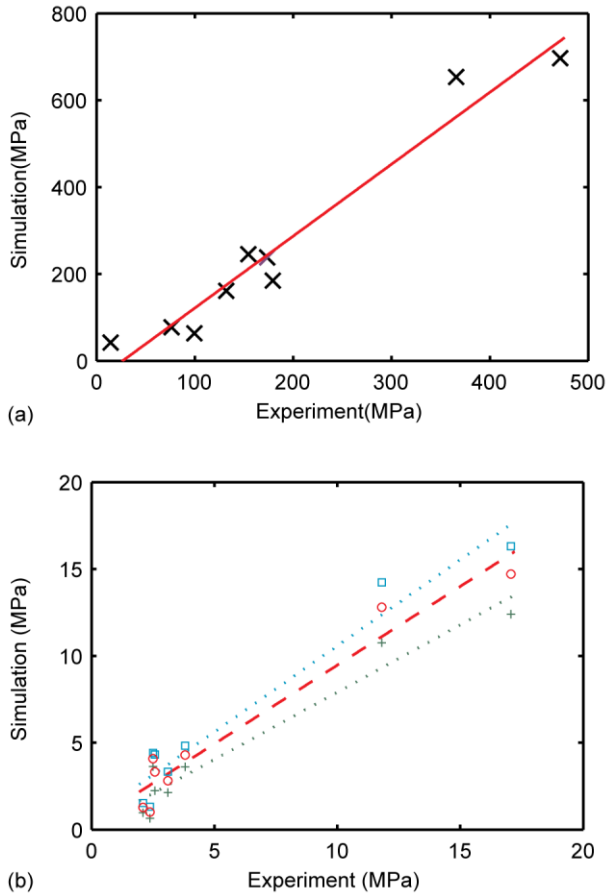

Fig 3.8 The relations between the simulated moduli and the experimental moduli of the fabricated scaffolds (a). The relations between the simulated yield stresses and the experimental yield stresses of the fabricated scaffolds (b). The green plots and fitting line indicates minimum $\varepsilon = 0.0001$, and the blue plots and line shows maximum $\varepsilon = 0.003$. The red plots and fitting line shows $\varepsilon = 0.001$ with the highest R-square (0.946).

3.5 Discussion

Controlling pore diameter and porosity of the scaffolds is necessary to control mechanical properties as well as tissue regeneration and scaffold degradation [37]. We successfully fabricated 50:50 PLGA scaffolds with designed strut sizes, pores sizes and porosities using IBD and indirect SFF techniques, and those were analyzed using μ-CT [43]. The scaffold outer shapes were designed in 7mm cubical shape to mimic the trabecular bone samples commonly used to test mechanical properties [51]. To examine

the effect of direction of casting on mechanical properties for the same specimen, the scaffolds with 1:1 ratio were examined instead of 2:1 ratio in the ASTM standard. The pore sizes of the scaffolds were designed similar or smaller compared to other SFF scaffolds for bone application [20,21]. Although the scaffolds have lower porosities, 50% and 70%, than the conventional scaffolds made by salt leaching and gas forming techniques, they have defined orthogonally interconnected pore architectures to allow mass transport into the scaffolds. In addition, lowering scaffold porosity may necessary to achieve high mechanical properties since the bulk property of this material is lower than bone.

Solid cubes were fabricated to find the best casting condition for porous scaffolds, and to obtain bulk material properties under our manufacturing conditions. The fabricated cubes had high volume fraction, and the bulk moduli and yield stresses which were much higher than those of trabecular bone [16,52,53], providing an upper bound on the attainable mechanical properties for porous scaffolds. The anisotropy of the mechanical properties may be explained that the fabrication process changed the polymer structures, such as crystallinity changes from differential scanning calorimetric tests (data not shown).

From the μ-CT data, it was confirmed that the pores of the 50% and 70 % porous scaffolds were orthogonally interconnected and that the molten polymers successfully penetrated into the HA secondary mold to form the internal architectures. The pore and strut sizes of the fabricated scaffolds were close to the designed ones, but the fabricated scaffolds had 8 - 10% lower volume fractions, or higher porosity, than the designed values due to some defects or air bubbles trapped inside of the scaffolds. However, this

difference was still smaller than those reported for early applications of direct SFF techniques, such as SLA (15-20%) [18]. Indirect SFF scaffolds made of PPF [27] also exhibited a larger deviation in volume fraction from designed ones. Compared with the previous scaffolds made by SFF techniques, the fabricated scaffolds had the same or better accuracy.

From the mechanical properties of both the 50% and 70% porous scaffolds, we obtained varying scaffold compressive moduli and yield stresses within the range of human trabecular bone, whose compressive modulus ranges from 10 to 900 MPa and yield stress from 0.2 to 14 MPa [16,52,53]. Our indirect SFF scaffolds also achieved higher compressive modulus and yield stress than scaffolds made by previous porogen leaching, phase separation and the composite techniques. In addition, 70% porous scaffold showed similar or higher modulus than other direct SFF techniques, such as 20 ~ 140 MPa of PPF scaffolds [18], 51.6 MPa of blended PCL/PLGA/TCP scaffolds [54] and 30 ~ 42 MPa of PCL scaffolds [21], although this is in part due to different bulk mechanical properties. The relation between the porosity of scaffolds and the mechanical properties showed increasing scaffold volume fraction increased the compressive modulus and yield stresses, consistent with other studies [5,11,23]. Furthermore, the mechanical properties of porous scaffolds are determined not only by their porosities but also by their architectures, including pore sizes and strut thicknesses [18]. Our scaffolds were composed with repeating unit cells which have similar diameter and different pore and strut sizes, and porosity. The 50% porous scaffolds had thicker walls than the 70% porous scaffolds which determined the mechanical properties depending on scaffold design.

When fabricating three dimensional porous scaffolds for load bearing applications, it is important to that the properties of the fabricated scaffolds match the designed properties their designs. According to the results of our study, there is no a significant difference of the compressive modulus or the yield stress among all directions of both the 70% and 50% porous scaffolds. These results are different than some of previous studies where the scaffolds mechanical properties followed the longitudinal alignments of microtubules [36] or a fabrication technique [55]. The anisotropy of their scaffolds relies on the design architecture, however, our 50% and 70% porous scaffolds had uniform architecture in three directions (X, Y, Z directions), and were not affected by the anisotropy of the casting process.

The files of the designed scaffolds and the μ-CT images of the fabricated scaffolds were further converted to simulate the mechanical properties of the fabricated scaffolds. The goal of the FE simulation is to predict mechanical properties of scaffolds without destroying the scaffolds [20,56]. Although some previous studies performed the simulation of designed scaffolds [57,58], these methods could not represent any potential manufacturing defects within the fabricated scaffolds. In addition, other investigators used geometry based FEM [45] to simulate scaffold designs, which required significant pre-processing time [59]. To solve these limitations, many investigators including our own group have used a voxel-based FE method to directly import CT data and automatically create voxel meshes [59,60]. Thus, μ-CT and the voxel-based FE analysis techniques were adapted in this study to build computer models representing actual fabricated scaffolds including defects. The voxel-based methods are powerful and allow simulation of large models in short time compared with a geometry based technique.

It is known that linear elements have a stiffer behavior than quadratic elements. In order to get accurate simulation, we used greater than a half million linear voxel elements in each model. In spite of the linear analysis, we applied various loadings to predict yield stress since the modified Weibull distribution of modulus is fit to a distribution of elements at a given stress, not an absolute value of stress. Thus, we are looking at the number of the elements that have a certain stress level. This function will not be linear as shown in Fig 3.7 (b), since it is the number of elements that exist at a given stress, and not the stress in a specific element. In other words, the number of elements at a given stress for a high load may not be linearly proportional to the number of elements at a given stress for a low load.

There have been some concerns that the voxel-based method may possess a certain amount of numerical errors inherent to its digitized modeling. Especially at the boundary, there can be oscillations in the responses or local stress concentrations at the stair-like boundary. To evaluate the accuracy of the digital image-based FE method, Guldberg et al., [61] compared voxel-based solutions to analytical solutions and showed that the error was less than 5% if a structural member is modeled with 10 voxel elements. They also confirmed oscillatory behavior of the stresses in the voxel-based solution; however, the oscillation was around the exact solution, which allowed filtering technique to minimize the errors. In this study, the smallest strut size of the scaffolds was about 300μm, and the voxel size was 30μm. The beam diameter to voxel ratio is 10, which indicates the error is small enough to be negligible, and the stress concentration was minimized in the simulation by averaging stress values [61].

We first performed the stress distributions and the scaffolds deformations under compression. Combining the bulk mechanical properties of 50:50 PLGA, the FE analysis could also be used to predict potential yield stress of the designed scaffolds. Although the simulation results of the designed scaffolds showed homogeneous stress distribution patterns, the stress distributions of the fabricated scaffolds were heterogeneous and showed tensile stresses besides compression stresses due to defects.

The predicted compressive moduli of the designed scaffolds were greater than the experimental compressive moduli of the fabricated scaffolds because the designed scaffolds do not contain any defects. Experimental scaffolds were mechanically inferior to the computational image based designs due to defects in the actual material such as microcracks, voids and rough layer boundaries. Using FE models alone based on a perfect design without defects can leads to overestimates of mechanical properties.

To achieve a more accurate prediction of scaffolds mechanical properties, the unique approach of combining post-fabrication imaging (μ-CT) and finite element analysis (Voxel FEM) was performed. This approach allows captured significant portion of the material defects in the computational model. Comparison between the experimental values and predicted values proved that our computational analysis correlated well with our experimental data. By introducing ε, a small fraction of voxels were allowed to undergo stresses higher than bulk yield even at the ultimate load. A fabricated porous scaffold may not suffer overall yielding even if it experiences local yield stress. We found that variation of ε causes a variation of the correlation, which implies that there may be an optimal value of ε to detect yield loads of the fabricated scaffolds, and further experiments are needed to find the optimal value. Our results showed that simulation

using the μ-CT data had better correlation than the designed scaffolds. Although ideally one would look for a 1 to 1 correlation between computational and experimental results, finding a significant correlation between their results is still very helpful for design purposes, especially if the correlation is conservative. Such a correlation would allow engineers to computationally predict how variations in architecture can affect elastic modulus and yield stress and rapidly examine a large range of architectural designs to determine a range of desired properties that would not be feasible using a purely experimental approach.

Limitations of our fabrication method are defects in the final product from the fabrication process, which include air bubbles and residual hydroxyapatite. Although we successfully fabricated solid cubes, there was unavoidable air rapped during casting of the polymer into the HA secondary molds [24], where molten PLGA was cast into the HA secondary molds. In addition, during decalcification of HA, PLGA may suffer some degradation due to the acidic solution of the RDO. These limitations may be minimized by modifying the design of the secondary molds or the decalcification method.

The difference between the simulations and the experiments may be explained by several factors during processing of images were processed from μ-CT to FE software. Since the grayscale images of the CT data included some noise and did not show clear boundaries of the scaffolds, some details of the scaffolds may be lost when they were exported to stl files. In addition, the resolutions of the original CT images were reduced due to the memory limitation of the FE software and the computer as well as the voxel representation that may lose some details of the scaffolds shapes. The actual material moduli of the base material that makes the scaffolds may be lower than the moduli input

for the base material in the FE model, perhaps due to some degradation of polymer material by the RDO acid.

3.6 Conclusions

It was demonstrated that indirect SFF technique can be used to fabricate designed scaffolds with interconnected porous architectures directly from image-based design techniques. These fabricated scaffolds could attain moduli and strength values in the range of human trabecular bone. Moreover, μ-CT structural measurements of 50:50 PLGA porous scaffolds showed scaffolds had consistent reliable volume fraction similar to designed volume fraction although some casting defects are still present. Thus, measured scaffold modulus and yield stress within trabecular bone range demonstrates that highly porous interconnected scaffolds can be fabricated with load bearing capacity. The mechanical properties of the scaffolds were also simulated using voxel-based finite element methods and the result showed strong correlations between the experiments and simulations for both compressive modulus and yield strength. The use of this nondestructive method to predict modulus and yield stress will allow rapid and rigorous evaluation of scaffold mechanical quality for *in vivo* applications. With further experimental validation more rigorous prediction may be possible.

Acknowledgments

This study was supported by National Institute of Health (NIH) R01 grant AR 053379. We also would like to thank for Prof. John Halloran in Materials Science and Engineering for letting us to use their tube furnace and sintering oven.

References

[1] Karageorgiou V, Kaplan D. Porosity of 3D biomaterial scaffolds and osteogenesis. Biomaterials 2005;26:5474-5491.

[2] Athanasiou KA, Agrawal CM, Barber FA, Burkhart SS. Orthopaedic applications for PLA-PGA biodegradable polymers. Arthroscopy 1998;14:726-737.

[3] Hutmacher DW. Scaffold design and fabrication technologies for engineering tissues--state of the art and future perspectives. J Biomater Sci Polym Ed 2001;12:107-124.

[4] Hollister SJ. Porous scaffold design for tissue engineering. Nat Mater 2005;4:518-524.

[5] Ma PX, Choi JW. Biodegradable polymer scaffolds with well-defined interconnected spherical pore network. Tissue Eng 2001;7:23-33.

[6] Murphy WL, Dennis RG, Kileny JL, Mooney DJ. Salt fusion: an approach to improve pore interconnectivity within tissue engineering scaffolds. Tissue Eng 2002;8:43-52.

[7] Guan L, Davies JE. Preparation and characterization of a highly macroporous biodegradable composite tissue engineering scaffold. J Biomed Mater Res A 2004;71:480-487.

[8] Huang YX, Ren J, Chen C, Ren TB, Zhou XY. Preparation and properties of poly(lactide-co-glycolide) (PLGA)/ nano-hydroxyapatite (NHA) scaffolds by thermally induced phase separation and rabbit MSCs culture on scaffolds. J Biomater Appl 2008;22:409-432.

[9] Hu Y, Grainger DW, Winn SR, Hollinger JO. Fabrication of poly(alpha-hydroxy acid) foam scaffolds using multiple solvent systems. J Biomed Mater Res 2002;59:563-572.

[10] Nam YS, Park TG. Porous biodegradable polymeric scaffolds prepared by thermally induced phase separation. J Biomed Mater Res 1999;47:8-17.

[11] Thomson RC, Yaszemski MJ, Powers JM, Mikos AG. Fabrication of biodegradable polymer scaffolds to engineer trabecular bone. J Biomater Sci Polym Ed 1995;7:23-38.

[12] Wu L, Zhang H, Zhang J, Ding J. Fabrication of three-dimensional porous scaffolds of complicated shape for tissue engineering. I. Compression molding based on flexible-rigid combined mold. Tissue Eng 2005;11:1105-1114.

[13] Harris LD, Kim BS, Mooney DJ. Open pore biodegradable matrices formed with gas foaming. J Biomed Mater Res 1998;42:396-402.

[14] Thomson RC, Yaszemski MJ, Powers JM, Mikos AG. Hydroxyapatite fiber reinforced poly(alpha-hydroxy ester) foams for bone regeneration. Biomaterials 1998;19:1935-1943.

[15] Lu HH, El-Amin SF, Scott KD, Laurencin CT. Three-dimensional, bioactive, biodegradable, polymer-bioactive glass composite scaffolds with improved mechanical properties support collagen synthesis and mineralization of human osteoblast-like cells in vitro. J Biomed Mater Res A 2003;64:465-474.

[16] Rezwan K, Chen QZ, Blaker JJ, Boccaccini AR. Biodegradable and bioactive porous polymer/inorganic composite scaffolds for bone tissue engineering. Biomaterials 2006;27:3413-3431.

[17] Karande TS, Ong JL, Agrawal CM. Diffusion in musculoskeletal tissue engineering scaffolds: design issues related to porosity, permeability, architecture, and nutrient mixing. Ann Biomed Eng 2004;32:1728-1743.

[18] Lee KW, Wang S, Fox BC, Ritman EL, Yaszemski MJ, Lu L. Poly(propylene fumarate) bone tissue engineering scaffold fabrication using stereolithography: effects of resin formulations and laser parameters. Biomacromolecules 2007;8:1077-1084.
[19] Hollister SJ, Lin CY, Saito E, Lin CY, Schek RD, Taboas JM, et al. Engineering craniofacial scaffolds. Orthod Craniofac Res 2005;8:162-173.
[20] Williams JM, Adewunmi A, Schek RM, Flanagan CL, Krebsbach PH, Feinberg SE, et al. Bone tissue engineering using polycaprolactone scaffolds fabricated via selective laser sintering. Biomaterials 2005;26:4817-4827.
[21] Hutmacher DW, Schantz T, Zein I, Ng KW, Teoh SH, Tan KC. Mechanical properties and cell cultural response of polycaprolactone scaffolds designed and fabricated via fused deposition modeling. J Biomed Mater Res 2001;55:203-216.
[22] Hsu SH, Yen HJ, Tseng CS, Cheng CS, Tsai CL. Evaluation of the growth of chondrocytes and osteoblasts seeded into precision scaffolds fabricated by fused deposition manufacturing. J Biomed Mater Res B Appl Biomater 2007;80:519-527.
[23] Sherwood JK, Riley SL, Palazzolo R, Brown SC, Monkhouse DC, Coates M, et al. A three-dimensional osteochondral composite scaffold for articular cartilage repair. Biomaterials 2002;23:4739-4751.
[24] Weigel T, Schinkel G, Lendlein A. Design and preparation of polymeric scaffolds for tissue engineering. Expert Rev Med Devices 2006;3:835-851.
[25] Taboas JM, Maddox RD, Krebsbach PH, Hollister SJ. Indirect solid free form fabrication of local and global porous, biomimetic and composite 3D polymer-ceramic scaffolds. Biomaterials 2003;24:181-194.
[26] Chen VJ, Smith LA, Ma PX. Bone regeneration on computer-designed nano-fibrous scaffolds. Biomaterials 2006;27:3973-3979.
[27] Lee KW, Wang S, Lu L, Jabbari E, Currier BL, Yaszemski MJ. Fabrication and characterization of poly(propylene fumarate) scaffolds with controlled pore structures using 3-dimensional printing and injection molding. Tissue Eng 2006;12:2801-2811.
[28] Liao E, Yaszemski M, Krebsbach P, Hollister S. Tissue-engineered cartilage constructs using composite hyaluronic acid/collagen I hydrogels and designed poly(propylene fumarate) scaffolds. Tissue Eng 2007;13:537-550.
[29] Roosa SM, Kemppainen JM, Moffitt EN, Krebsbach PH, Hollister SJ. The pore size of polycaprolactone scaffolds has limited influence on bone regeneration in an in vivo model. J Biomed Mater Res A 2010;92:359-368.
[30] Lin CY, Schek RM, Mistry AS, Shi X, Mikos AG, Krebsbach PH, et al. Functional bone engineering using ex vivo gene therapy and topology-optimized, biodegradable polymer composite scaffolds. Tissue Eng 2005;11:1589-1598.
[31] Howk D, Chu TM. Design variables for mechanical properties of bone tissue scaffolds. Biomed Sci Instrum 2006;42:278-283.
[32] Middleton JC, Tipton AJ. Synthetic biodegradable polymers as orthopedic devices. Biomaterials 2000;21:2335-2346.
[33] Sosnowski S, Wozniak P, Lewandowska-Szumiel M. Polyester scaffolds with bimodal pore size distribution for tissue engineering. Macromol Biosci 2006;6:425-434.

[34] Wu L, Ding J. In vitro degradation of three-dimensional porous poly(D,L-lactide-co-glycolide) scaffolds for tissue engineering. Biomaterials 2004;25:5821-5830.
[35] Kim SS, Sun Park M, Jeon O, Yong Choi C, Kim BS. Poly(lactide-co-glycolide)/hydroxyapatite composite scaffolds for bone tissue engineering. Biomaterials 2006;27:1399-1409.
[36] Ma PX, Zhang R. Microtubular architecture of biodegradable polymer scaffolds. J Biomed Mater Res 2001;56:469-477.
[37] Wu L, Ding J. Effects of porosity and pore size on in vitro degradation of three-dimensional porous poly(D,L-lactide-co-glycolide) scaffolds for tissue engineering. J Biomed Mater Res A 2005;75:767-777.
[38] Jiang T, Abdel-Fattah WI, Laurencin CT. In vitro evaluation of chitosan/poly(lactic acid-glycolic acid) sintered microsphere scaffolds for bone tissue engineering. Biomaterials 2006;27:4894-4903.
[39] Sun W, Starly B, Darling A, Gomez C. Computer-aided tissue engineering: application to biomimetic modelling and design of tissue scaffolds. Biotechnol Appl Biochem 2004;39:49-58.
[40] Hollister SJ, Levy RA, Chu TM, Halloran JW, Feinberg SE. An image-based approach for designing and manufacturing craniofacial scaffolds. Int J Oral Maxillofac Surg 2000;29:67-71.
[41] Hollister SJ, Maddox RD, Taboas JM. Optimal design and fabrication of scaffolds to mimic tissue properties and satisfy biological constraints. Biomaterials 2002;23:4095-4103.
[42] Lin CY, Kikuchi N, Hollister SJ. A novel method for biomaterial scaffold internal architecture design to match bone elastic properties with desired porosity. J Biomech 2004;37:623-636.
[43] Ho ST, Hutmacher DW. A comparison of micro CT with other techniques used in the characterization of scaffolds. Biomaterials 2006;27:1362-1376.
[44] van Lenthe GH, Hagenmuller H, Bohner M, Hollister SJ, Meinel L, Muller R. Nondestructive micro-computed tomography for biological imaging and quantification of scaffold-bone interaction in vivo. Biomaterials 2007;28:2479-2490.
[45] Charles-Harris M, del Valle S, Hentges E, Bleuet P, Lacroix D, Planell JA. Mechanical and structural characterisation of completely degradable polylactic acid/calcium phosphate glass scaffolds. Biomaterials 2007;28:4429-4438.
[46] Lacroix D, Chateau A, Ginebra MP, Planell JA. Micro-finite element models of bone tissue-engineering scaffolds. Biomaterials 2006;27:5326-5334.
[47] Duty AO, Oest ME, Guldberg RE. Cyclic mechanical compression increases mineralization of cell-seeded polymer scaffolds in vivo. J Biomech Eng 2007;129:531-539.
[48] Jaecques SV, Van Oosterwyck H, Muraru L, Van Cleynenbreugel T, De Smet E, Wevers M, et al. Individualised, micro CT-based finite element modelling as a tool for biomechanical analysis related to tissue engineering of bone. Biomaterials 2004;25:1683-1696.
[49] Chu TM, Halloran JW, Hollister SJ, Feinberg SE. Hydroxyapatite implants with designed internal architecture. J Mater Sci Mater Med 2001;12:471-478.

[50] Chu TM, Orton DG, Hollister SJ, Feinberg SE, Halloran JW. Mechanical and in vivo performance of hydroxyapatite implants with controlled architectures. Biomaterials 2002;23:1283-1293.
[51] Turner CH, Burr DB. Basic biomechanical measurements of bone: a tutorial. Bone 1993;14:595-608.
[52] Athanasiou KA, Zhu C, Lanctot DR, Agrawal CM, Wang X. Fundamentals of biomechanics in tissue engineering of bone. Tissue Eng 2000;6:361-381.
[53] Hutmacher DW, Schantz JT, Lam CX, Tan KC, Lim TC. State of the art and future directions of scaffold-based bone engineering from a biomaterials perspective. J Tissue Eng Regen Med 2007;1:245-260.
[54] Kim JY, Jin GZ, Park IS, Kim JN, Chun SY, Park EK, et al. Evaluation of SFF-based Scaffolds Seeded with Osteoblasts and HUVECs for Use in Vivo Osteogenesis. Tissue Eng Part A 2010.
[55] Mathieu LM, Mueller TL, Bourban PE, Pioletti DP, Muller R, Manson JA. Architecture and properties of anisotropic polymer composite scaffolds for bone tissue engineering. Biomaterials 2006;27:905-916.
[56] Alberich-Bayarri A, Moratal D, Ivirico JL, Rodriguez Hernandez JC, Valles-Lluch A, Marti-Bonmati L, et al. Microcomputed tomography and microfinite element modeling for evaluating polymer scaffolds architecture and their mechanical properties. J Biomed Mater Res B Appl Biomater 2009;91:191-202.
[57] Diego RB, Estelles JM, Sanz JA, Garcia-Aznar JM, Sanchez MS. Polymer scaffolds with interconnected spherical pores and controlled architecture for tissue engineering: fabrication, mechanical properties, and finite element modeling. J Biomed Mater Res B Appl Biomater 2007;81:448-455.
[58] Miranda P, Pajares A, Guiberteau F. Finite element modeling as a tool for predicting the fracture behavior of robocast scaffolds. Acta Biomater 2008.
[59] Lengsfeld M, Schmitt J, Alter P, Kaminsky J, Leppek R. Comparison of geometry-based and CT voxel-based finite element modelling and experimental validation. Med Eng Phys 1998;20:515-522.
[60] Hollister SJ, Brennan JM, Kikuchi N. A homogenization sampling procedure for calculating trabecular bone effective stiffness and tissue level stress. J Biomech 1994;27:433-444.
[61] Guldberg RE, Hollister SJ, Charras GT. The accuracy of digital image-based finite element models. J Biomech Eng 1998;120:289-295.

CHAPTER 4

Effects of Designed PLLA and 50:50PLGA Scaffold Architectures on Bone Formation *In Vivo*

4.1 Abstract

Biodegradable porous scaffolds have been investigated as an alternative approach to current metal, ceramic, and polymer bone graft substitutes for lost or damaged bone tissues. Although there have been many studies investigating the effects of scaffold architecture on bone formation, many of these scaffolds were fabricated using conventional methods, such as salt leaching and phase separation, and were constructed without designed architecture. To study the effects of both designed architecture and material on bone formation, we designed and fabricated three types of porous scaffold architecture from two biodegradable materials, poly (L-lactic acid) (PLLA) and 50:50Poly (lactic-co-glycolic acid) (PLGA) using image based design and indirect solid freeform fabrication techniques, seeded them with bone morphogenic protein-7 transduced human gingival fibroblasts and implanted them subcutaneously into mice for 4 and 8 weeks. Micro-computed tomography data confirmed that the fabricated porous scaffolds replicated the designed architectures. Histological analysis revealed that the 50:50PLGA scaffolds degraded and did not maintain their architecture after 4 weeks. The PLLA scaffolds maintained their architecture at both time points and showed

improved bone ingrowth which followed the internal architecture of the scaffolds. Mechanical properties of both PLLA and 50:50PLGA scaffolds decreased, but PLLA scaffolds maintained greater mechanical properties than 50:50PLGA after implantation. The increase of mineralized tissue helped to support mechanical properties of bone tissue and scaffold constructs from 4 to 8 weeks. The results indicated the importance of choice of scaffold materials and computationally designed scaffolds to control tissue formation and mechanical properties for desired bone tissue regeneration.

4.2 Introduction

Bone graft substitutes such as titanium and other metals have been used for reconstructing bone defects caused by injury, inflammatory disease or cancer. However, these implants are less than ideal because the materials are non-degradable and may cause stress shielding. Tissue engineered scaffolds have been studied as alternative implants to heal skeletal defects. To enhance bone tissue integration and bone growth into the tissue engineered scaffolds, the scaffolds should have porous architecture to encourage cell migration and blood vessel formation [1]. It is also necessary to have sufficient mechanical properties to support physiologic loading, and proper degradation profiles to transfer loads to regenerating tissues during healing [2-4].

Poly (L-lactic acid) (PLLA) and Poly (lactic-*co*-glycolic acid) (PLGA) have both been approved by the FDA for specific clinical indications [5]. They have been used as orthopaedic implants [2,6] and have been widely studied as scaffolds for bone regeneration both *in vitro* and *in vivo*. Due to different degrees of hydrophilicity, degradation ratios and by-products, PLLA and PLGA have different effects on cell

behavior and tissue regeneration, and have been compared in different matrices, including films, porous sponges, and fiber like shapes using various cell types [7-10]. It has been demonstrated that the degradation time changes depending on the ratio of lactic acid and glycolic acid polymer [8,9,11]. Thus, adjusting the polymer ratio should control the degradation time of these scaffolds and their distinct degradation profiles may influence bone regeneration.

In addition to the scaffold material composition, factors influencing scaffold architecture, such as porosity and pore size, play a critical role in cell migration and bone formation into the scaffolds [12,13]. It has been postulated that an approximately 100 μm pore diameter is suitable for *in vitro* cell migration and a 300 μm pore diameter is necessary for tissue ingrowth and nutrient diffusion [1,14]. However, the effects of scaffold architecture on bone tissue formation are not fully known, and vary significantly between studies [15-22]. Because the effects of scaffold architecture on bone formation may differ depending on the materials studied [22,23] and the ability to fabricate scaffolds with controlled pore architectures [24], it is necessary to investigate the effects of rigorously controlled architectures for each biodegradable scaffold to clearly delineate architecture versus material influence on bone regeneration.

Conventional biodegradable scaffolds, especially scaffolds made from PLLA and PLGA, have been commonly fabricated by salt leaching or gas foaming and have a wide range of pore sizes with poor or non-interconnected pores, and the scaffold architectures are not identically duplicated with repeated samples [25,26]. It is also difficult to control local pore and wall locations, and porosities of these scaffolds. Currently, scaffold architecture is controlled in the global or overall scaffold level. Furthermore, in order to

ensure pore interconnectivity, porosity needs to be increased, and as a result the mechanical properties of scaffolds may thus be reduced [27].

To overcome these limitations, the combination of computer aided design and solid freeform fabrication techniques have been developed [4,28-30]. These methods allow design and fabrication of scaffolds with controllable local pore architecture to generate reproducible and effective mechanical and mass transport properties. Our group has developed image based design techniques by which the internal architectures of scaffolds can be customized based on the mathematical concept of unit cells [31-33]. These unit cells are designed and fabricated to have the desired effective physical properties, such as compressive modulus, permeability and diffusivity. Furthermore, we have utilized the indirect solid freeform fabrication (SFF) method to fabricate scaffolds with designed pore diameters, struts sizes and porosities [34]. Utilizing these techniques, we have successfully designed and fabricated 50:50PLGA porous scaffolds which have compression moduli within the range of human trabecular bone [35].

Bone morphogenetic proteins (BMPs) belong to the TGF-β family and had been extensively applied using direct BMP delivery or *in vivo* or *ex vivo* delivery via gene therapy to induce bone formation for skeletal regeneration [36-38]. Our method to express BMPs *in vivo* uses human dermal and gingival fibroblasts that have been transduced by recombinant adenovirus encoding BMPs to induce bone formation in ectopic sites [39,40]. This technique has also been combined with porous SFF scaffolds to facilitate bone generation [15,41-43]. Consequently, this *ex vivo* gene therapy method can be applied to induce bone formation in our engineered scaffolds.

The goal of this study was to determine the influence of scaffold material and architecture, especially pore size, strut size and surface/volume ratio on bone formation *in vivo* and to evaluate the mechanical properties of the resulting scaffolds and tissue constructs. Six groups of scaffolds, (three different designs and two different materials, PLLA and 50:50PLGA scaffolds) were fabricated. These scaffolds were seeded with transduced human gingival fibroblasts expressing BMP-7, and then implanted into mice subcutaneous pockets for 4 and 8 weeks. The scaffolds and scaffold/regenerated bone tissue construct were evaluated using Micro-computed tomography (μ-CT), mechanical testing, and histological assessments.

4.3 Methods

4.3.1. Porous Scaffold Design and Fabrication

Porous scaffolds 5mm in diameter and 3mm high with three different pore diameters (280, 550, and 820μm) were designed using image-based techniques (Fig 4.1, a). Based on the designed pore sizes, each group of the scaffolds was named Large (pore size = 820μm), Medium (pore size = 550μm), or Small (pore size = 280μm). First, the unit cells of each design were determined, and then, generated in a repeating pattern to fill the external scaffold geometry. The resulting image representations were converted to stereolithography (STL) formats and sliced in the Modelworks software (Solidscape, Inc., Merrimack, NH) to fabricate wax molds using a ModelMaker II (for Large and Medium) or PatternMaster™ (Fig 4.1, b) (for Small) 3D printer (Solidscape, Inc., Merrimack, NH). These wax molds (Fig 4.1, c) were cast into hydroxyapatite ceramic (HA) secondary molds (Fig 4.1, d). Polymer pellets, PLLA (Inherent Viscosity = 0.65dL/g) and

50:50PLGA (Inherent Viscosity = 0.61dL/g) (Birmingham Polymers Inc., AL), were heated at 205ºC and 170 ºC, respectively, in a Teflon mold. The HA molds were then placed into the Teflon mold containing molten polymer, in order to force the polymer through the open pore network. The HA molds were then removed from the porous polymer scaffolds using RDO Rapid Decalcifier (APEX Engineering Products Corp, Plainfield, IL). The scaffolds were sterilized in 70% ethanol overnight and then left in 100% ethanol until the day of implantation.

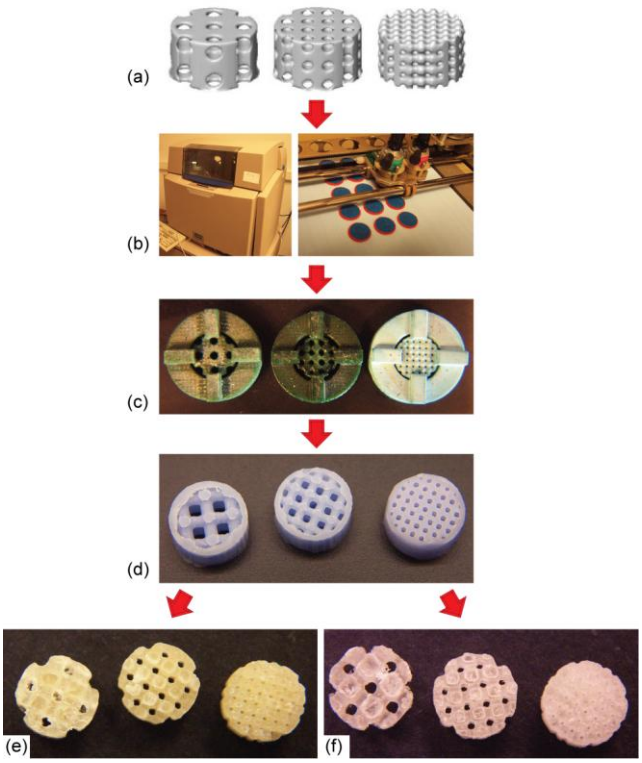

Fig 4.1 Porous scaffolds were designed using image based design techniques and exported into STL formats (Large, Medium and Small, from left to right) (a). The stl format files were imported to the rapid prototyping machines (b) to print the thermoplastic molds (c). The thermoplastic molds were casted into HA secondary molds (b), and finally the HA secondary molds were casted into either PLLA scaffolds (e) or 50:50PLGA scaffolds (f).

4.3.2. Cell preparation and scaffold implantation

Primary human gingival fibroblasts (HGFs) were prepared from explants of human surgical waste in compliance with the University of Michigan Institutional Review Board [39]. HGFs from passage 5- 10 were cultured near confluence in Alpha minimum essential medium (α-MEM) supplemented with 10% fetal bovine serum, and 1% penicillin and streptomycin (Gibco). 24 hours before implantation, the HGFs were infected with AdCMV-BMP-7, a recombinant adenovirus construct expressing murine BMP-7 gene under a cytomegalovirus (CMV) promoter, at a multiplicity of infection (MOI) of 1000 PFU/cell [44]. Two million cells were seeded into each scaffold by suspending them in 60µl of 5mg/ml bovine plasma-derived fibrinogen (Sigma), and gelled with 6µl of 100U/ml bovine plasma-derived thrombin (Sigma). The scaffolds seeded with 2 million cells were subcutaneously implanted into immunocompromised mice (N: NIH-bg-nu-xid, Charles River, Wilmington, MA). After animals were anesthetized with an injection of ketamine/xylazine, 4 subcutaneous pockets were created and 4 scaffolds were implanted into each mouse, and finally surgical sites were closed with wound clips in compliance with University Committee on Use and Care of Animal (UCUCA) regulations. The mice were sacrificed at 4 and 8 weeks after the implantation, and the scaffold and tissue constructs were harvested, fixed with Z-fix (Anatech, Battle Creek, MI) and left in 70% ethanol for further assay.

4.3.3. Assay of scaffolds and regenerated tissues

All of the scaffolds pre-implantation alone and post-implantation with tissues were scanned using a MS-130 high resolution µ-CT Scanner (GE Medical Systems, Toronto,

CAN) at a resolution of 16 μm. The scanned images were reconstructed using MicroView software (GE Healthcare). The reconstructed images were used to calculate the scaffold pore size, porosity and surface area prior to implantation and Bone volume (BV) and Tissue mineral density (TMD) were calculated for the scaffolds after implantation. The surfaces of pre-implanted scaffolds were also examined under a scanning electron microscope (XL30 ESEM, Philips). The environmental scanning electron microscopy (ESEM) mode was carried out at10kV and in a humid atmosphere of 0.7 Torr.

4.3.4. Mechanical test of scaffolds with regenerated tissue

Following μ-CT scanning, 4-7 replicates from each scaffold group were mechanically tested. Compression tests were performed after scaffolds were rehydrated for 30 minutes, using a MTS Alliance RT30 Electromechanical test frame (MTS Systems Corp., MN). The cross head speed was 1mm/min after a preload of 0.227kg (0.5 lbs) for PLLA scaffolds and 0.0227kg (0.05 lbs) for 50:50PLGA scaffolds. The heights of the scaffolds were measured with a caliper, and the TestWorks4 software (MTS Systems Corp., MN) was used to record load and displacement data. The stress-strain curves were calculated from the initial dimensions of specimens. The compressive modulus was defined by the slope at the initial linear section of the stress-strain curve.

4.3.5. Histological analysis

After scanning with the μ-CT machine, one harvested scaffold from each group was also used for histological assay. The scaffold and tissue constructs were demineralized

with RDO and the residual polymer in the tissue was removed using chloroform prior to paraffin-embedding. The scaffolds were then sectioned at 5 μm and stained with hematoxylin and eosin (H&E).

4.3.6. Statistical analysis

The statistical analysis was performed with SPSS (SPSS, Inc., Chicago, IL USA). Two groups were analyzed with Student's *t*-test for independent samples. Multiple comparison procedures were determined by one-way ANOVA followed by Tukey's Post Hoc multiple comparisons. Errors are reported in figures as the standard deviation (SD) and significance was determined using probability value of $p < 0.05$.

4.4 Results

4.4.1. Evaluation of the fabricated (pre-implanted) scaffolds

The schematics of the design and fabrication process of the scaffolds are depicted in Fig 4.1. HA secondary molds (Fig 4.1, d) ensured the fabrication process was identical between PLLA and 50:50PLGA scaffolds except for polymer casting temperatures. The architecture of the designs was the same for both the fabricated PLLA and 50:50PLGA scaffolds (Fig 4.1, e, f), which was also confirmed by μ-CT rendering images (Fig 4.2, a-f). The orthogonal pore locations and connections of the fabricated PLLA and 50:50PLGA scaffolds were also confirmed from the cross sectional images of μ-CT data (Fig 4.2, g-l). Low magnification ESEM images were similar in all groups (Fig 4.2, m-r), while the high magnification images showed slightly rougher surfaces on the PLLA scaffolds than the 50:50PLGA scaffolds (Fig 4.2, s-x, indicated by stars). Furthermore,

porosity, surface to volume ratio, pore sizes and strut sizes were measured using the µ-CT images (Table 4.1). For each parameter, there was no significant difference between the fabricated PLLA and 50:50PLGA scaffolds. These data support the concept that the scaffold architectures within each design group (Large, Medium, and Small) made of the two materials are identical to each other. Porosity, pore size and strut size of the fabricated scaffolds decreased in order from Large to Small pore designs. The Small group had a higher surface to volume ratio than the Large and Medium group for both PLLA and 50:50PLGA scaffolds.

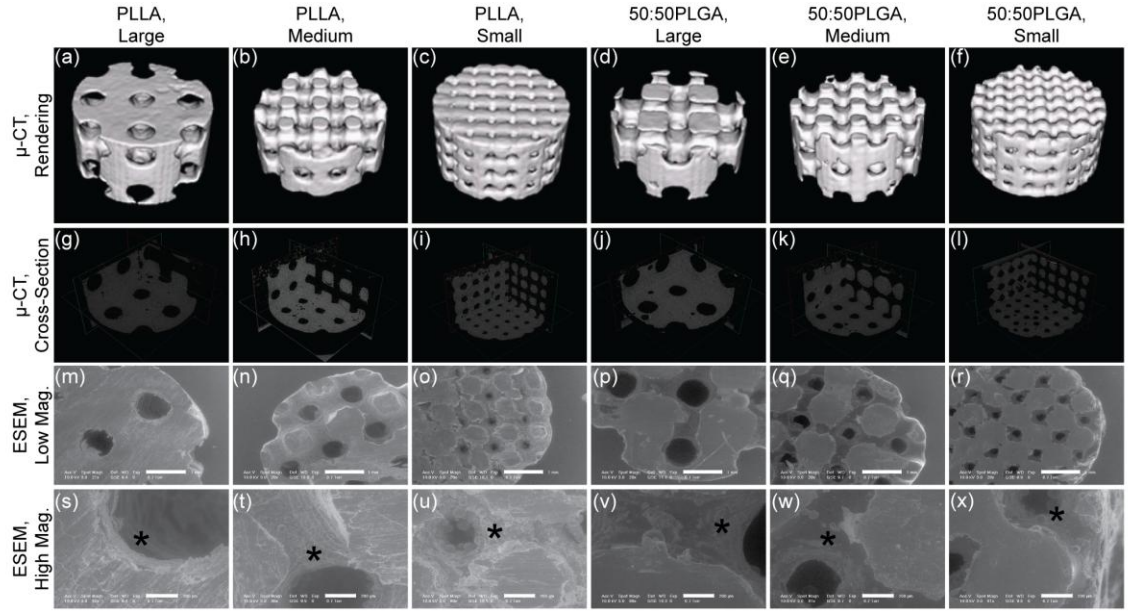

Fig 4.2 µ-CT rendering images (a-f), µ-CT images showing cross sectional x, y, and z planes (g-l), and ESEM images of fabricated PLLA and 50:50PLGA scaffolds (m-x). The scale bars in the ESEM images are 1mm and 200 µm for Low (m-r) and High magnifications (s-x), respectively. * indicates the surface around the pores for comparison of the surface morphologies of PLLA and 50:50PLGA scaffolds.

Table 4.1 Fabricated scaffold dimensions

	PLLA			50:50PLGA		
	Large	Medium	Small	Large	Medium	Small
Pore size (mm)	0.821 ± 0.041	0.580 ± 0.039	0.285 ± 0.026	0.840 ± 0.057	0.537 ± 0.033	0.258 ± 0.037
Strut size (mm)	0.914 ± 0.028	0.594 ± 0.033	0.413 ± 0.017	0.898 ± 0.045	0.622 ± 0.050	0.448 ± 0.039
Porosity (%)	52.1 ± 0.95	45.4 ± 3.21	32.1 ± 3.50	52.9 ± 2.17	43.8 ± 2.21	30.5 ± 3.30
Surface/Volume (mm^2/ mm^3)	4.57 ± 0.22	4.54 ± 0.15	5.40 ± 0.17	4.65 ± 0.25	4.88 ± 0.31	5.43 ± 0.59

4.4.2. Histological observations of implanted scaffolds

Due to the secretion of BMP-7 from the transduced HGFs, all of the implanted scaffolds had bone-like tissue formation after 4 and 8 weeks (Fig 4.3). The histological images show cortical bone-like tissues formed outer layers and bone marrow-like tissues, such as trabecular structures, endothelial cells and osteoblasts, were observed within the cortical layer and the scaffolds. In the 4 week implant groups, most of the marrow-like tissues were distributed in the peripheral regions of the specimen. However, more bone marrow-like tissues containing blood vessel-like tissues were observed in the 8 week implants than in the 4 week implants. We found marrow- like tissue both at the center of the scaffolds and also in the surrounding regions at 8 weeks.

The histological images also show that tissue formation differed between PLLA and 50:50PLGA scaffold groups. After 4 weeks of implantation, little degradation of PLLA was observed, and most of their architectures remained intact (Fig 4.3, a-c). However, 50:50PLGA scaffolds degraded more rapidly and lost their initial architectures (Fig 4.3, d-f). After 8 weeks of implantation, PLLA scaffolds maintained their architecture, while most of 50:50PLGA degraded, leaving very little polymer, and the bone constructs appeared flattened (Fig 4.3, h-m). After degradation of most of the 50:50PLGA scaffolds,

the histological images showed more bone marrow-like tissues containing blood vessel-like tissues in 8 week implants than in 4 week implants. For PLLA scaffolds, bone-like tissues formed mostly in the peripheral area of the scaffolds and very little bone ingrowth was observed (Fig 4.3, a-c, and g), and a few blood vessel-like tissues were seen inside of the scaffolds (Fig 4.3, g) at 4 weeks. At 8 weeks, advanced bone ingrowth was observed following the porous architectures of the Small PLLA scaffolds (Fig 4.3, j), and larger blood vessel tissues were also observed (Fig 4.3, n). In addition, there may be more fibrous tissue on PLLA scaffolds at 4 weeks than 8 weeks.

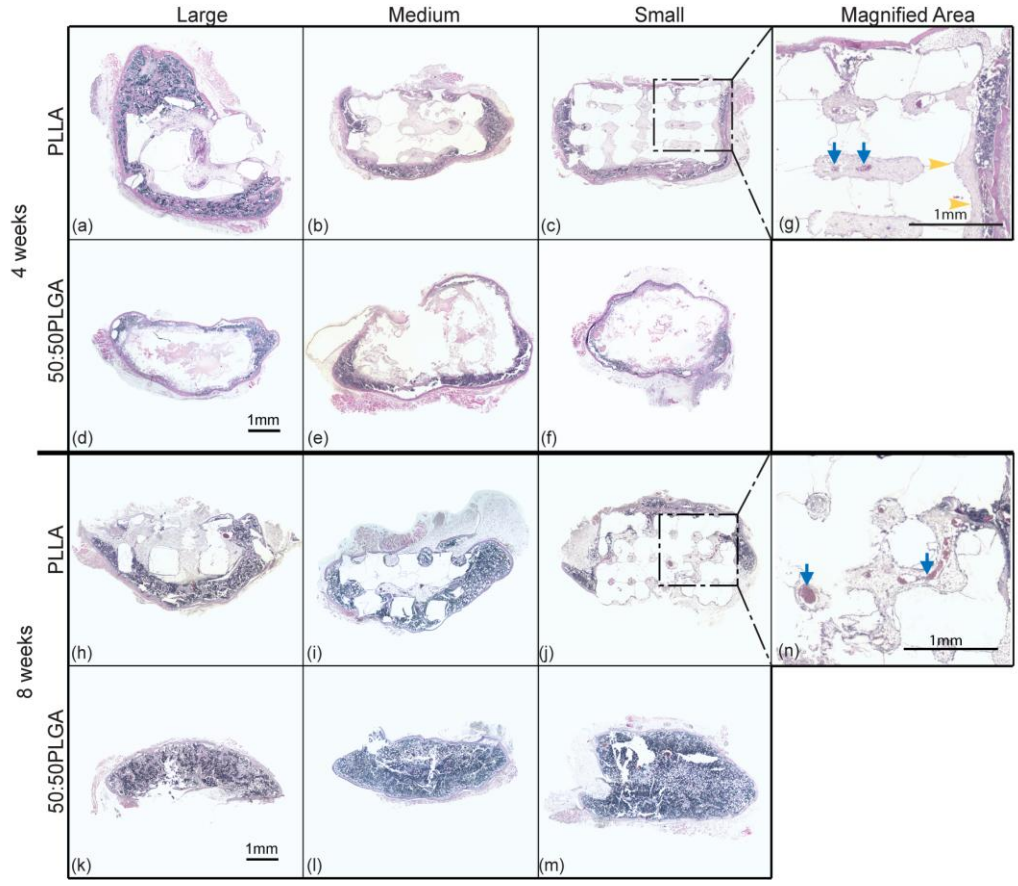

Fig 4.3 Histological images of PLLA (a, b, and c) and 50:50PLGA scaffolds (d, e, and f) at 4 weeks and PLLA (h,i and j) and 50:50PLGA scaffolds (k, l, and m) at 8 weeks. Porous architectures of PLLA scaffolds were maintained for all groups (a, b, and c) at 4 weeks and (h, i, and j) at 8 weeks. None of 50:50PLGA groups maintained the initial architectures, however, polymer material was still left inside of the bony shells at 4 weeks (d, e, and f). After 8 weeks, most of 50:50PLGA polymer had degraded and disappeared (k, l, and m). Magnified areas of Small PLLA scaffold at 4 weeks (c) were shown (h: dashed-dotted line). Yellow arrow indicates fibrous tissue between scaffold and trabecular like tissue, and a few blood vessel-like tissues were indicated by blue arrows (g). Magnified areas of Small PLLA scaffold at 8 weeks (j) were also shown (n: dashed-dotted line). Thicker blood vessel-like tissues were observed within the scaffold pores, shown by blue arrows (n).

4.4.3. Tissue observations using μ-CT

Three dimensional tissue representations were generated from μ-CT data (Fig 4.4). Mineralized tissues were highlighted, and color contours indicated the density of the regenerated tissues. Highly dense tissues were distributed only on the outside of the scaffolds. Due to the rapid degradation, there was no bone growth into the 50:50PLGA scaffolds. All PLLA scaffolds maintained their architectures at all time points. There

was some bone ingrowth into the PLLA scaffolds at 4 weeks, while there was slightly more bone ingrowth at 8 weeks. Maximum bone penetration was measured as the distance from the circular peripheral edge of each scaffold towards the center (N = 3-5 scaffolds). The bone penetration in the Small , Medium and Large PLLA scaffolds was 0.464 ± 0.024 mm, 0.723 ± 0.392 mm, and 0.457 ± 0.146 mm, respectively at 4 weeks, and 1.043 ± 0.292 mm, 0.834 ± 0.249 mm, and 0.773 ± 0.049 mm, respectively at 8 weeks. Small PLLA scaffolds supported a significant increase of bone penetration from 4 to 8 weeks. Large and Medium PLLA scaffolds also had increases in bone penetration, but these did not reach a statistically significant level. There was no significant difference between the scaffold groups at each time point. Also, the pattern of bone ingrowth followed the internal scaffold architectures, and bone tissues regenerated along the struts (Fig 4.4, g-i). More bone tissue distribution was observed at 8 weeks than at 4 weeks with the highest amounts seen in the Small PLLA group, which had more bone surrounding the struts (Fig 4.4, i).

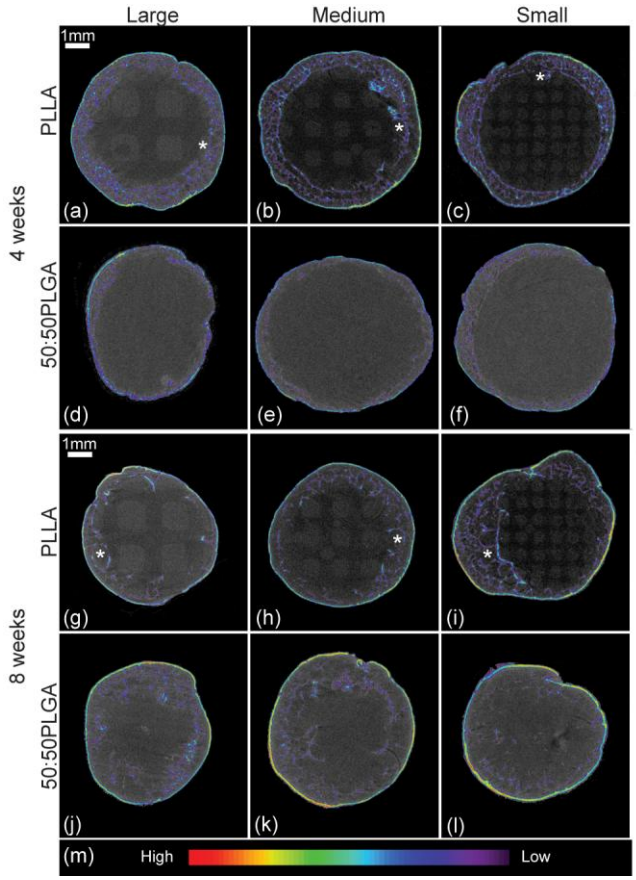

Fig 4.4 μ-CT images of PLLA (a, b, and c) and 50:50PLGA scaffolds (d, e, and f) at 4 weeks, and PLLA (g, h, and i) and 50:50PLGA scaffolds (j, k, and l) at 8 weeks. Some struts were surrounded by tissues are indicated by *. Relative density of the tissues are indicated with color scale (m)

4.4.4. Tissue mineral density and bone volume of implanted scaffolds

TMD and BV were also calculated using μ-CT data (Fig 4.5, Table 4.2). The data demonstrated that TMD significantly increased in all groups from 4 week implantation to 8 weeks. From the 4 week implantation data, although there was no significant difference, the Small PLLA scaffold group had higher TMD than the Large and Medium PLLA scaffold groups (Fig 4.5, a). In addition, Large and Medium 50:50PLGA scaffold groups had more mineralized tissues than the Large and Medium of PLLA scaffold groups at 4 weeks (no significant difference). Medium and Small PLLA scaffold groups showed slightly higher mineral density than Medium and Small 50:50PLGA scaffold

groups (Fig 4.5, b). The results of TMD were similar in all groups at both time points, while BV results showed different trends depending on the scaffold materials. Although only the Large 50:50PLGA showed a significant difference (Fig 4.5, c, d), the trends suggested that PLLA scaffolds lost their BV from 4 weeks to 8 weeks time points, while, 50:50PLGA increased BV during that time. In addition, other trends showed that PLLA scaffolds had more BV than 50:50PLGA scaffolds at the 4 weeks time point (Fig 4.5, c), however, after 8 weeks implantation, 50:50PLGA scaffolds showed higher BV (Fig 4.5, d) (no significant difference).

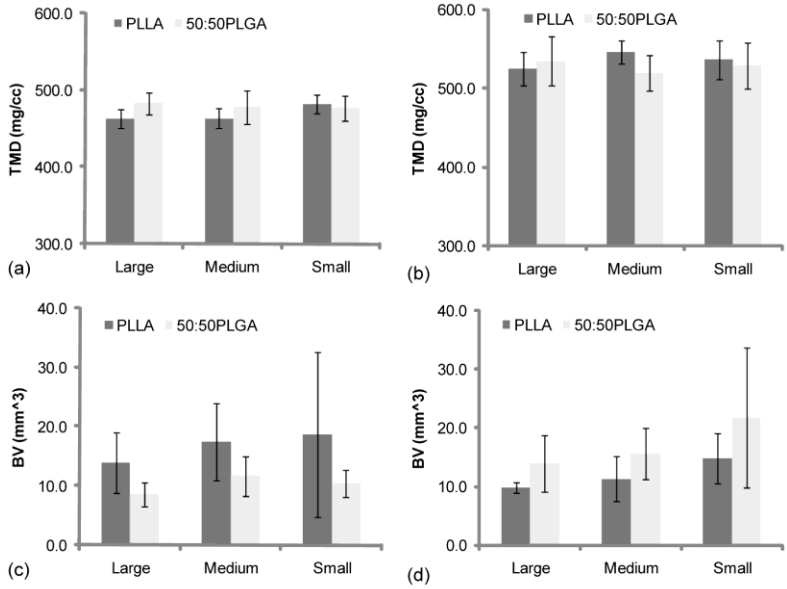

Fig 4.5 Tissue mineral density (TMD) at 4 (a) and 8 (b) weeks, and Bone volume (BV) at 4 (c) and 8 (d) weeks. There was no significant difference of TMD and BV values between PLLA and 50:50PLGA scaffolds.

Table 4.2 Tissue Mineral Density, Bone Volume and Modulus of scaffold and tissue constructs at 4 and 8 weeks

		PLLA			50:50PLGA		
		Large	Medium	Small	Large	Medium	Small
TMD (mg/cc)	4 wk	462.6 ± 12.4 (N=4)	463.4 ± 12.5 (N=5)	482.4 ± 12.1 (N=5)	482.8 ± 14.0 (N=8)	477.5 ± 21.7 (N=7)	476.2 ± 16.4 (N=5)
	8 wk	524.8 ± 21.4 (N=3)	546.0 ± 14.7 (N=5)	536.5 ± 24.4 (N=5)	534.5 ± 31.4 (N=5)	519.9 ± 22.5 (N=5)	528.7 ± 29.2 (N=5)
Bone Volume (mm^3)	4 wk	13.96 ± 5.14 (N=4)	17.37 ± 6.53 (N=5)	18.66 ± 13.87 (N=5)	8.58 ± 2.08 (N=8)	11.61 ± 3.28 (N=7)	10.39 ± 2.27 (N=5)
	8 wk	9.83 ± 0.89 (N=3)	11.25 ± 3.85 (N=5)	14.71 ± 4.28 (N=5)	13.88 ± 4.76 (N=5)	15.55 ± 4.38 (N=5)	21.77 ± 11.96 (N=5)
Modulus (MPa)	0 wk	100.4 ± 56.4 (N=7)	98.9 ± 30.6 (N=7)	196.4 ± 76.7 (N=7)	197.8 ± 53.7 (N=6)	239.0 ± 102.6 (N=6)	125.1 ± 63.2 (N=5)
	4 wk	13.0 ± 4.2 (N=4)	29.4 ± 14.2 (N=4)	90.5 ± 41.7 (N=7)	0.78 ± 0.35 (N=5)	1.30 ± 0.73 (N=6)	0.80 ± 0.40 (N=4)
	8 wk	32.2 ± 31.9 (N=3)	53.7 ± 28.1 (N=5)	83.4 ± 27.3 (N=5)	5.43 ± 5.97 (N=5)	4.15 ± 1.79 (N=4)	6.62 ± 3.52 (N=4)

4.4.5. Mechanical properties

A compressive test was performed to investigate the changes in scaffold mechanical properties during implantation (Fig 4.6, a,d). The average mechanical properties of PLLA and 50:50PLGA scaffolds were equal to or greater than 100 MPa prior to implantation. All PLLA scaffolds had significantly decreased mechanical properties after 4 weeks of implantation due to polymer degradation (Fig 4.6, a). Then, their mechanical properties were increased or maintained after 8 weeks implantation due to growth of mineralized tissues. All 50:50PLGA scaffolds had nearly a complete loss of mechanical properties at 4 weeks, but then slightly increased after 8 weeks of implantation (Fig 4.6, b). The mechanical properties of all of the 50:50PLGA scaffolds were significantly lower than Small PLLA scaffolds at 4 weeks and Medium and Small PLLA scaffolds at 8 weeks.

The correlation between the modulus and bone volume are shown in Fig 4.6 (b, c, e, f). PLLA scaffolds did not have any correlation at 4 ($R^2 = 0.0371$) and 8 ($R^2 = 0.0102$) weeks. However, 50:50PLGA scaffolds had some correlation at 4 ($R^2 = 0.4809$) and 8

(R^2 = 0.4043) weeks. The 8 week data had an outlier which lowered the correlation, which increased to R^2 = 0.8884 without the outlier. These results indicate that increased bone deposition increased the moduli of the regenerated tissues when the scaffold modulus was significantly reduced.

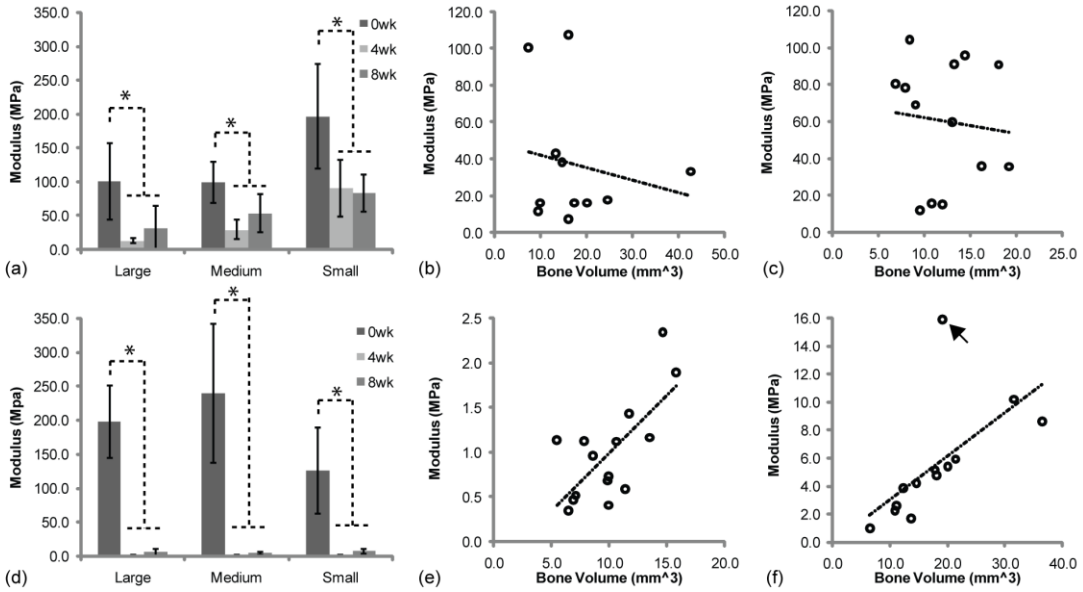

Fig 4.6 Mechanical test results of implanted PLLA (a) and 50:50PLGA (d). * indicates significant difference. Correlations between modulus and bone volume of PLLA scaffolds at 4 (b) and 8 (c) weeks and 50:50PLGA scaffolds at 4 (e) and 8 (f) weeks. R-square values are 0.0371 (b), 0.0102 (c), 0.4809 (e) and 0.4043 (f). The value of (f) increases to 0.8884 without the outlier (indicated with an arrow).

4.5 Discussion

Computer based scaffold design and SFF were used to determine the effect of porous scaffold material and architecture on bone regeneration. PLLA and 50:50PLGA scaffolds were fabricated using the identical procedure with the exception of their melting temperatures. The semi-crystalline structure of PLLA required a higher casting temperature, while the 50:50PLGA can be melted at a lower temperature than PLLA due to its amorphous structure. The μ-CT data demonstrated that the fabricated PLLA and 50:50PLGA scaffolds had similar defined pore sizes, strut sizes, porosities and surface to

volume ratios. In addition, the μ-CT results verified that the fabricated scaffolds in the same design groups had identical internal and external architectures between materials. Although the viscosities of the polymers were similar, the surface morphologies of the scaffolds were slightly different as shown in the ESEM images. This may be due to the difference of the chemical structures including crystallinity of the polymers.

Ex vivo gene therapy was used to induce bone formation from the surrounding tissues at the implant site. This regenerative gene therapy strategy using adenoviral vectors can be applied to transduce various cells, such as bone marrow stromal cells [45], and fibroblasts [40,46]. The consistent secretion of BMP-2 from adenovirus transduced HGFs up to 2 weeks *in vitro* has been reported [47]. Additionally, this approach has been studied to induce endochondral-like bone tissue formation by transduced HGFs [40,48]. Other methods of bone formation have previously been reported, including seeding bone marrow stromal cells [49], incorporation of BMP-7 into nanospheres [50], and BMP-2 conjugated with heparin [49]. However, these methods require pre-treatment of the scaffolds prior to implantation. The scaffolds may start degrading during the preparation, especially 50:50PLGA scaffolds due to their short degradation profile. Therefore, to minimize any alteration of the scaffolds before implantation and successfully regenerate bone tissue *in vivo*, *ex vivo* gene therapy was a suitable method for testing this study.

Scaffold tissue constructs differed between the PLLA and 50:50PLGA scaffolds due to polymer degradation. PLLA scaffolds maintained their architecture throughout the study period, while 50:50PLGA scaffolds completely lost the original designed pore structure, and there were only chunks remaining at the 4 week time point. The hydrophilicity of the PGA component in PLGA may induce faster water uptake and

hydrolysis leading to faster degradation [11]. In contrast, the methyl group of the PLLA side chain contributes to the hydrophobicity of the polymer, resulting in slower degradation [10]. As reported previously, the *in vivo* half-life of 50:50PLGA foams was about 2 weeks [11], our 50:50PLGA scaffolds may maintain their architectures for only a few weeks or less *in vivo*.

Due to the rapid degradation, little bone tissue was found inside the degraded 50:50PLGA scaffolds at 4 and 8 weeks. In contrast, the PLLA scaffolds had small amounts of bone ingrowth and some blood vessel-like tissues from the histological analysis. These differences may be attributed to the effects of degradation by-products on cell activities. PLLA nanofibers or porous membranes supported activities of chondrocytes and human mesenchymal stem cells and vascularization more than those of 50:50PLGA since rapid degradation of 50:50PLGA created acidic environments and prevented cell activities on or in the constructs [8,9]. In addition, reduction of pH negatively affected activities of bone marrow stromal cells during osteogenesis [51]. Although there are no data regarding pH change or acidic by-products in this study, there may be similar effects on cell activities and tissue formation for both the PLLA and 50:50PLGA scaffolds at the earlier time point. Additionally, the collapse of the PLGA porous architecture would prohibit cell migration and bone formation within the scaffold interior.

The trends of BV results show that BV was higher on the PLLA scaffolds than the 50:50PLGA scaffolds at 4 weeks, while the 50:50PLGA scaffolds had higher BV at 8 weeks. The acidic environment may also explain the change in bone volume over time. Initially, at 4 weeks, bone formation was inhibited by more acidic by-products in the

environment on the PLGA scaffolds, but, the removal of these degradation by-products allowed restoration of cellular activities which may have led to the bone volume increase observed at the 8 week time point. The PLLA scaffolds may have more degradation by-products which may lower BV at 8 weeks. From the data shown in this and previous studies [8,9,51], PLLA scaffolds may be more useful in this situation because it has a slower degradation rate that allows new tissue to generate while it still maintaining sufficient mechanical properties to support new tissue growth. In comparison, the 50:50PLGA is not able to support the tissue due to its fast degradation profile. It would be useful to study another polymer, such as 85:15PLGA that lasts longer *in vivo*, as SFF scaffolds for bone application. Furthermore, the effects of SFF scaffolds on degradation need to be investigated to better understand the interaction between scaffolds and tissue formation.

The PLLA scaffolds in this study showed much less bone ingrowth than porous HA scaffolds and porous poly (propylene fumerate)/tricalcium phosphate (PPF/TCP) scaffolds reported in our previous studies [15,42] since HA and TCP are known osteoconductive materials that have been shown to allow chemotactic adherence for enhanced bone growth. Furthermore, hydrophobic materials, like PLLA, may delay cell attachment and bone formation [52,53]. In addition, the layers of tissues or bony shell surrounding the PLLA scaffolds prevent diffusion of nutrients into the construct [54] and may cause accumulation of acidic by-product inside of the implants, which could prohibit cell migration and tissue ingrowth.

The importance of scaffolds pore sizes for bone formation has been discussed in many studies. The minimum pore size, 280 μm, in this study was chosen based on the required

diameters for blood vessel formation, which was approximated according to *in vivo* bone tissue formation in previous studies [19,52,55]. Although the effect of pore size of PLLA or PLGA porous scaffolds on bone regeneration has been explored in various studies, these results varied depending on the materials and methods of the study. For example, pore sizes of PLGA scaffolds did not affect osteoblast activities *in vitro* nor was *in vivo* bone formation influenced by pore sizes within the range of 150-710 μm and 125-500 μm [20-22]. In contrast, another group compared porous PLGA scaffolds with constant porosity and indicated that pore size between 400 and 600 μm were favorable for osteoblasts rather than 300 μm or smaller pore sizes [56,57]. Another study demonstrated that PLLA scaffolds with pores of 350 μm diameters induced more bone ingrowth than the smaller ones (100 and 200 μm) when implanted in rabbits' calvarias [58]. However, it is again critical to note that these previous studies, which suggested an influence of pore diameter [56-58], utilized conventional fabrication techniques which did not rigorously control pore diameter and interconnectivity. Our chosen pore size, 280, 550 and 820 μm, thus bracketed the range of pore sizes investigated in previous studies: with the difference being the controlled interconnected, repeatable architecture in this study. The pore range is also within the range of the reported trabecular pore sizes, 300 ~ 1000 μm [59,60].

Regarding bone ingrowth from μ-CT images, we did not observe any significant difference between the scaffolds designs, such as pore size, which is in agreement with our previous studies [15,43]. The distances of bone penetration into the PLLA scaffolds in this study was more than previously reported in PLGA foams implanted in the rat mesentery for 49 days [20]. The distances generally increased from 4 to 8 weeks in our

study, while the previous study showed that there was little increase over the implantation time. This may be due to their use of foam scaffolds, which have random oriented pores and non-controlled internal architectures, and a more tortuous pathway that may prevent nutrient diffusion and cell migration into the scaffolds [24]. Silva et al. demonstrated that porous HA and PLLA scaffolds with aligned channels could improve cell infiltration into the center of the scaffolds [61]. Their study and our results indicate that orthogonally interconnected porous architectures may not only help increase nutrient diffusion when compared to foam scaffolds, but may also guide tissue ingrowth.

Other scaffold design parameters, such as porosity and surface area, did not seem to have a significant effect on bone formation in this study. Although high porosity has been discussed as an important requirement of scaffolds [62], the effect of scaffold porosity on bone formation was not significant in this study. Since our scaffolds have fully and orthogonally interconnected pore architectures or channels, infiltration of nutrients into the scaffolds may not be different between the scaffold design groups. The pore sizes of the scaffolds varied the surface areas of the scaffolds onto which cells from host tissue can attach. The μ-CT data also showed that the patterns of bone ingrowth followed the internal architectures of the scaffolds. Small PLLA scaffolds had the smallest strut sizes and pore sizes which allowed the tissues to surround the struts and interlock, increasing tissue integration. This may help to form stronger bonds between the regenerated tissues and porous scaffolds. The scaffolds with smaller pores had more total surface area than the scaffolds with larger pores, which may create a larger surface area for cell adhesion and help bone formation. Furthermore, another scaffold design parameter may have a more impactful factor on increasing bone formation. For example, it has been postulated

that pore interconnectivity and permeability may be an important scaffold design parameters [24,63,64].

For functional use of these scaffolds at load bearing sites, it is important to understand the time dependent changes in scaffold/tissue construct mechanical properties. Initially, the fabricated PLLA and 50:50PLGA scaffolds had mechanical properties in the low to medium range of human trabecular bone [35]. After implantation, the mechanical properties decreased due to the degradation of materials. As shown in the histology and μ-CT images, 50:50PLGA scaffolds completely lost their designed architectures, and their mechanical properties decreased dramatically both at 4 and 8 weeks compared with the pre-implanted scaffolds and the PLLA scaffolds. Despite the retention of designed architecture, PLLA scaffolds also showed a decrease in their mechanical properties, which indicates some polymer degradation.

The mechanical properties of PLLA scaffolds with bone tissue were significantly higher than those of 50:50PLGA scaffolds at 4 and 8 weeks. There was no correlation between bone volume and PLLA/bone construct mechanical properties at 4 and 8 weeks. However, the 50:50PLGA/bone construct mechanical properties showed some correlation with bone volume at 4 weeks, which increased at 8 weeks. The mechanical properties of the PLLA scaffold constructs, due to the greater retention of polymer architecture and mechanical properties were likely more dependent on the polymer at 4 and 8 weeks. In contrast, the 50:50PLGA mechanical properties were solely dependent on the generated bone as the polymer was degraded by 4 weeks.

Although, the majority of PLLA mechanical properties relied on the scaffold material, Large and Medium PLLA scaffolds still exhibited an increasing trend in mechanical

properties due to higher mineralized tissues and bone growth on/into the scaffolds from 4 to 8 weeks. Small PLLA scaffolds had similar mechanical properties at both time points. Small PLLA scaffolds may have a slower degradation speed, maintaining their mechanical properties longer than the other groups.

One of the limitations in this study is that ectopic sites do not provide the same environment as orthotopic sites, including mechanical stimulation, nutrients, cell types and cell-cell interactions. For example, the bone volume of PLLA scaffolds decreased from 4 to 8 weeks, similar to findings by Lin et al. [42]. This may because there is little loading on the ectopic models to simulate bone remodeling and increases in mineralization of newly formed tissues [65] as well as less nutrient supply. In addition, mechanical loading on the scaffolds would increase the degradation of PLLA scaffolds in terms of molecular weight and mechanical properties [66].

4.6 Conclusions

In the present study, we compared the effect of materials and architectures of porous scaffolds on bone formation. Our data demonstrated that material choice significantly influences *in vivo* bone tissue regeneration and mechanical properties. We also found that scaffold architecture controls the patterns of bone ingrowth and mechanical properties of scaffold-bone constructs. The 50:50PLGA scaffolds degraded rapidly, providing little initial support for bone ingrowth, and had very low mechanical properties. In comparison, the PLLA scaffolds maintained their architectures throughout the study period and supported some blood vessel and bone ingrowth. Given the long tissue regeneration time seen in many clinical applications (e.g. spine fusion, long bone defects,

mandibular defects) the ability of a polymer scaffold to maintain structural and mechanical properties up to 6 month is critical. Pore size, if architecture is maintained and does not collapse, does not significantly influence bone regeneration. The patterns of bone tissue ingrowth were defined by the computer designed pores and struts of the scaffolds. Furthermore, mechanical properties of implanted scaffolds can be controlled by the initial architectures. All of these results support the importance of choosing suitable scaffold materials and designing conductive scaffold architectures that are ideal for bone tissue regeneration. Each of these factors will need to be fine tuned in order to find the desired properties for specific anatomical sites or defects.

Acknowledgment

This study was supported by National Institute of Health (NIH) R01 grant AR 053379.

References

[1] Karageorgiou V, Kaplan D. Porosity of 3D biomaterial scaffolds and osteogenesis. Biomaterials 2005;26:5474-5491.

[2] Athanasiou KA, Agrawal CM, Barber FA, Burkhart SS. Orthopaedic applications for PLA-PGA biodegradable polymers. Arthroscopy 1998;14:726-737.

[3] Hutmacher DW. Scaffold design and fabrication technologies for engineering tissues--state of the art and future perspectives. J Biomater Sci Polym Ed 2001;12:107-124.

[4] Hollister SJ. Porous scaffold design for tissue engineering. Nat Mater 2005;4:518-524.

[5] Middleton JC, Tipton AJ. Synthetic biodegradable polymers as orthopedic devices. Biomaterials 2000;21:2335-2346.

[6] Kontakis GM, Pagkalos JE, Tosounidis TI, Melissas J, Katonis P. Bioabsorbable materials in orthopaedics. Acta Orthop Belg 2007;73:159-169.

[7] Narayan D, Venkatraman SS. Effect of pore size and interpore distance on endothelial cell growth on polymers. J Biomed Mater Res A 2008;87:710-718.

[8] Li WJ, Cooper JA,Jr, Mauck RL, Tuan RS. Fabrication and characterization of six electrospun poly(alpha-hydroxy ester)-based fibrous scaffolds for tissue engineering applications. Acta Biomater 2006;2:377-385.

[9] Kaushiva A, Turzhitsky VM, Darmoc M, Backman V, Ameer GA. A biodegradable vascularizing membrane: a feasibility study. Acta Biomater 2007;3:631-642.

[10] Ishaug-Riley SL, Okun LE, Prado G, Applegate MA, Ratcliffe A. Human articular chondrocyte adhesion and proliferation on synthetic biodegradable polymer films. Biomaterials 1999;20:2245-2256.

[11] Lu L, Peter SJ, Lyman MD, Lai HL, Leite SM, Tamada JA, et al. In vitro and in vivo degradation of porous poly(DL-lactic-co-glycolic acid) foams. Biomaterials 2000;21:1837-1845.

[12] Gomes ME, Holtorf HL, Reis RL, Mikos AG. Influence of the porosity of starch-based fiber mesh scaffolds on the proliferation and osteogenic differentiation of bone marrow stromal cells cultured in a flow perfusion bioreactor. Tissue Eng 2006;12:801-809.

[13] Khan Y, Yaszemski MJ, Mikos AG, Laurencin CT. Tissue engineering of bone: material and matrix considerations. J Bone Joint Surg Am 2008;90 Suppl 1:36-42.

[14] Cao Y, Mitchell G, Messina A, Price L, Thompson E, Penington A, et al. The influence of architecture on degradation and tissue ingrowth into three-dimensional poly(lactic-co-glycolic acid) scaffolds in vitro and in vivo. Biomaterials 2006;27:2854-2864.

[15] Schek RM, Wilke EN, Hollister SJ, Krebsbach PH. Combined use of designed scaffolds and adenoviral gene therapy for skeletal tissue engineering. Biomaterials 2006;27:1160-1166.

[16] Li JP, Habibovic P, van den Doel M, Wilson CE, de Wijn JR, van Blitterswijk CA, et al. Bone ingrowth in porous titanium implants produced by 3D fiber deposition. Biomaterials 2007;28:2810-2820.

[17] Rose FR, Cyster LA, Grant DM, Scotchford CA, Howdle SM, Shakesheff KM. In vitro assessment of cell penetration into porous hydroxyapatite scaffolds with a central aligned channel. Biomaterials 2004;25:5507-5514.

[18] Tsuruga E, Takita H, Itoh H, Wakisaka Y, Kuboki Y. Pore size of porous hydroxyapatite as the cell-substratum controls BMP-induced osteogenesis. J Biochem 1997;121:317-324.
[19] Kuboki Y, Jin Q, Takita H. Geometry of carriers controlling phenotypic expression in BMP-induced osteogenesis and chondrogenesis. J Bone Joint Surg Am 2001;83-A Suppl 1:S105-15.
[20] Ishaug-Riley SL, Crane GM, Gurlek A, Miller MJ, Yasko AW, Yaszemski MJ, et al. Ectopic bone formation by marrow stromal osteoblast transplantation using poly(DL-lactic-co-glycolic acid) foams implanted into the rat mesentery. J Biomed Mater Res 1997;36:1-8.
[21] Ishaug-Riley SL, Crane-Kruger GM, Yaszemski MJ, Mikos AG. Three-dimensional culture of rat calvarial osteoblasts in porous biodegradable polymers. Biomaterials 1998;19:1405-1412.
[22] Wu YC, Shaw SY, Lin HR, Lee TM, Yang CY. Bone tissue engineering evaluation based on rat calvaria stromal cells cultured on modified PLGA scaffolds. Biomaterials 2006;27:896-904.
[23] Sinha RK, Morris F, Shah SA, Tuan RS. Surface composition of orthopaedic implant metals regulates cell attachment, spreading, and cytoskeletal organization of primary human osteoblasts in vitro. Clin Orthop Relat Res 1994;(305):258-272.
[24] Melchels FP, Barradas AM, van Blitterswijk CA, de Boer J, Feijen J, Grijpma DW. Effects of the architecture of tissue engineering scaffolds on cell seeding and culturing. Acta Biomater 2010;6:4208-4217.
[25] Hsu SH, Yen HJ, Tseng CS, Cheng CS, Tsai CL. Evaluation of the growth of chondrocytes and osteoblasts seeded into precision scaffolds fabricated by fused deposition manufacturing. J Biomed Mater Res B Appl Biomater 2007;80:519-527.
[26] Hutmacher DW, Schantz T, Zein I, Ng KW, Teoh SH, Tan KC. Mechanical properties and cell cultural response of polycaprolactone scaffolds designed and fabricated via fused deposition modeling. J Biomed Mater Res 2001;55:203-216.
[27] Goldstein AS, Zhu G, Morris GE, Meszlenyi RK, Mikos AG. Effect of osteoblastic culture conditions on the structure of poly(DL-lactic-co-glycolic acid) foam scaffolds. Tissue Eng 1999;5:421-434.
[28] Sun W, Starly B, Darling A, Gomez C. Computer-aided tissue engineering: application to biomimetic modelling and design of tissue scaffolds. Biotechnol Appl Biochem 2004;39:49-58.
[29] Hutmacher DW, Sittinger M, Risbud MV. Scaffold-based tissue engineering: rationale for computer-aided design and solid free-form fabrication systems. Trends Biotechnol 2004;22:354-362.
[30] Martins A, Chung S, Pedro AJ, Sousa RA, Marques AP, Reis RL, et al. Hierarchical starch-based fibrous scaffold for bone tissue engineering applications. J Tissue Eng Regen Med 2009;3:37-42.
[31] Hollister SJ, Levy RA, Chu TM, Halloran JW, Feinberg SE. An image-based approach for designing and manufacturing craniofacial scaffolds. Int J Oral Maxillofac Surg 2000;29:67-71.
[32] Hollister SJ, Maddox RD, Taboas JM. Optimal design and fabrication of scaffolds to mimic tissue properties and satisfy biological constraints. Biomaterials 2002;23:4095-4103.

[33] Lin CY, Kikuchi N, Hollister SJ. A novel method for biomaterial scaffold internal architecture design to match bone elastic properties with desired porosity. J Biomech 2004;37:623-636.
[34] Taboas JM, Maddox RD, Krebsbach PH, Hollister SJ. Indirect solid free form fabrication of local and global porous, biomimetic and composite 3D polymer-ceramic scaffolds. Biomaterials 2003;24:181-194.
[35] Saito E, Kang H, Taboas JM, Diggs A, Flanagan CL, Hollister SJ. Experimental and computational characterization of designed and fabricated 50:50 PLGA porous scaffolds for human trabecular bone applications. J Mater Sci Mater Med 2010;21:2371-2383.
[36] Bessa PC, Casal M, Reis RL. Bone morphogenetic proteins in tissue engineering: the road from laboratory to clinic, part II (BMP delivery). J Tissue Eng Regen Med 2008;2:81-96.
[37] Bessa PC, Casal M, Reis RL. Bone morphogenetic proteins in tissue engineering: the road from the laboratory to the clinic, part I (basic concepts). J Tissue Eng Regen Med 2008;2:1-13.
[38] Nussenbaum B, Krebsbach PH. The role of gene therapy for craniofacial and dental tissue engineering. Adv Drug Deliv Rev 2006;58:577-591.
[39] Rutherford RB, TrailSmith MD, Ryan ME, Charette MF. Synergistic effects of dexamethasone on platelet-derived growth factor mitogenesis in vitro. Arch Oral Biol 1992;37:139-145.
[40] Krebsbach PH, Gu K, Franceschi RT, Rutherford RB. Gene therapy-directed osteogenesis: BMP-7-transduced human fibroblasts form bone in vivo. Hum Gene Ther 2000;11:1201-1210.
[41] Williams JM, Adewunmi A, Schek RM, Flanagan CL, Krebsbach PH, Feinberg SE, et al. Bone tissue engineering using polycaprolactone scaffolds fabricated via selective laser sintering. Biomaterials 2005;26:4817-4827.
[42] Lin CY, Schek RM, Mistry AS, Shi X, Mikos AG, Krebsbach PH, et al. Functional bone engineering using ex vivo gene therapy and topology-optimized, biodegradable polymer composite scaffolds. Tissue Eng 2005;11:1589-1598.
[43] Roosa SM, Kemppainen JM, Moffitt EN, Krebsbach PH, Hollister SJ. The pore size of polycaprolactone scaffolds has limited influence on bone regeneration in an in vivo model. J Biomed Mater Res A 2010;92:359-368.
[44] Franceschi RT, Wang D, Krebsbach PH, Rutherford RB. Gene therapy for bone formation: in vitro and in vivo osteogenic activity of an adenovirus expressing BMP7. J Cell Biochem 2000;78:476-486.
[45] Chang SC, Chuang HL, Chen YR, Chen JK, Chung HY, Lu YL, et al. Ex vivo gene therapy in autologous bone marrow stromal stem cells for tissue-engineered maxillofacial bone regeneration. Gene Ther 2003;10:2013-2019.
[46] Hirata K, Tsukazaki T, Kadowaki A, Furukawa K, Shibata Y, Moriishi T, et al. Transplantation of skin fibroblasts expressing BMP-2 promotes bone repair more effectively than those expressing Runx2. Bone 2003;32:502-512.
[47] Shin JH, Kim KH, Kim SH, Koo KT, Kim TI, Seol YJ, et al. Ex vivo bone morphogenetic protein-2 gene delivery using gingival fibroblasts promotes bone regeneration in rats. J Clin Periodontol 2010;37:305-311.

[48] Rutherford RB, Moalli M, Franceschi RT, Wang D, Gu K, Krebsbach PH. Bone morphogenetic protein-transduced human fibroblasts convert to osteoblasts and form bone in vivo. Tissue Eng 2002;8:441-452.
[49] Claase MB, de Bruijn JD, Grijpma DW, Feijen J. Ectopic bone formation in cell-seeded poly(ethylene oxide)/poly(butylene terephthalate) copolymer scaffolds of varying porosity. J Mater Sci Mater Med 2007;18:1299-1307.
[50] Wei G, Jin Q, Giannobile WV, Ma PX. The enhancement of osteogenesis by nano-fibrous scaffolds incorporating rhBMP-7 nanospheres. Biomaterials 2007;28:2087-2096.
[51] Kohn DH, Sarmadi M, Helman JI, Krebsbach PH. Effects of pH on human bone marrow stromal cells in vitro: implications for tissue engineering of bone. J Biomed Mater Res 2002;60:292-299.
[52] Oh SH, Park IK, Kim JM, Lee JH. In vitro and in vivo characteristics of PCL scaffolds with pore size gradient fabricated by a centrifugation method. Biomaterials 2007;28:1664-1671.
[53] Oh SH, Kang SG, Kim ES, Cho SH, Lee JH. Fabrication and characterization of hydrophilic poly(lactic-co-glycolic acid)/poly(vinyl alcohol) blend cell scaffolds by melt-molding particulate-leaching method. Biomaterials 2003;24:4011-4021.
[54] Kruyt MC, Dhert WJ, Oner FC, van Blitterswijk CA, Verbout AJ, de Bruijn JD. Analysis of ectopic and orthotopic bone formation in cell-based tissue-engineered constructs in goats. Biomaterials 2007;28:1798-1805.
[55] Druecke D, Langer S, Lamme E, Pieper J, Ugarkovic M, Steinau HU, et al. Neovascularization of poly(ether ester) block-copolymer scaffolds in vivo: long-term investigations using intravital fluorescent microscopy. J Biomed Mater Res A 2004;68:10-18.
[56] Pamula E, Bacakova L, Filova E, Buczynska J, Dobrzynski P, Noskova L, et al. The influence of pore size on colonization of poly(L-lactide-glycolide) scaffolds with human osteoblast-like MG 63 cells in vitro. J Mater Sci Mater Med 2008;19:425-435.
[57] Pamula E, Filova E, Bacakova L, Lisa V, Adamczyk D. Resorbable polymeric scaffolds for bone tissue engineering: The influence of their microstructure on the growth of human osteoblast-like MG 63 cells. J Biomed Mater Res A 2008.
[58] Robinson BP, Hollinger JO, Szachowicz EH, Brekke J. Calvarial bone repair with porous D,L-polylactide. Otolaryngol Head Neck Surg 1995;112:707-713.
[59] Keaveny TM, Morgan EF, Niebur GL, Yeh OC. Biomechanics of trabecular bone. Annu Rev Biomed Eng 2001;3:307-333.
[60] Rezwan K, Chen QZ, Blaker JJ, Boccaccini AR. Biodegradable and bioactive porous polymer/inorganic composite scaffolds for bone tissue engineering. Biomaterials 2006;27:3413-3431.
[61] Silva MM, Cyster LA, Barry JJ, Yang XB, Oreffo RO, Grant DM, et al. The effect of anisotropic architecture on cell and tissue infiltration into tissue engineering scaffolds. Biomaterials 2006;27:5909-5917.
[62] Sosnowski S, Wozniak P, Lewandowska-Szumiel M. Polyester scaffolds with bimodal pore size distribution for tissue engineering. Macromol Biosci 2006;6:425-434.
[63] Hui PW, Leung PC, Sher A. Fluid conductance of cancellous bone graft as a predictor for graft-host interface healing. J Biomech 1996;29:123-132.

[64] Jones AC, Arns CH, Hutmacher DW, Milthorpe BK, Sheppard AP, Knackstedt MA. The correlation of pore morphology, interconnectivity and physical properties of 3D ceramic scaffolds with bone ingrowth. Biomaterials 2009;30:1440-1451.
[65] Duty AO, Oest ME, Guldberg RE. Cyclic mechanical compression increases mineralization of cell-seeded polymer scaffolds in vivo. J Biomech Eng 2007;129:531-539.
[66] Kang Y, Yao Y, Yin G, Huang Z, Liao X, Xu X, et al. A study on the in vitro degradation properties of poly(L-lactic acid)/beta-tricalcuim phosphate (PLLA/beta-TCP) scaffold under dynamic loading. Med Eng Phys 2009;31:589-594.

CHAPTER 5

Architecture Effects on Long Term *In Vivo* Degradation in Computer Designed Poly (L-lactic acid) 3D Porous Scaffolds

5.1 Abstract

Current developments of computer aided design and solid freeform fabrication (SFF) techniques enable fabrication of scaffolds with precisely designed architectures and mechanical properties. The present study demonstrates the effect of precisely designed 3D scaffold architectures on *in vivo* degradation. Specifically, three types of porous Poly (L-lactic acid) (PLLA) scaffolds with variable pore size strut size, porosity, and surface area fabricated by SFF, and one PLLA solid cylinder design were implanted into mice subcutaneously for 6, 12 and 21 weeks. The solid cylinders exhibited faster mass loss than all porous scaffolds. Among the porous scaffolds, the group with the largest strut size lost mass faster than the other two groups. Strong correlations between surface area and weight loss were found at 12 (R^2=0.681) and 21 (R^2=0.671) weeks. Scaffold porosity, however, was not significantly correlated with degradation rate. Changes of molecular weight and crystallinity also showed changing of the chemical structures due to degradation, and the solid cylinders had faster crystallization due to advanced degradation than the porous scaffolds. Scaffold mechanical properties decreased with degradation, but maintained modulus in the lower range of the human trabecular bone

even after 21 weeks. The loss in mechanical properties, however, was a complex function of both degradation and the initial scaffold architecture. This study suggests that computer aided design and fabrication, within a given material, can significantly influence scaffold degradation profiles.

5.2 Introduction

Bone graft substitutes, such as metal, have been historically used to repair bone defects. However, these implants are not ideal since they do not degrade in the body, which may lead to chronic problems, such as implant loosening and infection. Furthermore, most metal implants are much stiffer than bone, often causing stress shielding and bone resorption. As an alternative approach, tissue engineered scaffolds have been developed using biodegradable materials. The role of tissue engineered scaffolds is to fill defects and support new tissue generation during healing process. During the process, scaffolds should degrade in concert with newly generating bone, providing a smooth transition in load bearing from scaffold to tissue [1].

The rate of scaffold degradation is affected by various factors including molecular weight, ratio of co-polymers, crystallinity, morphology, stress, *in vitro* or *in vivo* environment, and implantation sites [2-4]. The influence of polymer scaffold architecture on degradation has been widely postulated. For example, poly (lactic-co-glycolic acid) (PLGA) films or solid materials degrade faster than the porous PLGA scaffolds, and more homogeneous degradation occurs in the scaffolds than the films [5,6]. Lower porosity and permeability accelerated PLGA scaffold degradation *in vitro* [5,7]. Several studies have examined the degradation of porous poly (L-lactic acid) (PLLA) scaffolds *in*

vitro [8-13], and showed that thicker walls degrade faster than thinner ones due to the autocatalysis of lactic acid, and a higher surface per volume ratio decreases degradation rate [11,13].

Although the previous studies examined the relationship between scaffold architectures and degradation behavior, most of the porous scaffolds were sponge shaped or nanofibrous scaffolds whose internal architectures, such as pore interconnectivity, location, and strut size, could not rigorously be controlled and did not have sufficient mechanical properties for bone tissue engineering applications [14-19]. The significant architectural variations often lead to conflicting and confusing conclusions. For example, porous scaffolds were found to degrade faster than solid block polymers [20,21], which contradicts aforementioned results of faster degradation in solid materials versus porous materials [5,6]. In addition there have only been a few studies examining the degradation of PLLA scaffolds *in vivo* [9,22,23]. *In vivo* studies are obviously critical to simulate the clinical application, and furthermore are necessary to understand degradation profiles of PLLA scaffolds, since poly ester scaffolds tend to degrade faster *in vivo* than *in vitro* [22-24].

To have better controlled scaffold architectures for desired properties, our group and others have utilized computer aided design and solid freeform fabrication (SFF) techniques [25-28]. SFF techniques allow for the fabrication of porous scaffolds with specific architectures and have sufficient mechanical properties for load bearing application [16]. In addition, various SFF fabricated scaffolds have been tested in animals for bone applications [29-33]. A few studies have also shown the degradation of SFF scaffolds *in vitro* [12,34,35]. However, the effects of specific designed SFF scaffold

architectures on *in vivo* degradation (including mechanical properties) have not been rigorously studied. Since scaffold degradation in concert with bone regeneration is critical to attaining eventual clinical success, understanding how scaffold architecture affects scaffold degradation is important for improved bone reconstruction outcomes.

PLLA, is a widely used biomaterial for orthopaedic [36] and spine implants [37], and is being researched for tissue engineered scaffolds [9-12,38]. Under physiological conditions, PLLA degrades by hydrolysis of ester bonds and forms lactic acid. Lactic acid is further broken down to pyruvate by lactate dehydrogenase, and enters the citric acid cycle, where it is converted and removed from the body as carbon dioxide and water [4,9,39,40]. It is also well known that PLLA degradation entails molecular weight (M_w) loss, mechanical property reduction, and then morphology changes [41]. During degradation, other important physical properties also change, including melting point (T_m), glass transition temperature (T_g), crystallinity and mass of implants [7,11,12,38].

The goal of this study was to determine the effect of architecture on *in vivo* degradation of the designed porous PLLA scaffolds. We specifically hypothesized that architectural parameters affecting autocatalysis, namely strut thickness that controls acid diffusion and surface area, which controls acid removal from the scaffold, would affect degradation rate more significantly than other widely studied architectural variables like porosity and pore size. Three types of scaffolds were designed and fabricated using image based design and indirect SFF techniques [42]. In addition, solid cylinders were fabricated at the same time. All of the fabricated scaffolds and cylinders were implanted into subcutaneous sites of mice for 6, 12 and 21 weeks. Mass loss, mechanical property, molecular weight, crystallinity, and morphology were analyzed and correlated with

specific measurements of scaffolds architecture, including pore and strut size, porosity, and surface area.

5.3 Methods

5.3.1 Porous Scaffold Design and Fabrication

Cylindrical porous scaffolds of 5mm diameter and 3mm height with three different pore diameters (280, 550, and 820μm), were designed using image-based techniques (Fig 5.1 (a)). Based on the designed pore sizes, scaffolds were denoted as PLLA-L (Large pore size = 820μm), PLLA-M (Medium pore size = 550μm), or PLLA-S (Small pore size = 280μm). The resulting image representations were converted to stereolithography (STL) formats and sliced in Modelworks software (Solidscape, Inc., Merrimack, NH) to fabricate wax molds using a ModelMaker II (for PLLA-L and PLLA-M) or PatternMaster™ (for PLLA-S) 3D printer (Solidscape, Inc., Merrimack, NH). These wax molds were used to cast hydroxyapatite ceramic (HA) secondary molds. PLLA polymer pellets (Birmingham Polymers Inc., AL) were heated at 210ºC in a Teflon mold in Lindberg/Blue M Vacuum Oven (Thermo Scientific, Asheville, NC), and polymers were periodically added until the desired volume was achieved. The HA molds were then placed into the Teflon mold containing molten polymer, in order to force the polymer through the open pore network. The polymer and HA composites were cooled down at the room temperature in the oven, and cooling rate in the oven was monitored using a Traceable Expanded-Range Thermometer (Fisher Scientific). The HA molds were then removed from the porous polymer scaffolds using RDO Rapid Decalcifier (APEX Engineering Products Corp, Plainfield, IL) and rinsed in 100% ethanol. The PLLA solid

cylinders (PLLA-C) were also cast in the Teflon mold at the same time as the porous scaffolds. The cast PLLA-Cs were trimmed on top and bottom using a diamond saw (Crystalite Co., Westerville OH), to achieve 3mm height. Over 8 scaffolds per group were cast each time, and 4 casting cycles were performed to obtain enough number of scaffolds.

5.3.2 μ-CT analysis of pre- and post- implanted scaffolds

All of the scaffolds were scanned using a MS-130 high resolution μ-CT Scanner (GE Medical Systems, Toronto, CAN) at a resolution of 16μm before and after implantation. The scanned images were reconstructed using MicroView software (GE Healthcare, Milwaukee, WI) and stored as .vff files. The reconstructed images were used to calculate architectures of the pre-implanted scaffold, regarding pore size, strut size, volume, surface area and porosity.

5.3.3 Scaffold implantation

All animal implants were performed in compliance with University Committee on Use and Care of Animal (UCUCA) regulations. Prior to implantation, the scaffolds and cylinders were sterilized in 70% ethanol overnight, and filled with 60μl of 5mg/ml bovine plasma-derived fibrinogen (Sigma), and gelled with 6μl of 100U/ml bovine plasma-derived thrombin (Sigma). Immunocompromised mice (N: NIH-bg-nu-xid, Charles River, Wilmington, MA) were anesthetized with an injection of ketamine/xylazine, and then 4 subcutaneous pockets were created by blunt dissection. Each animal received a total of 4 implants (one scaffold or cylinder from each group) by

placing one individual implant into each pocket. Finally, all the surgical sites were closed using wound clips. The mice were sacrificed at 6, 12 and 21 weeks after the implantation, and the scaffolds and surrounding tissues were harvested.

5.3.4 Weight analysis of scaffolds

Tissues surrounding the harvested scaffolds were removed using collagenase solution as previously reported [43,44]. Briefly, the samples were treated with type 1 collagenase solution (collagenase (Sigma, C-9891): 2000U/ml + buffer (0.05M Tris-HCl and 0.36mM $CaCl_2$)) solution at 37ºC for 24 hours followed by 1% v/v of aqueous solution of Triton-100 washing for 24 hours. The samples were then rinsed in deionized water for 24 hours. Then, the samples were frozen at -20ºC freezer for 12 hours and lyophilized at -80ºC for 24 hours using a lyophilizer (FreeZone 6, Labconco Corp.) and weighed using an analytical balance (Sartorius Extend Balance). The weight loss was defined as $(W_0-W_t)/W_0 * 100\%$, where W_0 and W_t are the weights of scaffolds before and after implantation respectively [3,9].

5.3.5. Mechanical testing of scaffolds

Following post-implantation μ-CT scanning, compression tests were performed using a MTS Alliance RT30 Electromechanical test frame (MTS Systems Corp., MN) with a cross head speed of 1mm/min after scaffolds were immersed in phosphate buffer solution for 30 minutes. The heights and the diameters of the scaffolds were measured with a caliper (ABS Digimatic Solar Caliper, Mitutoyo Corp.) and TestWorksk4 software (MTS Systems Corp., MN) was used to record load and displacement data. The stress-strain

curves were calculated from the initial dimensions of specimens. The compressive modulus was defined by the slope at the initial linear section of the stress-strain curve.

5.3.6 Differential Scanning Calorimetry

To determine crystallinity, the enthalpy of the polymers was measured using differential scanning calorimetry (DSC). 3 to 5 mg of each sample were weighed using an analytical balance and sealed in volatile aluminum sample pans. The samples were heated in a Perkin-Elmer DSC-7 from 25 to 200 ºC at a rate of 10 ºC/min. An empty pan was used as a reference.

5.3.7 Gel Permeation Chromatography (GPC)

Samples were placed in glass vials and dissolved in HPLC reagent grade chloroform (Fisher, C607-4) with 3mg/mL concentration. The vials were capped to prevent evaporation of the chloroform and left for 10-24 hours. The solution was filtered with 0.2-PTFE syringe filters. GPC analysis of the samples was performed in chloroform at 1mL/min flow rate on a Waters GPC system equipped with a refractive index detector. The dissolved samples were eluted through a Waters column (Styragel HR4, WAT044225, 7.8mm I.D. x 300mm). Polymer molecular weights were calculated relative to selected polystyrene standers of molecular weights of 400000, 300000, 200000, 50000, 25000, and 1000 (PolySience Inc., Warrington, PA). Data was analyzed using Millennium software (Waters Corporation).

5.3.8 Statistical analysis

Statistical analysis was performed using SPSS (SPSS, Inc., Chicago, IL USA). N = 5 or 6 scaffolds were used for weight analysis, and N = 4 or 5 scaffolds were used for polymer crystallinity, molecular weight analysis and mechanical tests. One-way ANOVA followed by Tukey's Post Hoc multiple comparisons test was used. Errors were reported in figures as the standard deviation (SD) and significance was determined using probability value of $p<0.05$.

5.4 Results

5.4.1 Fabrication and Evaluation of the fabricated scaffolds

The designed scaffolds shown in Fig 5.1 (a) were fabricated using indirect SFF. The cooling rates of the polymers after heating were also monitored as shown in Fig 5.1 (b) and the cooling profiles to ambient temperature were consistent throughout the all casting cycles. The fabricated scaffolds were scanned using μ-CT to assess the morphologies of the scaffolds, regarding pore and strut sizes, volume, and surface area (Fig 5.2, Table 5.1). It was confirmed that the fabricated porous scaffolds had orthogonally interconnected pores or channels, and closely matched the computer design. The high R-squared values reflected the high correlations between the computer design and the fabricated scaffolds which were 0.9821, 0.9998, 0.9994 and 0.9890, for pore size, strut size, total volume and surface area, respectively (Fig 5.2 (a-c)). The pore and strut sizes were significantly different between the porous scaffold groups, ranging from largest to smallest as PLLA-L to PLLA-M to PLLA-S (Fig 5.2 (a)). The porosities of PLLA-L and PLLA-M were similar, and higher than those of PLLA-S and PLLA-C (Fig 5.2 (b)). Due to some air

bubbles from the casting process, PLLA-C did not achieve 0% porosity. The magnitude of scaffold surface area as follows PLLA-S, PLLA-M, PLLA-L and PLLA-C (Fig 5.2 (c)).

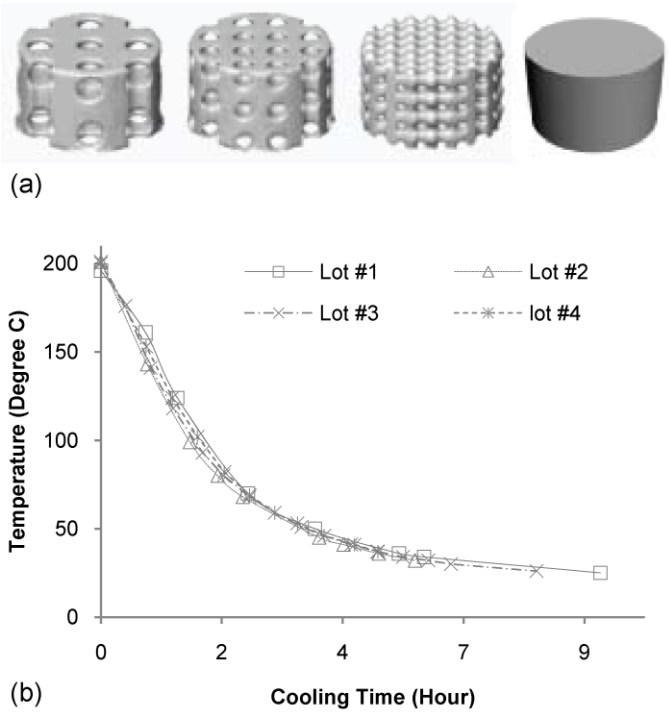

Fig 5.1 Computationally designed scaffolds (PLLA-L, PLLA-M, and PLLA-S) and solid cylinder (PLLA-C) from left to right (a). Oven temperature profiles after casting scaffolds (b).

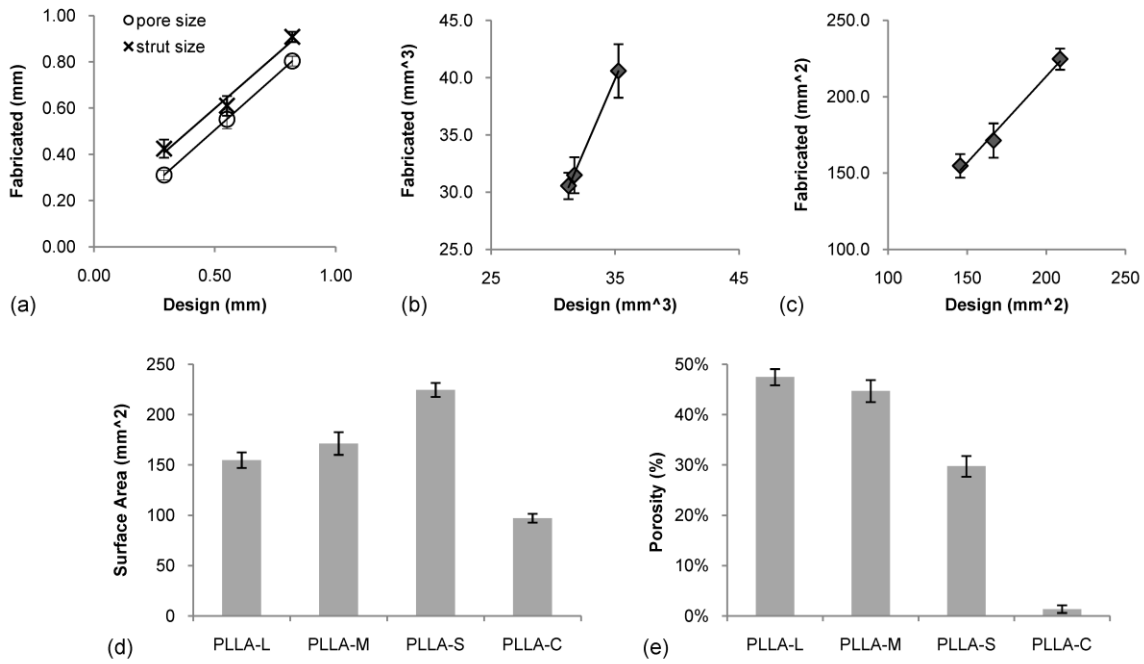

Fig 5.2 The relation between the design and the fabricated scaffolds, pore and strut sizes (a) volume (b) and surface area (c). These results indicate that architectures of the fabricated scaffolds match to those of the design. Surface (d) area and porosity (e) of the fabricated scaffolds and cylinders were highly reproducible within designs.

Table 5.1 Dimension of design and fabricated scaffolds and cylinder

		PLLA-L	**PLLA-M**	**PLLA-S**	**PLLA-C**
Pore Size (mm)	Design	0.82	0.55	0.28	
	Fabricated	0.80 ± 0.02	0.55 ± 0.04	0.31 ± 0.02	
Strut Size (mm)	Design	0.90	0.61	0.42	
	Fabricated	0.91 ± 0.02	0.61 ± 0.04	0.042 ± 0.04	
Total Volume	Design	31.24	31.72	35.27	
(mm^3)	Fabricated	30.55 ± 1.16	31.48 ± 1.57	40.39 ± 2.34	62.57 ± 2.08
Surface Area	Design	145.59	166.63	208.72	
(mm^2)	Fabricated	154.76 ± 7.70	171.31 ± 11.26	224.67 ± 6.95	97.29 ± 4.37
Porosity (%)	Fabricated	47.47 ± 1.60	44.70 ± 2.20	29.74 ± 2.03	1.35 ± 0.76

5.4.2 Morphology of the implanted scaffolds

The outer shapes of the scaffolds were still visible on the back of the mice at 21 weeks. After removing the fibrous tissues, visual inspection confirmed the existences of the original porous architectures for all scaffolds at all time points. Color changes were also observed especially in PLLA-C (Fig 5.3). Initially, PLLA-C was yellow-like color (Fig 5.3 (a)) and then, turned into white after degradation in the animal. μ-CT also confirmed the continued existences of the designed 3D internal architectures at 21 weeks and the absence of residual tissues in the scaffolds after collagenase treatment (Fig 5.3(e)).

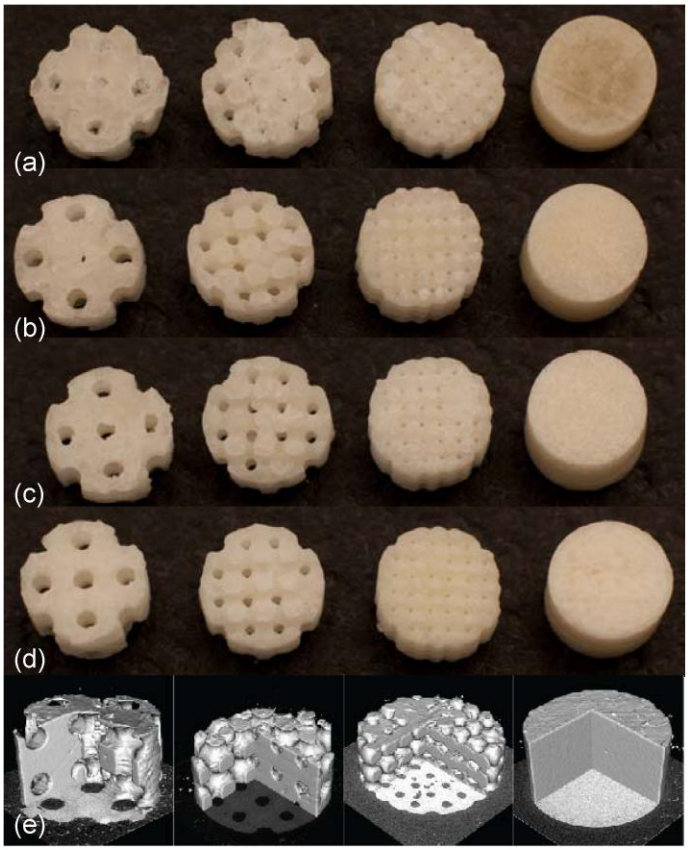

Fig 5.3 Pictures of implanted scaffolds and cylinders at 0 (a), 6 (b), 12 (c), and 21 (d) weeks. The colors of implants turned from yellow to white along to the implantation times. The rendering images from μ-CT show the existing architectures of porous scaffolds at 12 weeks (e). All images show PLLA-L, PLLA-M, PLLA-S, and PLLA-C from left to right.

5.4.3 Mass loss of the scaffolds

We first examined the effects of the collagenase solution used to remove tissues on scaffold mass. Weight differences before and after the collagenase treatment were -0.14 ± 0.56 %, -0.04 ± 0.17 %, -0.16 ± 0.14 %, and -0.32 ± 0.25 % for PLLA-L, PLLA-M, PLLA-S and PLLA-C, respectively. These are within the tolerances of the scale used; therefore, we concluded the effect of the collagenase treatment on scaffold degradation was negligible. The percentage of implants' mass loss at each time point is shown in Fig 5.4 and Table 5.2. PLLA-C lost significantly more percentage mass than all other groups at 12 and 21 weeks and more than PLLA-S at 6 weeks. PLLA-S showed significantly less percentage of mass loss than PLLA-M and PLLA-L at 21 weeks. These results suggest that larger strut sizes may cause faster degradation than smaller ones. The relationship of scaffold surface area to percent mass loss was also examined (Fig 5.5). Although a weak correlation was seen at 6 weeks (R^2=0.397) (Fig 5.5(a)), the correlation became stronger with longer time points, 12 weeks (R^2=0.681) (Fig 5.5(b)) and 21 weeks (R^2=0.671) (Fig 5.5 (c)). Among the design parameters, larger surface area was correlated with less mass loss. There was no relation between scaffold porosity and percent mass loss.

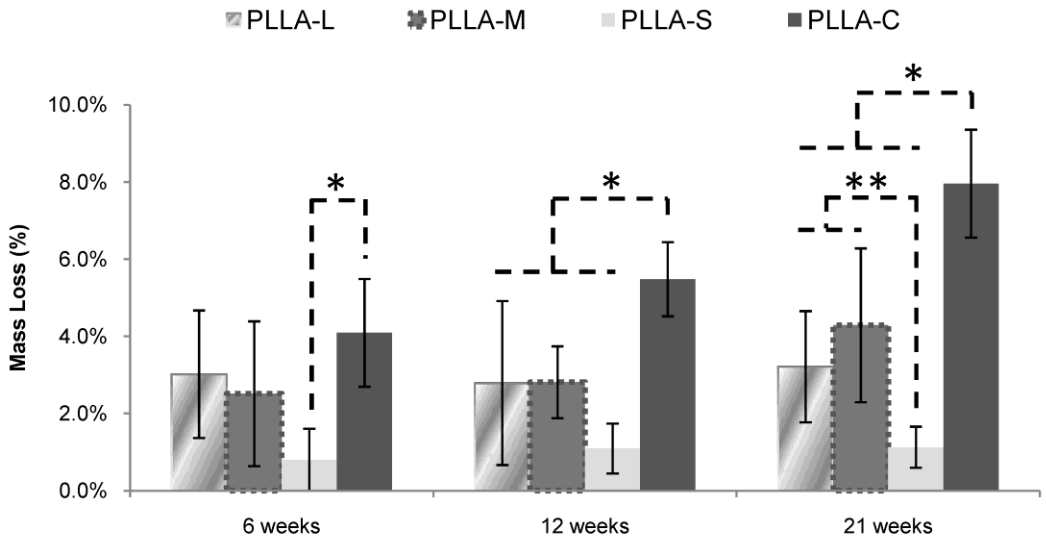

Fig 5.4 Mass loss of the scaffolds and cylinder each time point. * and ** indicate significant difference. With further implantation time, more significant differences were seen between the groups.

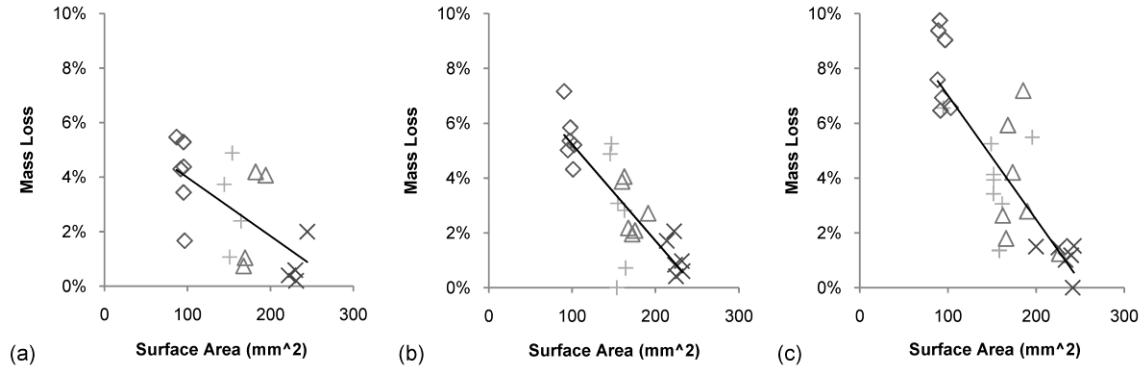

Fig 5.5 The relation between the initial surface area of implants and their mass loss at 6 (a), 12 (b) and 21 (c) weeks. +, △, ×, and ◇indicate PLLA-L, PLLA-M, PLLA-S, and PLLA-C, respectively. The R-squared values are 0.397 at 6 weeks (a), 0.681 at 12 weeks (b) and 0.671 at 21 weeks (c).

5.4.4 Crystallinity of the scaffolds

Scaffold cystallinity was determined by enthalpy measured with DSC (Fig 5.6, Table 5.2). Enthalpy increased in all porous scaffolds up to 21 weeks due to degradation of their amorphous regions, and there was no significant difference between the porous scaffolds. Meanwhile, the enthalpy of PLLA-C increased up to 12 weeks and decreased thereafter. The enthalpy value of PLLA-C was significantly higher than PLLA-S ($p = 0.048$) and PLLA-M ($p = 0.044$) at 6 weeks, and also higher but not reaching significance for PLLA-

L ($p = 0.050$). At 12 weeks, the solid cylinder enthalpy was significantly higher than the porous scaffolds with p values of 0.003, 0.001 and 0.001 for PLLA-L, PLLA-M and PLLA-S, respectively. These results indicate that PLLA-C degraded faster than the porous scaffolds with its crystal regions degrading after its amorphous regions.

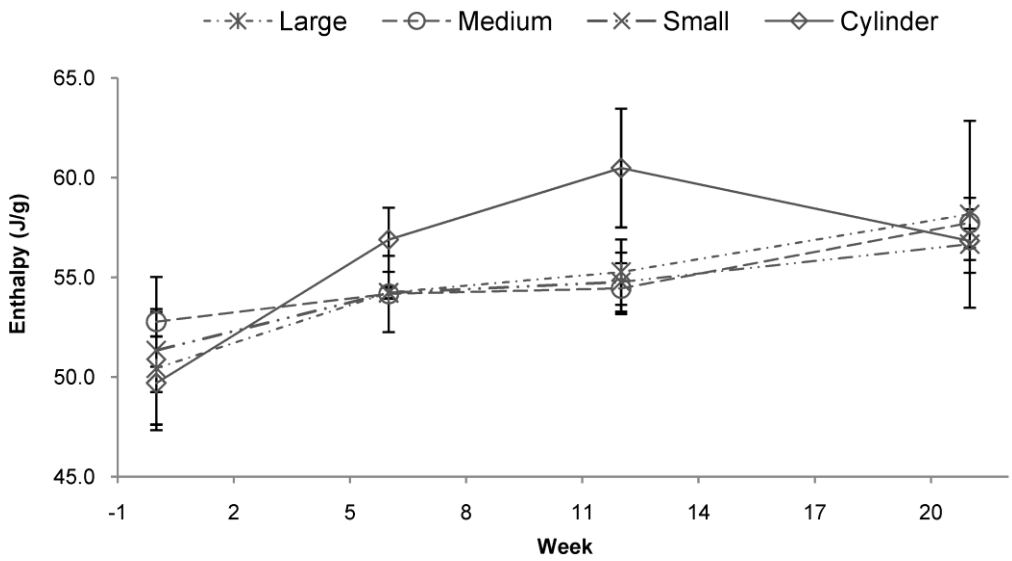

Fig 5.6 Enthalpy change of PLLA-L, PLLA-M, PLLA-S and PLLA-C. PLLA-L, PLLA-M, and PLLA-S increased their enthalpy which indicate increased their crystalinity. While, PLLA-C increased its enthalpy up to 12 weeks and then decreased at 21 weeks. PLLA-C may be exposed advanced degradation.

Table 5.2 Mass loss, Crystallinity, Molecular weight, Polydispersity index and Moduli of the implanted scaffolds

		PLLA-L	PLLA-M	PLLA-S	PLLA-C
0 week	Mass Loss (%)	-0.14 ± 0.56	-0.04 ± 0.17	-0.16 ± 0.14	-0.32 ± 0.25
	Enthalpy (J/g)	50.45 ± 2.82	52.78 ± 2.25	51.34 ± 2.08	49.70 ± 2.35
	Molecular Weight (Da)	48565 ± 2257	47800 ± 2636	49784 ± 3298	
	Polydispersity Index (PDI)	2.027 ± 0.022	1.999 ± 0.057	1.950 ± 0.077	
	Modulus (MPa)	85.80±37.70	149.84±72.37	209.96±65.90	642.26±161.54
6 weeks	Mass Loss (%)	3.02 ± 1.65	2.51 ± 1.88	0.79 ± 0.82	4.09 ± 1.40
	Enthalpy (J/g)	54.24 ± 0.31	54.17 ± 1.91	54.22 ± 0.26	56.89 ± 1.60
	Molecular Weight (Da)	41986 ± 3225	43557 ± 4279	44914 ± 2520	
	Polydispersity Index (PDI)	2.109 ± 0.084	2.088 ± 0.026	2.030 ± 0.174	
	Modulus (MPa)	46.18±13.15	134.75±108.20	149.84±54.59	539.49±126.80
12 weeks	Mass Loss (%)	2.79 ± 2.12	2.81 ± 0.93	1.10 ± 0.65	5.48 ± 0.96
	Enthalpy (J/g)	55.27 ± 1.64	54.45 ± 1.28	54.77 ± 1.48	60.49 ± 2.98
	Molecular Weight (Da)	37368 ± 3634	37626 ± 2852	37686 ± 3658	
	Polydispersity Index (PDI)	2.173 ± 0.146	2.077 ± 0.046	2.160 ± 0.087	
	Modulus (MPa)	73.09±30.16	77.89±38.98	106.88±59.97	437.66±83.35
21 weeks	Mass Loss (%)	3.22 ± 1.44	4.29 ± 1.99	1.13 ± 0.53	7.96 ± 1.40
	Enthalpy (J/g)	58.17 ± 4.69	57.73 ± 1.27	56.67 ± 0.79	56.83 ± 1.59
	Molecular Weight (Da)	28898 ± 3332	30346 ± 3127	29307 ± 1235	
	Polydispersity Index (PDI)	2.099 ± 0.129	2.153 ± 0.027	2.127 ± 0.082	
	Modulus (MPa)	50.08±40.98	56.38±17.16	88.83±36.55	288.11±106.69

5.4.5 Scaffold molecular weights and polydispersity index

GPC analysis was performed for the porous scaffolds to measure molecular weight (M_w) and polydispersity index (PDI) (Fig 5.7(a, b), Table 5.2). M_w of the scaffolds decreased as the duration of the implantation time increased indicating that polymer chains were cleaved due to the result of *in vivo* degradation (Fig 5.7 (a)). However, there was no significant difference between the scaffold groups. PDI also did not show any significant difference between groups and implantation times (Fig 5.7 (b)). The distribution of molecular weight showed further molecule change in the polymer of each scaffold group. The early time point shows more homogeneity in polymer chain length, while the later time points show a heterogeneous distribution of the polymer which indicates the

polymer chains may be randomly cleaved into pieces (Fig 5.7 (c, d, e)). These results also indicate that more random polymer chain lengths due to degradation.

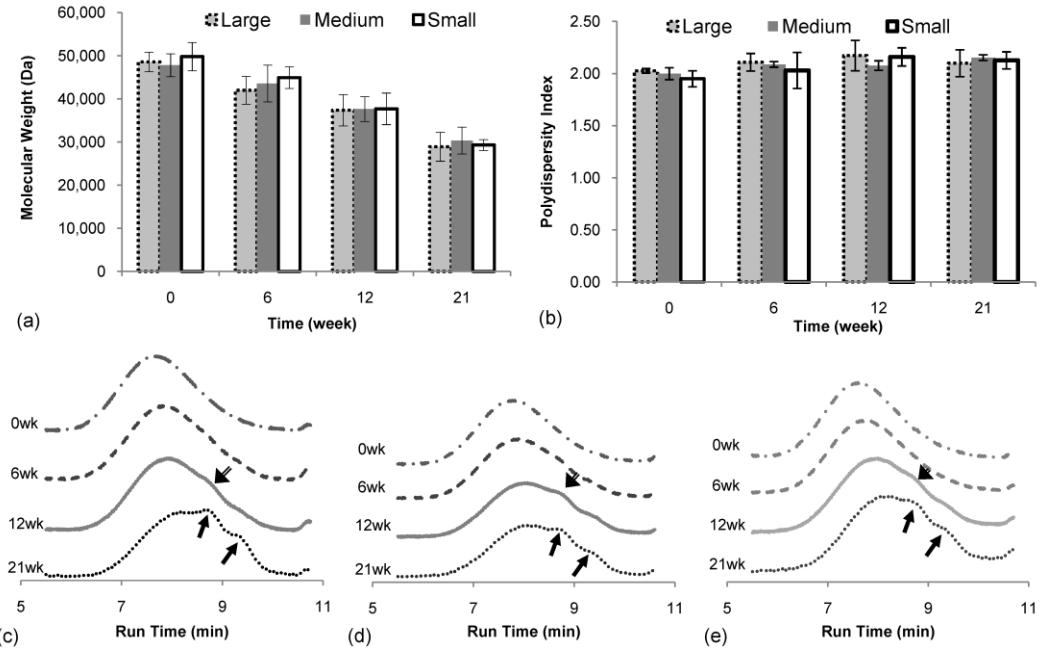

Fig 5.7 The results of molecular weight (M_w) (a) and polydispersity index (PDI) (b) of porous scaffolds were measured at each time point (N= 4-5). M_w decreased with implantation time for all porous scaffolds, while PDI was constant for all the porous scaffolds. There is no significant difference for either M_w or PDI between the groups. M_w distributions of PLLA-L (c), PLLA-M (b) and PLLA-S (e) show bimodal and multimodal distributions (arrows) appeared at 12 weeks and 21 weeks. These results indicate that the all scaffolds were developing a wider range of chain length, with an increase in the number of smaller chains.

5.4.6 Mechanical properties of the scaffolds

The changes of scaffold and cylinder compressive moduli in relation to implantation time were also measured (Fig 5.8 (a), Table 5.2). The mechanical properties were higher for implants with less porosity. Although all of the implants underwent a decrease in mechanical properties from 0 week to 21 weeks, all of the porous scaffold moduli were equal or greater than 50MPa. The decreases of the moduli were not monotonic as shown in the ratio of moduli at the given time point divided by the 0 week moduli of that group (Fig 5.8 (b)). The cylinder and small strut scaffolds had a more linear, monotonic

decrease in elastic modulus than the medium or larger pore scaffolds. The larger porous scaffolds had less numbers of struts in each scaffolds. Thus, when one strut broke or cracked, the construct tended to break easier than the scaffolds with more numbers of struts, which created a more random alteration in compressive modulus.

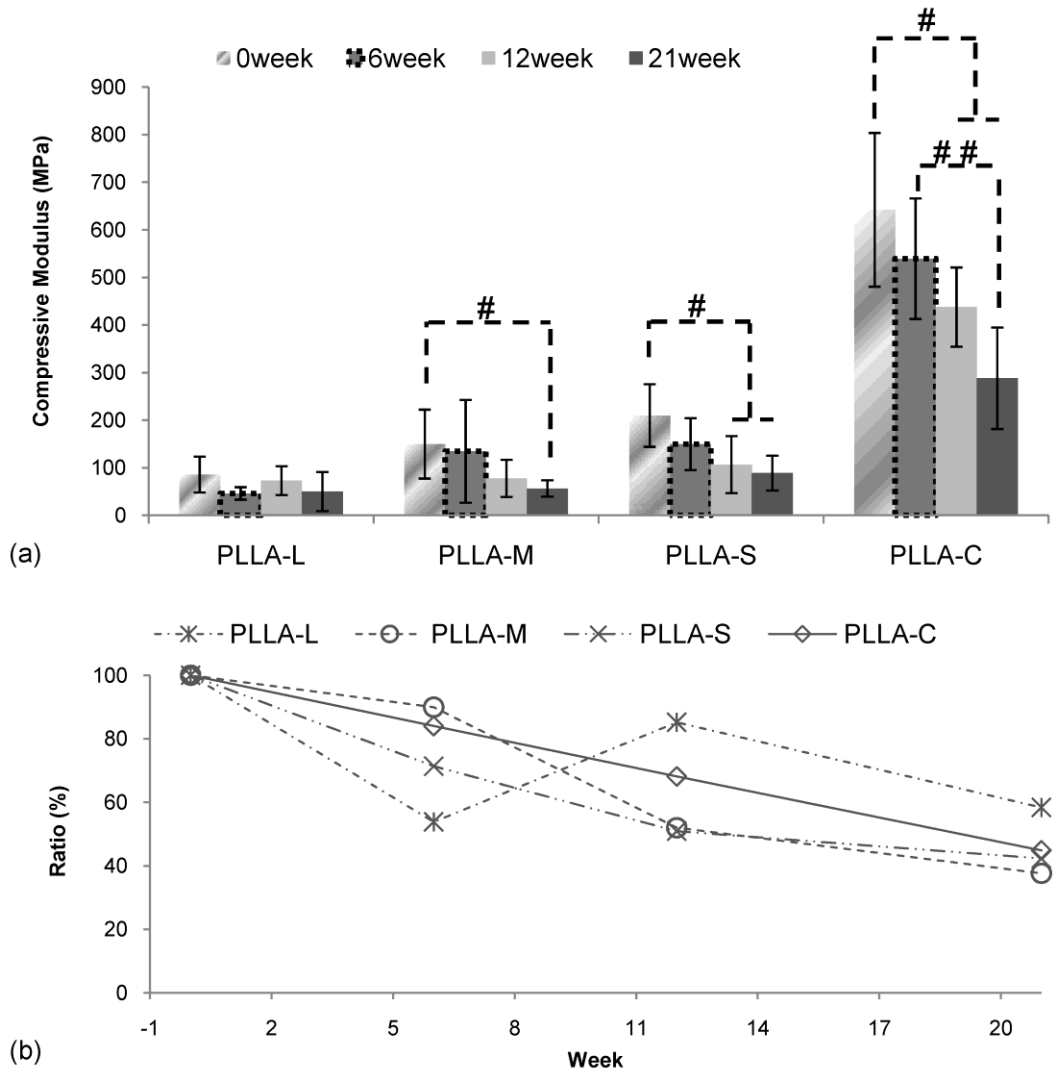

Fig 5.8 Modulus of scaffolds at the implantation time (a) show loss mechanical properties at each time point. Profiles of mechanical properties were unique of each group, which may indicate that mechanical properties depend on scaffold architectures as well as degradation ration. The average ratio of the moduli at each time point to 0 week (b) shows that decrease of mechanical properties more linear on PLLA-C, PLLA-S, PLLA-M, and PLLA-L in this order.

5.5 Discussion

This study demonstrated the specific effect of scaffold architecture created via computer aided design and fabricated techniques on *in vivo* degradation. Clinically used PLLA implants, such as bone screws and plates, have degradation times reported on the order of several years [45,46]. The implantation time in this study, up to 21 weeks, was much shorter than the previously tested time periods to avoid the implants completely losing their mechanical strength or internal architecture, allowing us to relate changes in scaffold properties to the initial design. The importance of PLLA scaffold architectures on their degradation has been examined using rods and porous scaffolds [3,11,12,38]. PLLA, specifically implants greater than 300μm thickness, were shown to undergo heterogeneous degradation [20,47,48]. Since the diameter of the current scaffold struts are larger than 300μm, all of the implants in this study are assumed to heterogeneously degrade.

To test our hypothesis, it is important to confirm factors in our process which may affect polymer degradation. The oven cooling temperature may affect properties of the fabricated scaffolds, including crystallinity and degradation rate [49,50]. The rate of cooling or temperature change was consistent thought all 4 casting cycles for all scaffolds' fabrication. In addition, acid solution in the RDO decalcifier used to remove HA molds may potentially degrade PLLA scaffolds. Since multiple fabrication runs were used to make all groups, an equal number of scaffolds per each experimental group were selected from each fabrication run to minimize bias due to inter-process variability.

The measurements of the fabricated scaffolds showed good correlation with the computer designs indicating that our fabrication technique can generate scaffolds with

desired architectures [16]. The porosity and surface area of the porous scaffolds and the solid cylinders were also compared to test the effect of the parameters on scaffold degradation profiles. All the data supported that the pore size, strut size, porosity and surface areas were unique for each group to evaluate the effect of scaffold architectures on their degradation.

A challenge for *in vivo* degradation studies of porous scaffolds is that implanted scaffolds become surrounded and infiltrated by tissues, which are often difficult to remove [22]. Since this makes some analyses impossible, especially weight measurement, we implanted our scaffolds into ectopic sites and used collagenase solution upon harvesting, to digest and remove the fibrous surrounding tissues. μ-CT data confirmed in fact that no residual tissue was present within the scaffolds. The open pore channels of our scaffolds might allow easy solution penetration inside of the scaffolds compared with scaffold with random pores. Also, there was no significant effect of the collagenase treatment on scaffold weight change. All of these results indicated that the implanted scaffolds and cylinders were properly treated for the following evaluations.

All of the implanted porous scaffolds and solid cylinders maintained their internal and external architectures during the study period. The existence of the architectures allowed testing for weight change and mechanical properties of the implants. However, polymer degradation was indicated by visual examination and the environmental scanning electron microscope (data not shown) demonstrating that color of polymers were changed, and small cracks were visible especially on PLLA-C at longer time points [3,51,52].

During the *in vivo* degradation period, the PLLA scaffolds and solid cylinders lost mass as shown in previous studies [3,9,11-13,52]. In particular, solid cylinders showed

faster percentage mass loss than the porous scaffolds, indicating that porous scaffolds degrade slower on a normalized basis than solid materials [5,6,13]. Among the porous scaffold groups, the weight loss depended on the initial designed architecture, confirming that degradation is significantly influenced by initial scaffold design. The solid cylinder and the scaffolds with larger strut size showed faster degradation through the longer implantation time, which may be explained by autocatalysis causing thicker materials to degrade faster than thinner materials [11,53]. In fact, when polymer degrades, lactic acid is released decreasing local pH, causing the autocatalysis process [2,11]. This may be seen in the solid cylinder and larger struts of the scaffolds due to more acid by-products trapped inside of the material.

On the other hand, the porous scaffolds had a higher surface to volume ratio than the solid cylinders, which helped to more efficiently remove acidic by-products due to polymer degradation [11]. Since there was no significant difference of surface to volume ratio between the scaffold groups, we did not see any significant correlation between surface to volume ratio and scaffold degradation. However, our study suggested that the overall scaffold surface area exhibited a significant correlation with scaffold degradation as measured by percent mass loss. This could be explained by the diffusion of soluble oligomers from the surface and from inside of the scaffolds. On the surface of the matrix, the oligomer can be removed or the carboxyl group can be neutralized by body fluid and cells to reduce acidity, while these effects are not present inside of the matrix, which leads to an increase in acidity [54]. Thus, increasing surface area with constant surface to volume ratio may still help to reduce acidic buildup and to slow down degradation.

The influence of PLLA scaffold porosity on degradation has been widely studied [5,13]. Although our scaffolds had lower porosity than many of previously reported porous foams or sponges, our scaffolds degraded slower than the porous PLLA scaffolds made with a particle leaching method [9]. Furthermore, in our study, PLLA-S had the lowest porosity, but degraded slower than PLLA-M and PLLA-L scaffolds with higher porosity. The possible reason for this is that porous scaffolds with random architectures and low interconnectivity inhibit fluid flow that removes acid by-products, and the remaining by-products increase local acidity inside of the porous scaffolds. In contrast, it is likely that the orthogonally interconnected pores or channels of our designed scaffolds in this study easily allowed body fluid infiltration to remove by-products, which may lead to slower scaffold degradation.

It was reported that the crystallinity increases at the early stage of degradation as a result of the degradation of the amorphous regions, and then it decreases at later stages [3,11,38,51]. All the porous scaffolds showed increased crystallinity over time, indicating that the amorphous regions of semi-crystalline PLLA were degraded increasing the portion of crystal regions [3,11]. The crystallinity of the solid cylinder increased up to 12 weeks and then decreased at 21 weeks indicating that the majority of the amorphous regions degraded first and followed by the degradation of the crystalline regions. These results also support that the solid materials degrade faster than the porous scaffolds.

Although there was no significant difference in molecular weight and polydispersity index between the scaffold groups, a decrease in molecular weight was observed in all scaffold designs and the solid cylinder with respect to implantation time. The decrease of

molecular weight indicates that longer polymer chains were cleaved into shorter chains due to degradation. Furthermore, a bimodal distribution of the GPC results was seen at the later time points, which indicates heterogeneous distributions of PLLA polymer chain, because of the faster degradation of amorphous region of semi-crystalline structures or various polymer degradation rate inside of the scaffold constructs [52,54].

Design and fabrication of scaffolds which gradually transfer load to newly generating bone [1,55], require an understanding of how the choice of material and design affect *in vivo* degradation. The results showed that the porous scaffold mechanical properties began at the lower to middle range of human trabecular bone, and then decreased to around the lower end of human trabecular bone range [56-58]. This suggests that these porous scaffolds may be applied to load bearing sites depending on the level of anatomic specific loads. Our previous study showed that newly generated bone tissue improves the mechanical properties of scaffold/bone constructs. Therefore, adjusting scaffold architecture via strut size and surface area (based on the degradation characteristics of a chosen material) may allow fine tuning of scaffold degradation rate to coincide with bone regeneration (depending on the chosen osteobiologic) enabling a smoother load transfer between scaffold and new bone.

However, the interaction between degradation and load bearing mediated by scaffold architecture is complex. Solid cylinders showed a linear decrease in mechanical properties, in the range of the previously reported *in vivo* degradation of rods (49% at 20weeks) or tensile specimens (35% at 20 weeks) [3,51]. Porous scaffolds with designed architecture exhibited a more variable decrease of mechanical properties. The numbers of the struts were different between the scaffolds groups, and the scaffolds with less

numbers of struts might have easily yielded if one of the struts broke during compression. This complicated dependency of reduced mechanical properties based on scaffold architecture can be evaluated using a combination of μ-CT and the finite element method to predict strength [16].

This study has some limitations. Since we used a mouse ectopic site, the implants were not exposed to mechanical loads during their implantation. Mechanical loading is an important factor that can accelerate degradation of scaffolds [59,60]. The degradation profile may differ in orthotopic sites than ectopic sties, due to the presence of osteoclasts or other macrophage type cells. Bone regeneration may also affect mass transport within the scaffold, affecting acid transport, which may also influence degradation. However, the ectopic model represented a simpler *in vivo* model to directly study architecture effects on scaffold degradation.

5.6 Conclusion

Porous scaffolds with computational designed architectures were successfully fabricated using indirect SFF. All implants showed changes of surface morphology, mass, molecular weight, and crystallinity, which indicate degradation of the implants. The ratios of scaffolds degradation were determined by their initial designed architectures. Porous scaffolds degraded slower than the cylinders, and scaffolds with larger struts degraded faster than scaffolds with smaller struts. In addition, scaffolds with greater surface area degraded more slowly. Larger porosity and pore size did not affect scaffold degradation. Our study suggests that computer design of scaffold architectures is an important factor influencing degradation profiles. Thus, scaffolds may be

computationally designed and fabricated to modulate degradation rate, within the degradation boundaries determined by the choice of biomaterial.

Acknowledgment

This study was supported by National Institute of Health (NIH) R01 grant AR 053379. Authors would like to thank Dr. Akira Abe, Dr. Huina Zhang, and Dr. Po-Chun Chang at the University of Michigan for technical assistances. We also acknowledge Prof. William Giannobile, Prof. Helena Ritchie, and Prof. Mohammad El-Sayed at the University of Michigan for the use of their equipments and lab spaces.

References

[1] Hutmacher DW. Scaffold design and fabrication technologies for engineering tissues--state of the art and future perspectives. J Biomater Sci Polym Ed 2001;12:107-124.

[2] Lu L, Peter SJ, Lyman MD, Lai HL, Leite SM, Tamada JA, et al. In vitro and in vivo degradation of porous poly(DL-lactic-co-glycolic acid) foams. Biomaterials 2000;21:1837-1845.

[3] Weir NA, Buchanan FJ, Orr JF, Dickson GR. Degradation of poly-L-lactide. Part 1: in vitro and in vivo physiological temperature degradation. Proc Inst Mech Eng [H] 2004;218:307-319.

[4] Gunatillake PA, Adhikari R. Biodegradable synthetic polymers for tissue engineering. Eur Cell Mater 2003;5:1-16; discussion 16.

[5] Wu L, Ding J. Effects of porosity and pore size on in vitro degradation of three-dimensional porous poly(D,L-lactide-co-glycolide) scaffolds for tissue engineering. J Biomed Mater Res A 2005;75:767-777.

[6] Pamula E, Menaszek E. In vitro and in vivo degradation of poly(L: -lactide-co-glycolide) films and scaffolds. J Mater Sci Mater Med 2008;19:2063-2070.

[7] Agrawal CM, McKinney JS, Lanctot D, Athanasiou KA. Effects of fluid flow on the in vitro degradation kinetics of biodegradable scaffolds for tissue engineering. Biomaterials 2000;21:2443-2452.

[8] Li WJ, Cooper JA,Jr, Mauck RL, Tuan RS. Fabrication and characterization of six electrospun poly(alpha-hydroxy ester)-based fibrous scaffolds for tissue engineering applications. Acta Biomater 2006;2:377-385.

[9] Gong Y, Zhou Q, Gao C, Shen J. In vitro and in vivo degradability and cytocompatibility of poly(l-lactic acid) scaffold fabricated by a gelatin particle leaching method. Acta Biomater 2007;3:531-540.

[10] Lu HH, Cooper JA,Jr, Manuel S, Freeman JW, Attawia MA, Ko FK, et al. Anterior cruciate ligament regeneration using braided biodegradable scaffolds: in vitro optimization studies. Biomaterials 2005;26:4805-4816.

[11] Lu L, Peter SJ, Lyman MD, Lai HL, Leite SM, Tamada JA, et al. In vitro degradation of porous poly(L-lactic acid) foams. Biomaterials 2000;21:1595-1605.

[12] Chen VJ, Ma PX. The effect of surface area on the degradation rate of nano-fibrous poly(L-lactic acid) foams. Biomaterials 2006;27:3708-3715.

[13] Odelius K, Hoglund A, Kumar S, Hakkarainen M, Ghosh AK, Bhatnagar N, et al. Porosity and Pore Size Regulate the Degradation Product Profile of Polylactide. Biomacromolecules 2011.

[14] Karande TS, Ong JL, Agrawal CM. Diffusion in musculoskeletal tissue engineering scaffolds: design issues related to porosity, permeability, architecture, and nutrient mixing. Ann Biomed Eng 2004;32:1728-1743.

[15] Melchels FP, Barradas AM, van Blitterswijk CA, de Boer J, Feijen J, Grijpma DW. Effects of the architecture of tissue engineering scaffolds on cell seeding and culturing. Acta Biomater 2010;6:4208-4217.

[16] Saito E, Kang H, Taboas JM, Diggs A, Flanagan CL, Hollister SJ. Experimental and computational characterization of designed and fabricated 50:50 PLGA porous scaffolds for human trabecular bone applications. J Mater Sci Mater Med 2010;21:2371-2383.

[17] Choi SW, Zhang Y, Xia Y. Three-dimensional scaffolds for tissue engineering: the importance of uniformity in pore size and structure. Langmuir 2010;26:19001-19006.
[18] Lee KW, Wang S, Dadsetan M, Yaszemski MJ, Lu L. Enhanced cell ingrowth and proliferation through three-dimensional nanocomposite scaffolds with controlled pore structures. Biomacromolecules 2010;11:682-689.
[19] Kim K, Dean D, Wallace J, Breithaupt R, Mikos AG, Fisher JP. The influence of stereolithographic scaffold architecture and composition on osteogenic signal expression with rat bone marrow stromal cells. Biomaterials 2011;32:3750-3763.
[20] Grizzi I, Garreau H, Li S, Vert M. Hydrolytic degradation of devices based on poly(DL-lactic acid) size-dependence. Biomaterials 1995;16:305-311.
[21] Wu L, Ding J. In vitro degradation of three-dimensional porous poly(D,L-lactide-co-glycolide) scaffolds for tissue engineering. Biomaterials 2004;25:5821-5830.
[22] Liao SS, Cui FZ. In vitro and in vivo degradation of mineralized collagen-based composite scaffold: nanohydroxyapatite/collagen/poly(L-lactide). Tissue Eng 2004;10:73-80.
[23] Sung HJ, Meredith C, Johnson C, Galis ZS. The effect of scaffold degradation rate on three-dimensional cell growth and angiogenesis. Biomaterials 2004;25:5735-5742.
[24] Ishaug-Riley SL, Crane GM, Gurlek A, Miller MJ, Yasko AW, Yaszemski MJ, et al. Ectopic bone formation by marrow stromal osteoblast transplantation using poly(DL-lactic-co-glycolic acid) foams implanted into the rat mesentery. J Biomed Mater Res 1997;36:1-8.
[25] Sun W, Starly B, Darling A, Gomez C. Computer-aided tissue engineering: application to biomimetic modelling and design of tissue scaffolds. Biotechnol Appl Biochem 2004;39:49-58.
[26] Hutmacher DW, Sittinger M, Risbud MV. Scaffold-based tissue engineering: rationale for computer-aided design and solid free-form fabrication systems. Trends Biotechnol 2004;22:354-362.
[27] Hollister SJ. Porous scaffold design for tissue engineering. Nat Mater 2005;4:518-524.
[28] Martins A, Chung S, Pedro AJ, Sousa RA, Marques AP, Reis RL, et al. Hierarchical starch-based fibrous scaffold for bone tissue engineering applications. J Tissue Eng Regen Med 2009;3:37-42.
[29] Roy TD, Simon JL, Ricci JL, Rekow ED, Thompson VP, Parsons JR. Performance of degradable composite bone repair products made via three-dimensional fabrication techniques. J Biomed Mater Res A 2003;66:283-291.
[30] Williams JM, Adewunmi A, Schek RM, Flanagan CL, Krebsbach PH, Feinberg SE, et al. Bone tissue engineering using polycaprolactone scaffolds fabricated via selective laser sintering. Biomaterials 2005;26:4817-4827.
[31] Roosa SM, Kemppainen JM, Moffitt EN, Krebsbach PH, Hollister SJ. The pore size of polycaprolactone scaffolds has limited influence on bone regeneration in an in vivo model. J Biomed Mater Res A 2010;92:359-368.
[32] Ho ST, Hutmacher DW, Ekaputra AK, Hitendra D, Hui JH. The evaluation of a biphasic osteochondral implant coupled with an electrospun membrane in a large animal model. Tissue Eng Part A 2010;16:1123-1141.

[33] Kang SW, Kim JS, Park KS, Cha BH, Shim JH, Kim JY, et al. Surface modification with fibrin/hyaluronic acid hydrogel on solid-free form-based scaffolds followed by BMP-2 loading to enhance bone regeneration. Bone 2010.
[34] Gomes ME, Azevedo HS, Moreira AR, Ella V, Kellomaki M, Reis RL. Starch-poly(epsilon-caprolactone) and starch-poly(lactic acid) fibre-mesh scaffolds for bone tissue engineering applications: structure, mechanical properties and degradation behaviour. J Tissue Eng Regen Med 2008;2:243-252.
[35] Shim JH, Kim JY, Park JK, Hahn SK, Rhie JW, Kang SW, et al. Effect of thermal degradation of SFF-based PLGA scaffolds fabricated using a multi-head deposition system followed by change of cell growth rate. J Biomater Sci Polym Ed 2010;21:1069-1080.
[36] Kontakis GM, Pagkalos JE, Tosounidis TI, Melissas J, Katonis P. Bioabsorbable materials in orthopaedics. Acta Orthop Belg 2007;73:159-169.
[37] Madigan L, Vaccaro AR, Lim MR, Lee JY. Bioabsorbable interbody spacers. J Am Acad Orthop Surg 2007;15:274-280.
[38] Barbanti SH, Santos AR,Jr, Zavaglia CA, Duek EA. Porous and dense poly(L-lactic acid) and poly(D,L-lactic acid-co-glycolic acid) scaffolds: in vitro degradation in culture medium and osteoblasts culture. J Mater Sci Mater Med 2004;15:1315-1321.
[39] Chen CC, Chueh JY, Tseng H, Huang HM, Lee SY. Preparation and characterization of biodegradable PLA polymeric blends. Biomaterials 2003;24:1167-1173.
[40] Peltoniemi H, Ashammakhi N, Kontio R, Waris T, Salo A, Lindqvist C, et al. The use of bioabsorbable osteofixation devices in craniomaxillofacial surgery. Oral Surg Oral Med Oral Pathol Oral Radiol Endod 2002;94:5-14.
[41] Middleton JC, Tipton AJ. Synthetic biodegradable polymers as orthopedic devices. Biomaterials 2000;21:2335-2346.
[42] Taboas JM, Maddox RD, Krebsbach PH, Hollister SJ. Indirect solid free form fabrication of local and global porous, biomimetic and composite 3D polymer-ceramic scaffolds. Biomaterials 2003;24:181-194.
[43] Wan Y, Yu A, Wu H, Wang Z, Wen D. Porous-conductive chitosan scaffolds for tissue engineering II. in vitro and in vivo degradation. J Mater Sci Mater Med 2005;16:1017-1028.
[44] Zhang Z, Guidoin R, King MW, How TV, Marois Y, Laroche G. Removing fresh tissue from explanted polyurethane prostheses: which approach facilitates physico-chemical analysis? Biomaterials 1995;16:369-380.
[45] Bergsma JE, de Bruijn WC, Rozema FR, Bos RR, Boering G. Late degradation tissue response to poly(L-lactide) bone plates and screws. Biomaterials 1995;16:25-31.
[46] Barber FA, Dockery WD. Long-term absorption of poly-L-lactic Acid interference screws. Arthroscopy 2006;22:820-826.
[47] Shive MS, Anderson JM. Biodegradation and biocompatibility of PLA and PLGA microspheres. Adv Drug Deliv Rev 1997;28:5-24.
[48] Schwach G, Vert M. In vitro and in vivo degradation of lactic acid-based interference screws used in cruciate ligament reconstruction. Int J Biol Macromol 1999;25:283-291.

[49] Iannace S, Maffezzoli A, Leo G, Nicolais L. Influence of crystal and amorphous phase morphology on hydrolytic degradation of PLLA subjected to different processing conditions. Polymer 2001;42:3799-3807.
[50] Weir NA, Buchanan FJ, Orr JF, Farrar DF, Boyd A. Processing, annealing and sterilisation of poly-L-lactide. Biomaterials 2004;25:3939-3949.
[51] Pistner H, Stallforth H, Gutwald R, Muhling J, Reuther J, Michel C. Poly(L-lactide): a long-term degradation study in vivo. Part II: Physico-mechanical behaviour of implants. Biomaterials 1994;15:439-450.
[52] Li SM, Garreau H, Vert M. Structure-Property Relationships in the Case of the Degradation of Massive Poly(alpha-Hydroxy Acids) in Aqueous-Media .3. Influence of the Morphology of Poly(l-Lactic Acid). J Mater Sci -Mater Med 1990;1:198-206.
[53] Grayson AC, Cima MJ, Langer R. Size and temperature effects on poly(lactic-co-glycolic acid) degradation and microreservoir device performance. Biomaterials 2005;26:2137-2145.
[54] Li S. Hydrolytic degradation characteristics of aliphatic polyesters derived from lactic and glycolic acids. J Biomed Mater Res 1999;48:342-353.
[55] Fini M, Giannini S, Giardino R, Giavaresi G, Grimaldi M, Aldini NN, et al. Resorbable device for fracture fixation: in vivo degradation and mechanical behaviour. Int J Artif Organs 1995;18:772-776.
[56] Athanasiou KA, Zhu C, Lanctot DR, Agrawal CM, Wang X. Fundamentals of biomechanics in tissue engineering of bone. Tissue Eng 2000;6:361-381.
[57] Hutmacher DW, Schantz JT, Lam CX, Tan KC, Lim TC. State of the art and future directions of scaffold-based bone engineering from a biomaterials perspective. J Tissue Eng Regen Med 2007;1:245-260.
[58] Rezwan K, Chen QZ, Blaker JJ, Boccaccini AR. Biodegradable and bioactive porous polymer/inorganic composite scaffolds for bone tissue engineering. Biomaterials 2006;27:3413-3431.
[59] Kang Y, Yao Y, Yin G, Huang Z, Liao X, Xu X, et al. A study on the in vitro degradation properties of poly(L-lactic acid)/beta-tricalcuim phosphate (PLLA/beta-TCP) scaffold under dynamic loading. Med Eng Phys 2009;31:589-594.
[60] Yang Y, Tang G, Zhao Y, Yuan X, Fan Y. Effect of cyclic loading on in vitro degradation of poly(L-lactide-co-glycolide) scaffolds. J Biomater Sci Polym Ed 2010;21:53-66.

CHAPTER 6

Effect of Hydroxyapatite-Coated PLLA and PCL Porous Scaffolds on Bone Formation *In Vivo*

6.1 Abstract

Biodegradable polymer scaffolds fabricated by computer aided design and solid freeform fabrication techniques have desired architectures and mechanical properties for bone applications. However, these polymer scaffolds typically have poor osteoconductivity and poor bone ingrowth compared with osteoconductive scaffolds, such as, hydroxyapatite and calcium phosphate scaffolds. We combined SFF techniques and biomineral coating to fabricate biodegradable scaffolds with designed interconnected architectures and improved osteoconductivity. PLLA and PCL scaffolds with the same design were fabricated using SFF and coated with biomineral layers using modified simulated body fluid. μ-CT results showed that both PLLA and PCL scaffolds had the identical structures with orthogonally interconnected pores. XRD, SEM and μ-CT data demonstrated mineral layers were on the surface of the PLLA and PCL scaffolds. The scaffolds were seeded with human gingival fibroblasts either trandsuced with bone morphogenic protein 7 (BMP-7) or green fluorescent protein (GFP), and implanted into mice subcutaneous sites for 3 and 10 weeks. From μ-CT and histological data at 3 weeks, there was no significant bone ingrowth difference between the coated scaffolds and

uncoated scaffolds for both PLLA and PCL. At 10 weeks, however, the coated scaffolds had significantly more bone ingrowth than the uncoated scaffolds. The bone tissues inside of the coated scaffolds had bone marrow-like tissue, while the uncoated scaffolds had more fibrous-like tissues. Mechanical properties of the coated PLLA scaffolds improved due to the advanced bone ingrowth compared with the uncoated PLLA scaffolds. This study concludes that combination of the SFF technique and biomineral coating improve bone ingrowth of PLLA and PCL scaffolds, and advanced bone ingrowth improve mechanical properties of PLLA scaffolds.

6.2 Introduction

Engineered scaffolds have been researched and developed for bone defect applications. Ideal scaffolds should be fabricated to fit to defect shapes, and support mechanical loads. Furthermore, they should enhance tissue ingrowth and degrade in conjunction with tissue healing [1]. To achieve these goals, computer aided design (CAD) and solid freeform fabrication (SFF) techniques have been utilized to fabricate biodegradable scaffolds from various material and shapes [2-5]. SFF scaffolds have well controlled and interconnected pores to enhance cell migration as well as generate higher mechanical properties for load bearing applications compared with conventional scaffolds, such as salt leaching [6-10].

FDA approved biodegradable Poly (α-hydroxy esters), including Poly (L-lactic acid) (PLLA) and Poly (ε-caprolactone) (PCL), have been widely used for orthopaedic implants, tissue engineering scaffolds and drug delivery [11,12]. PCL and PLLA both degrade by hydrolysis, but show different degradation profiles. Generally, PCL shows a more hydrophobic surface and slower degradation than PLLA [13-15]. Both PLLA and

PCL have also been used as scaffolds materials using SFF, and been implanted into animals to prove their application for bone formation as shown in the chapter 4 and other researches[16,17].

One of the disadvantages of the above biodegradable scaffolds is their poor osteoconductive property to support bone cell functions and tissue ingrowth into the scaffolds compared with hydroxyapatite (HA) and tricalcium phosphate (TCP) scaffolds. Biomineral coating of substrate surfaces using simulated body fluid (SBF), which contains similar ion components to human blood, is a promising technique to improve the osteoconductivity of tissue engineered constructs [18-20]. In this technique, biomaterials are immersed in SBF, and then carbonate apatite minerals, which are similar to the mineral component of bone tissue, precipitate on the negatively charged biomaterial surfaces [19,21,22]. .

Biomineralization has successfully been applied to various biomaterials including metals [23-25], polymers [21,26-29], and the composites of polymers and hydroxyapatite or calcium phosphate [27,30,31] to enhance bone cell function and bone tissue regeneration. The mineral coated titanium implants enhance bone ingrowth into the channels and more direct bone contact on the surface than the uncoated titanium implants which had more fibrous tissue formations [24,25,32]. A few coated biodegradable substrates, such as PLGA scaffolds and microspheres, have also shown improved bone formation *in vivo* [33,34]. These studies also showed that biomineral coatings inhibited fibrous tissue formation and supported direct bone formation [31,32,34].

Although the previous studies have shown a positive effect of apatite-coatings on bone tissue formation, some studies have not agreed with these results. Mineral coated salt

leaching scaffolds tend to have less open pore structures limiting effective coating at the center of the scaffolds and have undeveloped bone ingrowth towards the center of the scaffolds [35]. Some other studies showed a diminished effect of biomineral coatings on bone formation and fibrovascular tissues, with increased numbers of body giant cells *in vivo* using porous poly (ε-caprolactone-co-L-lactide) scaffolds, SFF PCL scaffolds or SFF porous Titanium scaffolds [27,28,36]. All together, these studies indicate that the effect of biomineral coatings of biodegradable scaffolds on *in vivo* bone formations is still not well understood. Furthermore, the effect of mineralization on different base materials has not been studied.

In the present study, we combined SFF scaffolds with biomineral coating using two types of biodegradable polymers with different degradability, PLLA and PCL. We hypothesized that biomineral coated SFF scaffolds would have improved bone ingrowth, and the biomineral coating would affect PLLA more than PCL scaffolds. PLLA and PCL scaffolds with the same designs were fabricated using the indirect SFF and coated with modified SBF technique. The fabricated scaffolds were seeded with either bone morphogenic protein 7 (BMP-7) or green fluorescent protein (GFP) transduced human gingival fibroblasts (HGF), and then, subcutaneously implanted into mice for 3 and 10 weeks.

6.3 Methods

6.3.1 Porous Scaffold Design and Fabrication

Porous scaffolds 5mm in diameter and 3mm in height with 550μm pore diameters were designed using image-based techniques. The resulting image representations were

converted to stereolithography (STL) formats and sliced in the Modelworks software (Solidscape, Inc., Merrimack, NH) to fabricate wax molds using a PatternMaster™ 3D printer (Solidscape, Inc., Merrimack, NH). These wax molds were cast into hydroxyapatite ceramic (HA) secondary molds. Polymer pellets, PLLA (Inherent Viscosity = 0.65dL/g, Birmingham Polymers Inc., AL) and PCL (Molecular weight: 43,000-50,000, Polyscience Inc.), were heated at 205ºC and 120 ºC, respectively, in a Teflon mold. The HA molds were then placed into the Teflon mold containing molten polymer, in order to force the polymer through the open pore network. The HA molds were then removed from the porous polymer scaffolds using RDO (APEX Engineering Products Corp, Plainfield, IL) and washed with 100% ethanol.

6.3.2 Mineral coating incubation in mSBF

Biomineral coating of PLLA and PCL scaffolds were performed by Darilis Suarez-Gonzalez from Prof. William Murphy's group at the University of Michigan. PLLA and PCL scaffolds were hydrolyzed in a 0.1M NaOH for 60 minutes to expose carboxylate anions that serve as nucleation sites. After hydrolysis samples were rinsed at least 3 times with deionized H_2O. Each scaffold was incubated at 37 °C in 15 ml of modified simulated body fluids (mSBF) for 14 days under continuous rotation. The mSBF solution had a similar composition to that of human plasma but with double the concentration of calcium and phosphate, and was prepared as previously reported by Dr. Suarez-Gonzalez et.al [22]. Specifically, the following reagents were added to ddH_2O heated to 37 °C in the order shown; 141mM NaCl, 4.0 mM KCl, 0.5 mM $MgSO_4$, 1.0 mM $MgCl_2$, 4.2 mM $NaHCO_3$, 20.0 mM Tris, 5.0 mM $CaCl_2$, and 2.0 mM KH_2PO_4. The solution was then

adjusted to a final pH of 6.8. The mSBF solution was renewed daily in order to maintain a consistent ionic strength throughout the experiment.

6.3.3 Scaffold surface characterization

The surfaces of pre-implanted scaffolds were also examined under a scanning electron microscope (XL30 ESEM, Philips). The environmental scanning electron microscopy (ESEM) mode was carried out at10kV and in a humid atmosphere of 0.7 Torr. The surfaces of the coated scaffolds were further investigated using electron scanning microscope with energy disperse X-ray spectroscopy (EDS), which was done by Darilis Suarez-Gonzalez.

6.3.4 Cell preparation and BMP-7 measurement

Primary human gingival fibroblasts (HGFs) were purchased (ScienCell, CA). HGFs were cultured and expanded on passage 6 near confluence in Dulbecco's Modification of Eagles Medium (DMEM) supplemented with 10% fetal bovine serum, and 1% penicillin and streptomycin (Gibco). The HGFs were infected with AdCMV-BMP-7, a recombinant adenovirus construct expressing murine BMP-7 gene under a cytomegalovirus (CMV) promoter, at a multiplicity of infection (MOI) of 500 PFU/cell for 20hours. 0.5 million cells were seeded into each scaffold by suspending them in 40µl of 5mg/ml collagen gel. The gelation procedure was as follows: Rat tail collagen high concentration (stock concentration = 9.03mg/mL, BD Bioscience Discovery Labs, San Jose, CA) were diluted with cold sterile 0.02N acetic acid to make 5mg/mL. As soon as 0.5N sodium hydroxide with 220 mg/mL sodium bicarbonate to initiate gelation is added

to Col I gel mixture, gel contents were mixed with cell and evenly re-suspended. 40µL of cell and gel mixture was placed each hole of sterilized custom made Teflon mold, and the scaffolds were place on top of gel to enforce infiltration. This was followed by incubation at 37°C for 40 min to solidify gels further. The scaffolds seeded with HGFs were transferred in ultra-low cluster 24 well plate (Corning Incorporated, NY) with DMEM containing 2% FBS were incubated on an orbital shaker. The media was changed for 2 or 3 days and collected every 48 hours at 7, 24, 21 and 28 days. The collected media was stored at -20 °C, and amount of BMP-7 in the media was measured using Human BMP-7 Quantikine ELISA kit (R&D Systems) according to manufacturer's instruction.

6.3.5 Scaffold implantation in mice subcutaneous sites

Passage 6 HGFs were cultured, transduced with AdCMV-BMP-7 or AdCMV-GFP, a recombinant adenovirus construct expressing murine GFP gene under a cytomegalovirus (CMV) promoter, with 500MOI. The transduced HGFs were seeded into scaffolds as the same way as the previous section, incubated for 24 hours, and subcutaneously implanted into 6-7 weeks old (46-53 days old) female immunocompromised mice (NIHS-bg-nu-xid, Harlan,). After animals were anesthetized with an injection of ketamine/xylazine, 4 subcutaneous pockets were created and 4 scaffolds (one scaffold from each group) were implanted into each mouse, and finally surgical sites were closed with wound clips in compliance with University Committee on Use and Care of Animal (UCUCA) regulations. The mice were sacrificed at 3 and 10 weeks after the implantation, and the

scaffold and tissue constructs were harvested, fixed with Z-fix (Anatech, Battle Creek, MI), and left in 70% ethanol for further assay.

6.3.6 Assay of scaffolds, regenerated tissues, and amount of mineral using μ-CT

All of the scaffolds pre-implantation alone and post-implantation with tissues were scanned using a MS-130 high resolution μ-CT Scanner (GE Medical Systems, Toronto, CAN) at a resolution of 16 μm. The scanned images were reconstructed using MicroView software (GE Healthcare). The reconstructed images were used to calculate the scaffold pore size, strut size, volume and surface area prior to implantation and Bone volume (BV) and Tissue mineral density (TMD) were calculated for the scaffolds after implantation. For bone ingrowth calculation, region of interest (ROI) was selected with size of 5mm diameter and 1.8mm height located within the center of a scaffold. The bone ingrowth was determined by subtracting the amount of mineral in the ROI before implantation from the total amount of mineralized tissue after implantation. To determine the amount of mineral deposition the scaffold surfaces, ROI with 5.6mm diameter and 3.5mm height was chosen, and then amount of mineral was calculated subtracting before implantation from after implantation.

6.3.7 Quantitative Polymerase Chain-reaction (qPCR)

The harvested scaffold and tissue constructs were homogenized in Trizol (Invitrogen, Carlsbad, CA, USA), and RNA extraction was performed using a PureLink RNA Mini kit (Invitrogen, Carlsbad, CA, USA) according to the manufacturer's instructions. 1μg of RNA from each sample was converted to cDNA by means of the SuperScript III First

Strand Synthese kit (Cat#11752 Invitrogen, Carlsbad, CA, USA). The converted cDNA was diluted 1:20 and used for 20μL reactions containing CYBER Green PCR mix (Cat#4309155 Applied Biosystems). As an internal control, GAPDH was simultaneously quantified. Primers for osteocalcin (OCN), Runx2 and GAPDH are shown in Table 6.1.

Table 6.1 Primers used for qPCR

	Right	Left
Osteocalcine (OCN)	CAAGCAGGGTTAAGCTCACA	GGTAGTGAACAGACTCCGGC
Runx2	GCTCACGTCGCTCATCTTG	ACACCGTGTCAGCAAAGC
GAPDH	TGAAGCAGGCATCTGAGGG	CGAAGGTGGAAGAGTGGGAG

6.3.8 Mechanical test of scaffolds with regenerated tissue

Following μ-CT scanning, compression tests were performed after scaffolds were undergone series of ethanol and rehydrated in Milli-Q water for 30 minutes, using a MTS Alliance RT30 Electromechanical test frame (MTS Systems Corp., MN). The cross head speed was 1mm/min after a preload of 0.227kg (0.5 lbs). The heights of the scaffolds were measured with a caliper, and the TestWorks4 software (MTS Systems Corp., MN) was used to record load and displacement data. The stress-strain curves were calculated from the initial dimensions of specimens. The compressive modulus was defined by the slope at the initial linear section of the stress-strain curve.

6.3.9 Histological analysis

After scanning with the μ-CT machine, one harvested scaffold from each group was also used for histological assay. The scaffold and tissue constructs were demineralized with RDO and the residual polymer in the tissue was removed using chloroform prior to

paraffin-embedding. The scaffolds were then sectioned at 5 μm and stained with hematoxylin and eosin (H&E) and Masson's Trichrome.

6.3.10 Statistical analysis

The statistical analysis was performed with SPSS (SPSS, Inc., Chicago, IL USA). Two groups were analyzed with Student's *t*-test for independent samples. Multiple comparison procedures were determined by one-way ANOVA followed by Tukey's Post Hoc multiple comparisons. Errors are reported in figures as the standard deviation (SD) and significance was determined using probability value of $p < 0.05$.

6.4 Results

6.4.1 Morphology of coated and non-coated scaffolds

The gross images of the fabricated scaffolds are shown in Fig 6.1 (a-d). The scaffolds have similar morphology, and become less transparent after mineral coatings. Architectures, including pore interconnection, of the non-coated PLLA and PCL scaffolds were analyzed using μ-CT (Fig 6.1 (f) and (h)). Pore size, strut size, volume, surface area and surface to volume ratio of non-coated PLLA and PCL scaffolds were measured (Table 6.2). These values were same between the PLLA and PCL scaffolds, which support that the scaffolds had identical architectures. μ-CT data also showed the existence of mineral layers inside of the scaffolds architectures (Fig 6.1 (e) and (g)). The surfaces of the scaffolds were further characterized using ESEM (Fig 6.1 (i-p)). Non-coated PLLA and PCL scaffolds had smooth surface (Fig 6.1 (j, l, n, p)), while mineral coated scaffolds show rough surface (Fig 6.1 (i, k, m, o)). The surface of the mineral

were also characterized, and nanoscale plate-like crystalline structures were observed on both coated PLLA and PCL scaffolds (Fig 6.2 (a, b)). Analysis of the composition of the biomineral by energy dispersive x-ray spectroscopy (EDS) showed that the mineral was composed primarily of calcium and phosphorous with a Ca/P ratio of 1.58 for coated PLLA scaffold (Fig 6.2 (c)) and 1.56 for coated PCL scaffold (Fig 6.2 (d)) which are in the rage of biological minerals. These data support growth of bone-like minerals on the surface of the scaffolds.

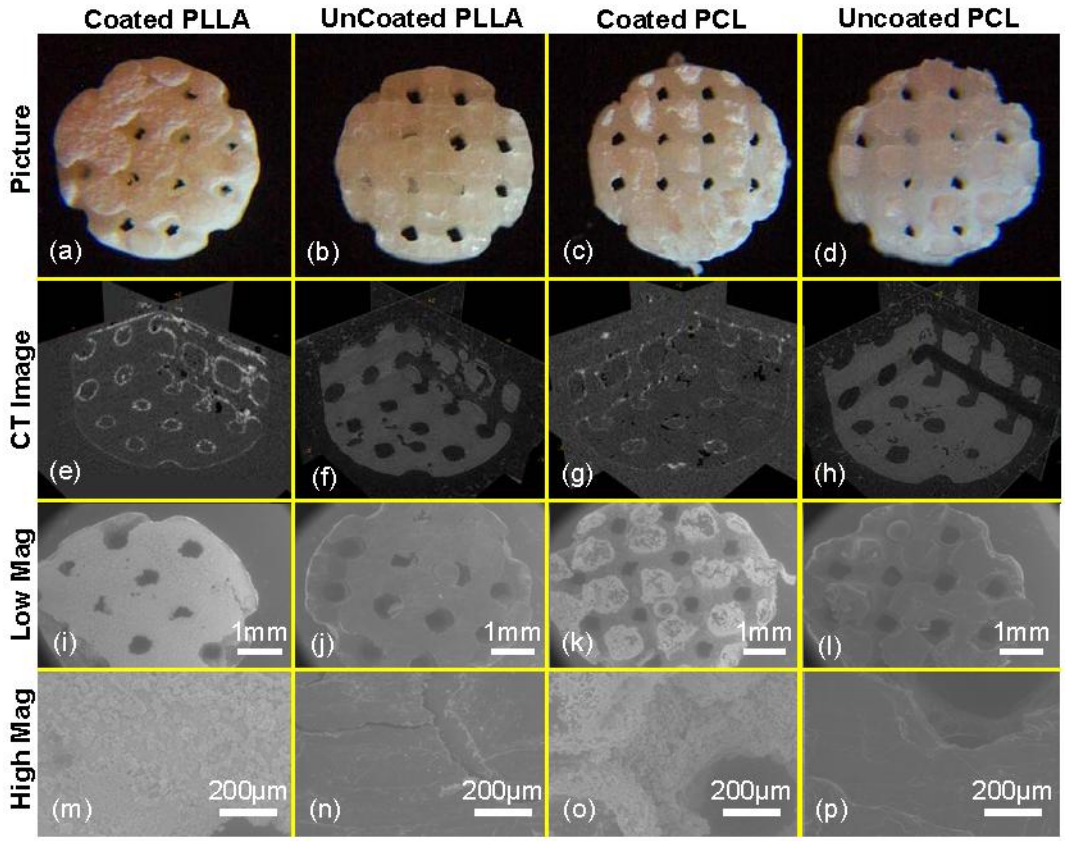

Fig 6.1 Pictures, µ-CT images, and ESEM images of Coated PLLA (a, e, i, m), Uncoated PLLA (b, f, j, n), Coaed PCL (c, g, k, o) and Uncoated PCL (d, h, l, p), respectively. µ-CT images confirm that mineral layer covered the surface of both PLLA and PCL scaffolds (e,g). ESEM images show that rough surface of the coated PLLA and PCL scaffolds (m, o), while relatively smooth surface of the uncoated PLLA and PCL scaffolds (n,p).

Table 6.2 Fabricated uncated PLLA and PCL scaffolds

	Pore Size (mm)	Strut Size (mm)	Volume (mm3)	Surface (mm2)	Surface/Volume
PLLA Scaffold	0.60 ± 0.03	0.67 ± 0.03	33.259 ± 2.194	187.126 ± 13.753	5.627 ± 0.204
PCL Scaffold	0.61 ± 0.04	0.67 ± 0.03	30.972 ± 1.290	182.220 ± 10.819	5.880 ± 0.131

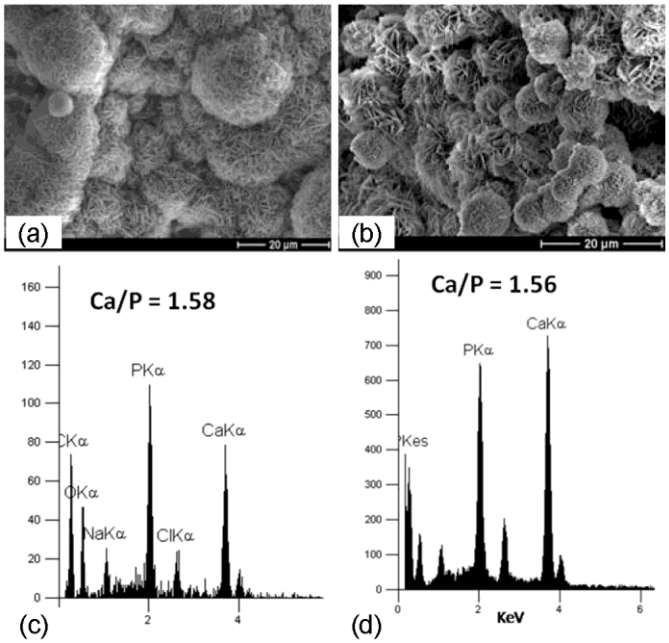

Fig 6.2 SEM images and EDS data of coated minerals of PLLA (a, c) and PCL (b, d) scaffolds. SEM images show that nucleated bone like mineral structures on the coated PLLA and PCL scaffolds (a, b). EDS data confirmed that existence of calcium and phosphorous peaks (c, d)

6.4.2 Crystallinity

Crystallinity data of the coated and uncoated scaffolds was shown in Fig 6.3. The uncoated PLLA scaffold showed many peaks due to its semi-crystalline structures (Fig 6.3 (b)), while the coated PLLA scaffold shows their peak at 2θ = 25.9 and 31.95 (Fig 6.3 (a)). The peak at 2θ = 31.95 is wider than that of 2θ = 25.9 due to the combination of crystal peaks of mineral and polymer. In contrast to non-coated PLLA scaffold, non-coated PCL scaffolds did not show crystal peaks of polymer (Fig 6.3 (d)). The coated PCL also show their crystal peaks at 2θ = 25.9 and 31.95 (Fig 6.3 (c)).

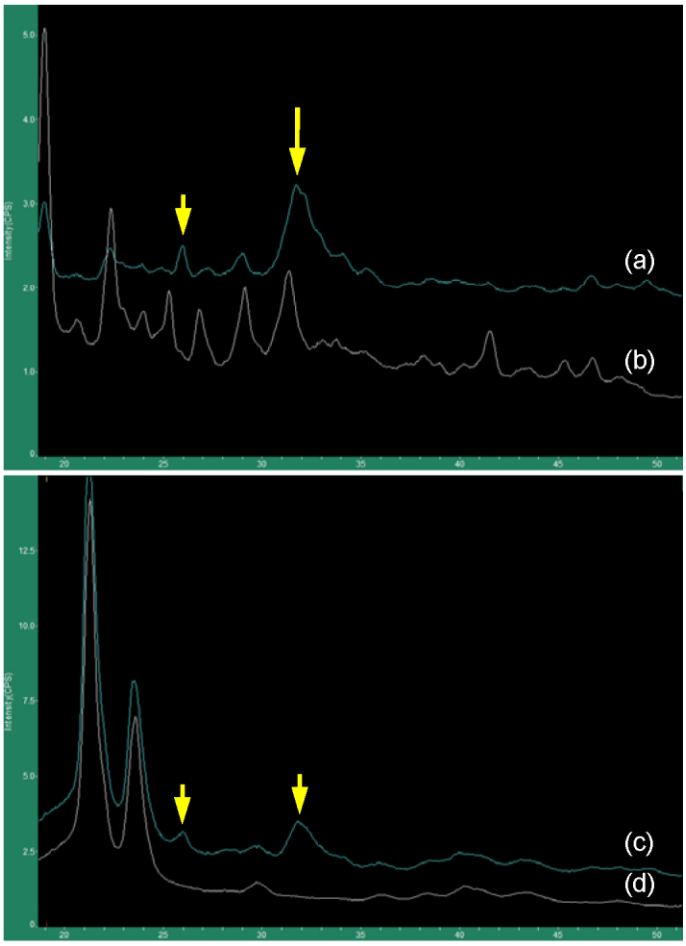

Fig 6.3 XRD data of Coated PLLA (a), Uncoated PLLA (b), Coated PCL (c) and Uncoated PCL (d)., and the coated PLLA scaffold shows their peak at 2θ = 25.9 and 31.95 (a), and the uncoated PLLA scaffold shows many peaks due to its semi-crystalline structures (b). The coated PCL also show their crystal peaks at 2θ = 25.9 and 31.95 (c).

6.4.3 BMP-7 expression *in vitro*

BMP-7 secretion from the transduced HGFs was measured *in vitro* for up to 28days (Fig 6.4). All of the scaffold groups showed expression of BMP-7 up to 4 weeks, and the amount of secretion decreased for longer time points. There is no significant difference between groups. The coated PLLA scaffolds had less amount and greater standard deviation.

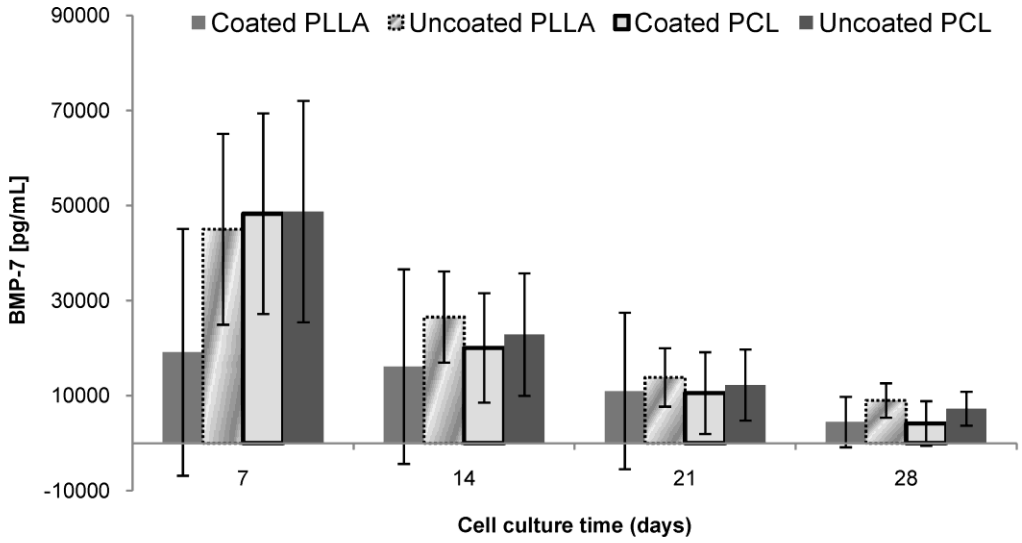

Fig 6.4 BMP-7 secretion from the scaffolds seeded with BMP-7 transduced HGFs using ELISA.

6.4.4 Bone formation

The scaffolds with BMP-7 virus transduced HGFs showed bone formation and were covered by bone tissues after 3 and 10 weeks implantations from μ-CT images (Fig 6.6), while scaffolds with GFP transduced HGFs did not have a boney shell. The results of qPCR show that osteogenic gene expression from all of scaffold groups with transduced HGFs (Fig 6.5). There is a small amount of bone ingrowth into the scaffold constructs at 3 weeks, and there is no significant difference between the groups (Fig 6.6 (a-d)). At 10 weeks, the coated scaffolds showed more bone ingrowth than the non-coated scaffolds, and the bone formation followed the architectures of the scaffolds (Fig 6.6 (e-h)).

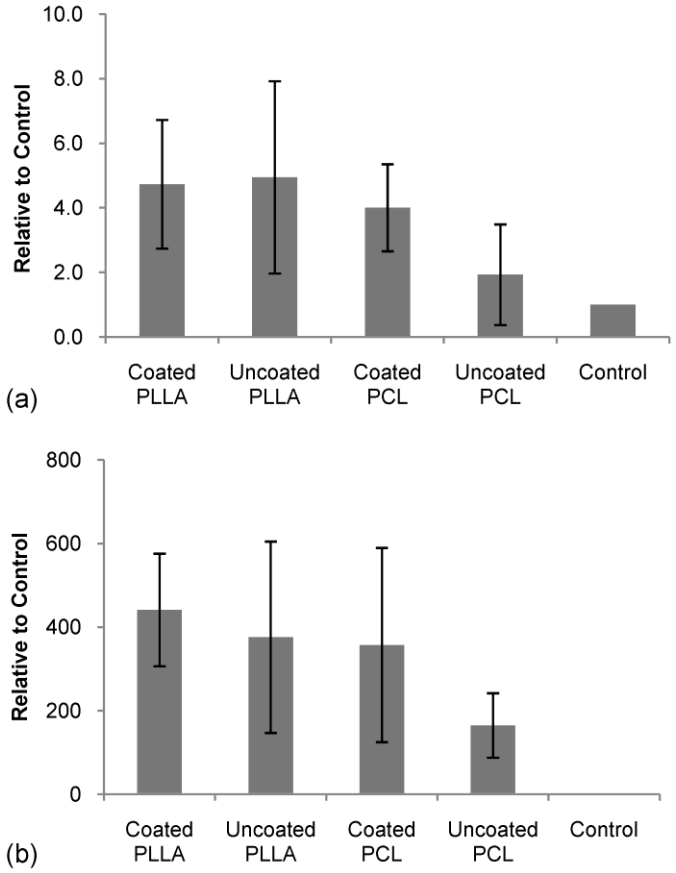

Fig 6.5 Runx 2 (a) and OCN (b) expression at 10 weeks.

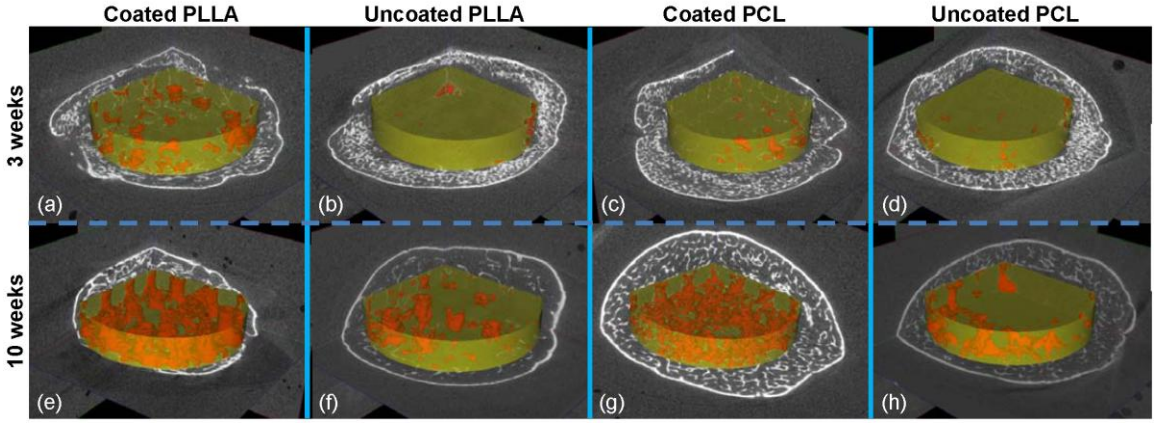

Fig 6.6 Bone ingrowth into Coated PLLA (a,e), Uncoated PLLA (b, f), Coated PCL (e, g) and Uncoated PCL (d, h) at 3 and 10 weeks implantation. There was a little bone ingrwoth in the all scaffolds at 3 weeks (e-h). Advanced bone ingrowth followed the designed architectures of the coated PLLA and PCL scaffolds at 10 weeks (e, h).

Bone ingrowth was calculated as the amount of bone in the ROI (Fig 6.7 (a)), and tissue mineral density of ROI was also calculated (Fig 6.7 (b)). There was no significant difference between the groups at 3 weeks. At 10 weeks, the coated PLLA and PCL scaffolds had significantly greater bone ingrowth than uncoated PLLA, and PCL scaffolds. In addition, bone ingrowth of the coated PLLA scaffolds was significantly higher than that of non-coated PCL scaffolds. All of the scaffolds increased their tissue mineral density from 3 to 10 weeks. Tissue mineral density of the coated PLLA was significantly higher than that of the non-coated PLLA scaffolds which indicates that mineral coatings may also help to increase mineralization of tissues on PLLA scaffolds.

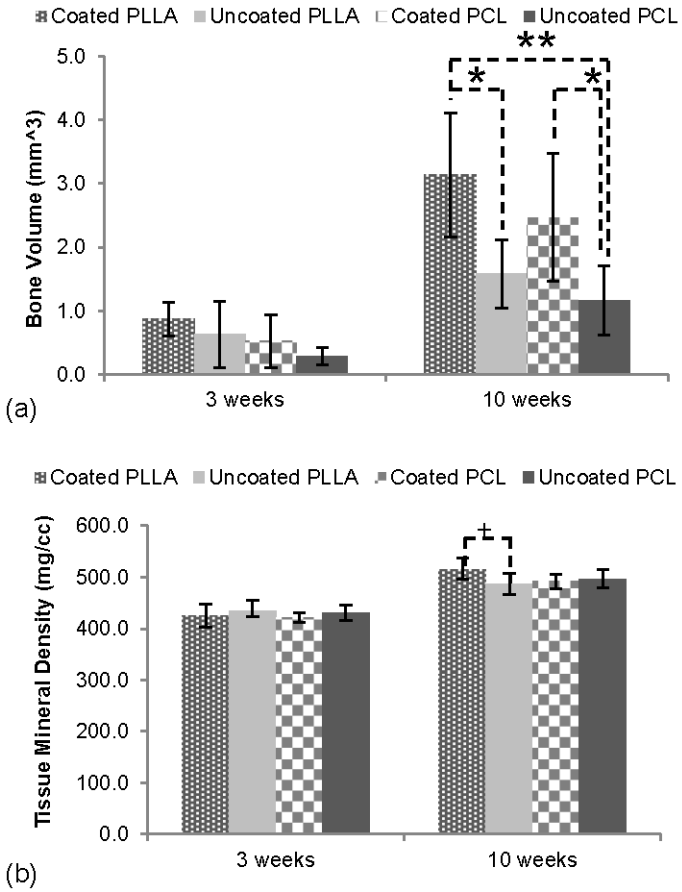

Fig 6.7 Calculated bone ingrowth (a) and tissue mineral density (b) in the ROI. There is no significant difference between the scaffolds at 3 weeks. And, the coated PLLA and PCL scaffolds showed significantly more bone ingrowth than the uncoated PLLA and PCL scaffolds at 10 weeks.

6.4.5 Deposition of biomineral coating

Layers of mineral coatings were observed through the study period on control scaffolds seeded with GFP transduced HGFs (Fig 6.8 (a-d)), and slightly higher intensity of coatings were observed at 10 weeks compared to 3 weeks. The amount of deposited mineral layers calculated from μ-CT also show that more deposition at 10 weeks than 3weeks period (Fig 6.8 (e)). All of these data indicates that the more mineral deposition occurred in our study instead of mineral dissolution.

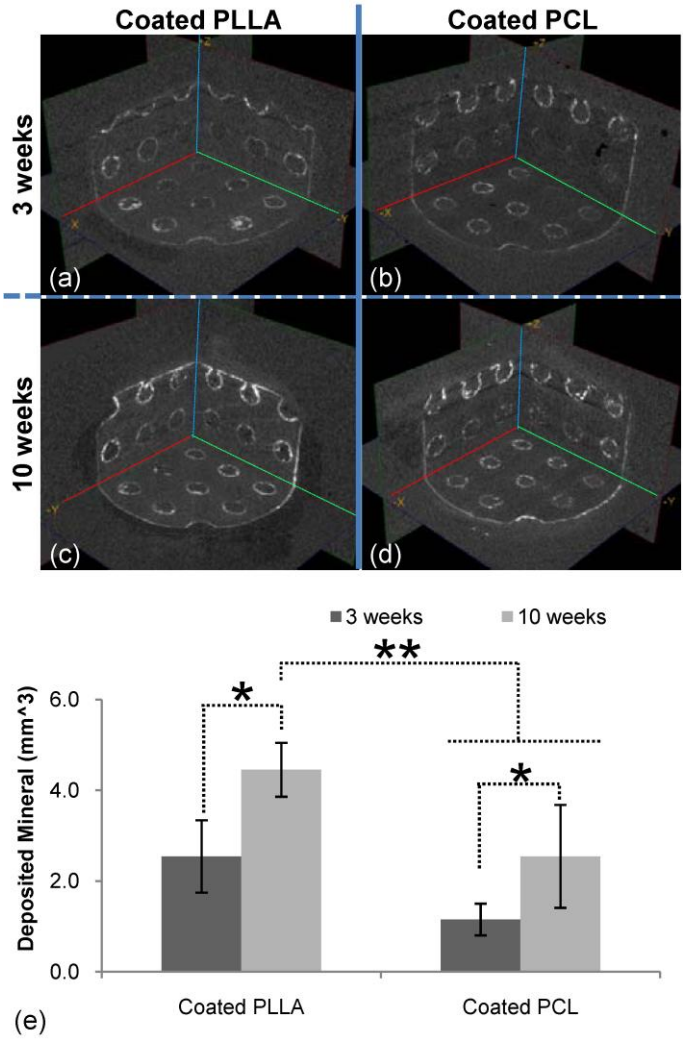

Fig 6.8 Scaffolds seeded with GFP transduced HGFs had no bone shell. The existence of mineral layers on the surface of the coated PLLA and PCL scaffolds were observed at 3 (a, b) and 10 (c, d) weeks. Deposition of mineral was calculated by CT, and there are increases of mineral from 3 to 10 weeks (e).

6.4.6 Histology data

Harvested scaffolds with BMP-7 transduced HGFs were evaluated using histological techniques, H&E (Fig 6.9 and Fig 6.10 (a-d)) and Masson's Trichrome (Fig 6.9 and Fig 6.10 (e-h)). H&E staining shows that there was little bone formation in the pores of the coated and uncoated PLLA and PCL scaffolds at 3weeks (Fig 6.9 and Fig 6.10 (a, b)). However, the pores of the coated scaffolds contained blood vessel like tissues, which may be precursor of bone ingrowth (Fig 6.9 and Fig 6.10 (a)). In contrast, the uncoated scaffolds showed few blood vessels (Fig 6.9 and Fig 6.10 (b)). Then, well developed bone tissue ingrowths was observed in the pores of the coated PLLA and PCL scaffolds at 10 weeks (Fig 6.9 and Fig 6.10 (c)). The bone tissue followed the pore architectures of the scaffolds containing bone marrow like tissues. The uncoated PLLA and PCL did not have much bone ingrowth at 10 weeks point and contains fat-like tissues in the pores (Fig 6.9 and Fig 6.10 (d)). Masson's trichrome staining also showed little bone tissue in the pores of coated and uncoated PLLA and PCL scaffolds at 3 weeks (Fig 6.9 and Fig 6.10 (e, f)). At 10 weeks, however, the coated PLLA and PCL scaffolds had well developed bone tissue containing osteoid, unmineralized matrix (Fig 6.9 and Fig 6.10 (g)), indicating active deposition of bone minerals in comparison to the uncoated scaffolds.

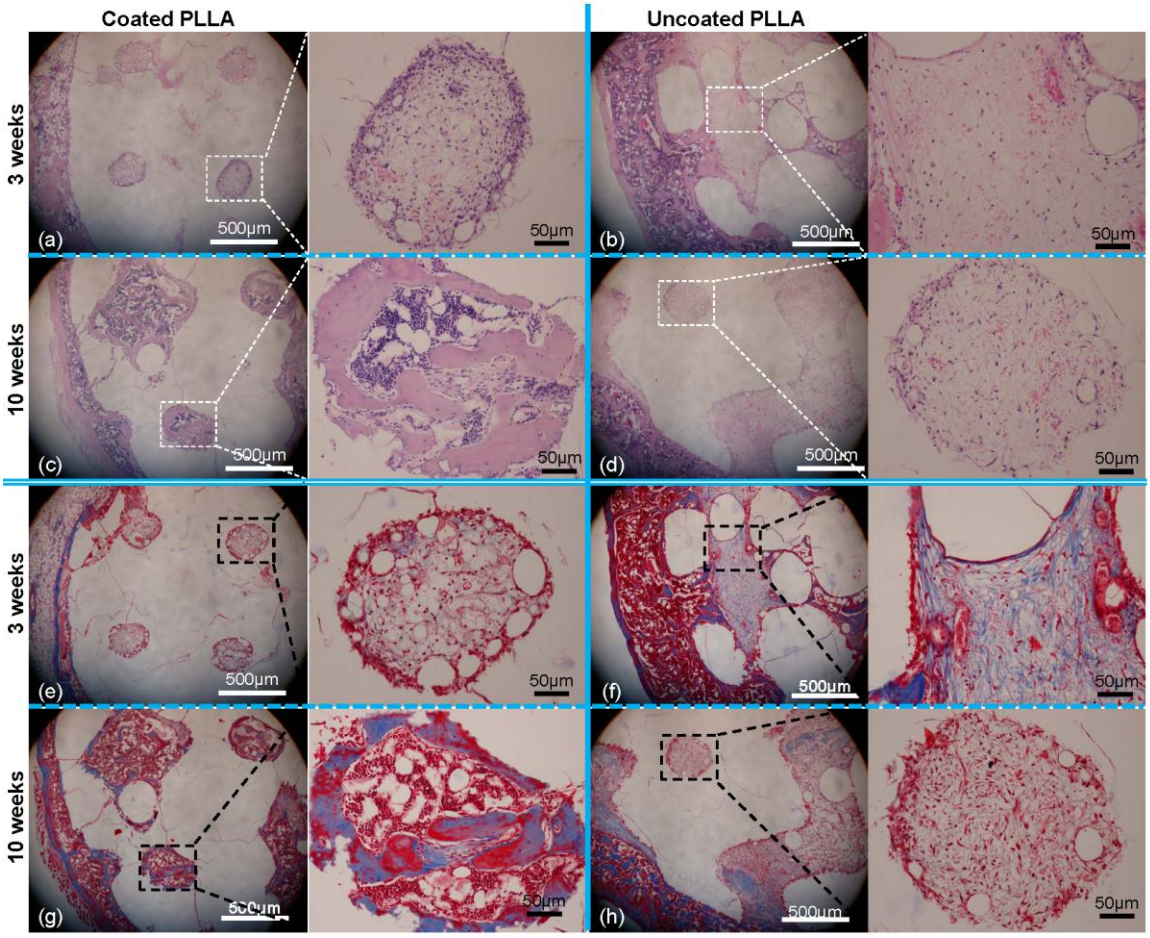

Fig 6.9 Histological evaluation of implanted PLLA scaffolds. H&E staining shows that little bone ingrowth in both the coated and uncoated PLLA scaffolds (a, b). At 10 weeks, there are well developed bone ingrowth containing marrow like tissues in the coated PLLA scaffolds (c), and more fibrous like tissues in the uncoated PLLA scaffolds (d). Masson's Trichrome staining also shows similar results to the H&E staining, and further show the osteoid deposition in the coated PLLA scaffolds at 10 weeks.

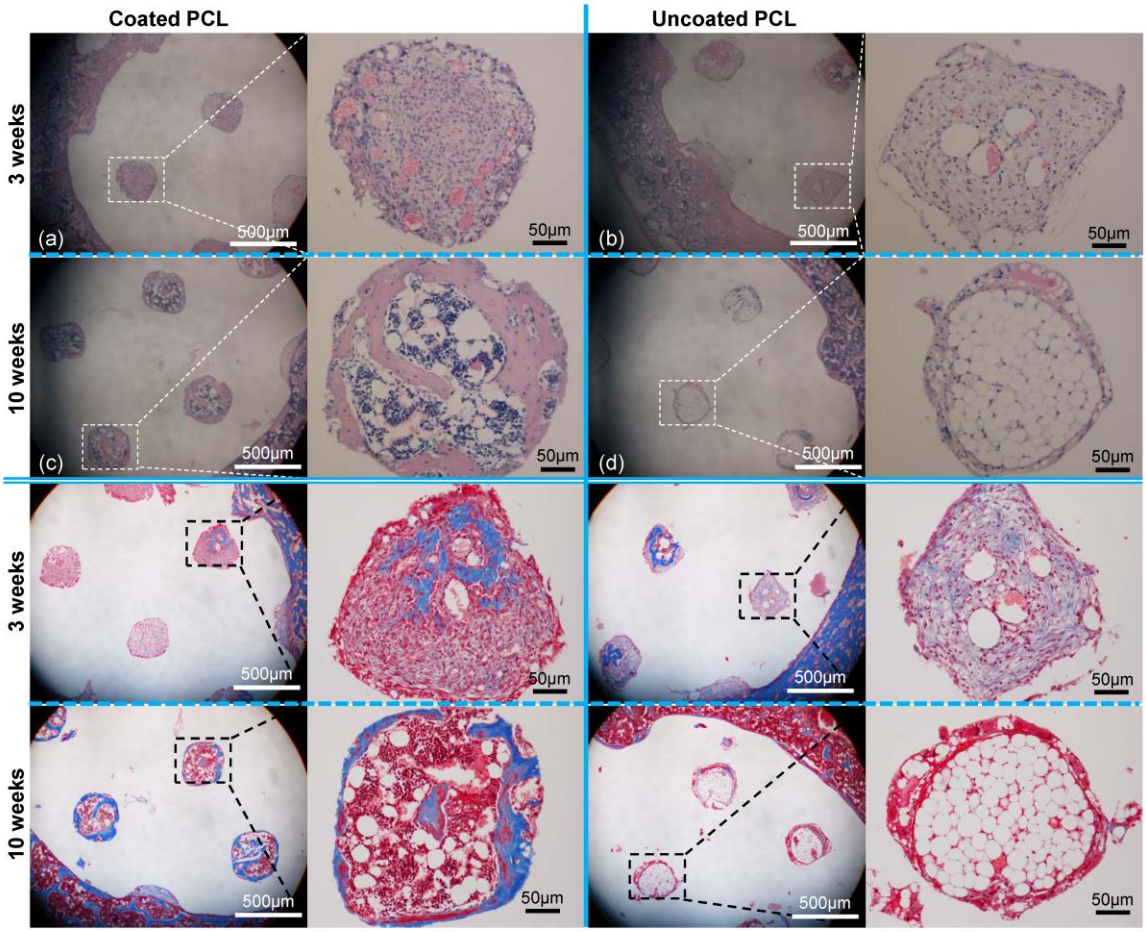

Fig 6.10 Histological evaluation of implanted PCL scaffolds. H&E staining shows that little bone ingrowth in both the coated and uncoated PCL scaffolds, however, more blood vessel like tissues in the coated PCL scaffolds at 3 weeks (a, b). At 10 weeks, there are well developed bone ingrowth containing marrow like tissues in the coated PCL scaffolds (c), and more fibrous like tissues in the uncoated PCL scaffolds (d). Masson's Trichrome staining also shows similar results to the H&E staining, and further show the osteoid deposition in the coated PCL scaffolds at 10 weeks.

6.4.7 Mechanical testing of scaffolds with and without bone tissue

Elastic modulli of scaffolds with BMP-7 transduced HGFs were determined at both time points (Fig 6.11 (a)). Elastic moduli of both coated and uncoated PLLA scaffolds decreased after scaffold implantations from 0 to 3 weeks due to polymer degradation ($p=0.046$ and 0.001, respectively). The moduli of the coated PLLA scaffolds significantly increased from 3 to 10 weeks ($p = 0.046$), however, the increase of uncoated PLLA scaffolds was not significant ($p = 0.590$). Uncoated PCL scaffolds also

significantly increased their mechanical properties from 3 to 10 weeks ($p = 0.028$). Although the coated PCL scaffolds did not have significant improvement of their mechanical properties, the p value was close to the significant level ($p = 0.073$).

Elastic moduli of the scaffolds with GFP transduced HGFs were also tested (Fig 6.11 (b)). Only uncoated PLLA scaffold showed significant decrease of moduli from 0 to 3 weeks. Moduli of coated and uncoated PLLA scaffold also increased from 3 to 10 weeks, but not significantly, maybe, due to more fibrous tissue formation due to polymer degradation. The coated and uncoated PCL scaffolds show constant moduli throughout the study period.

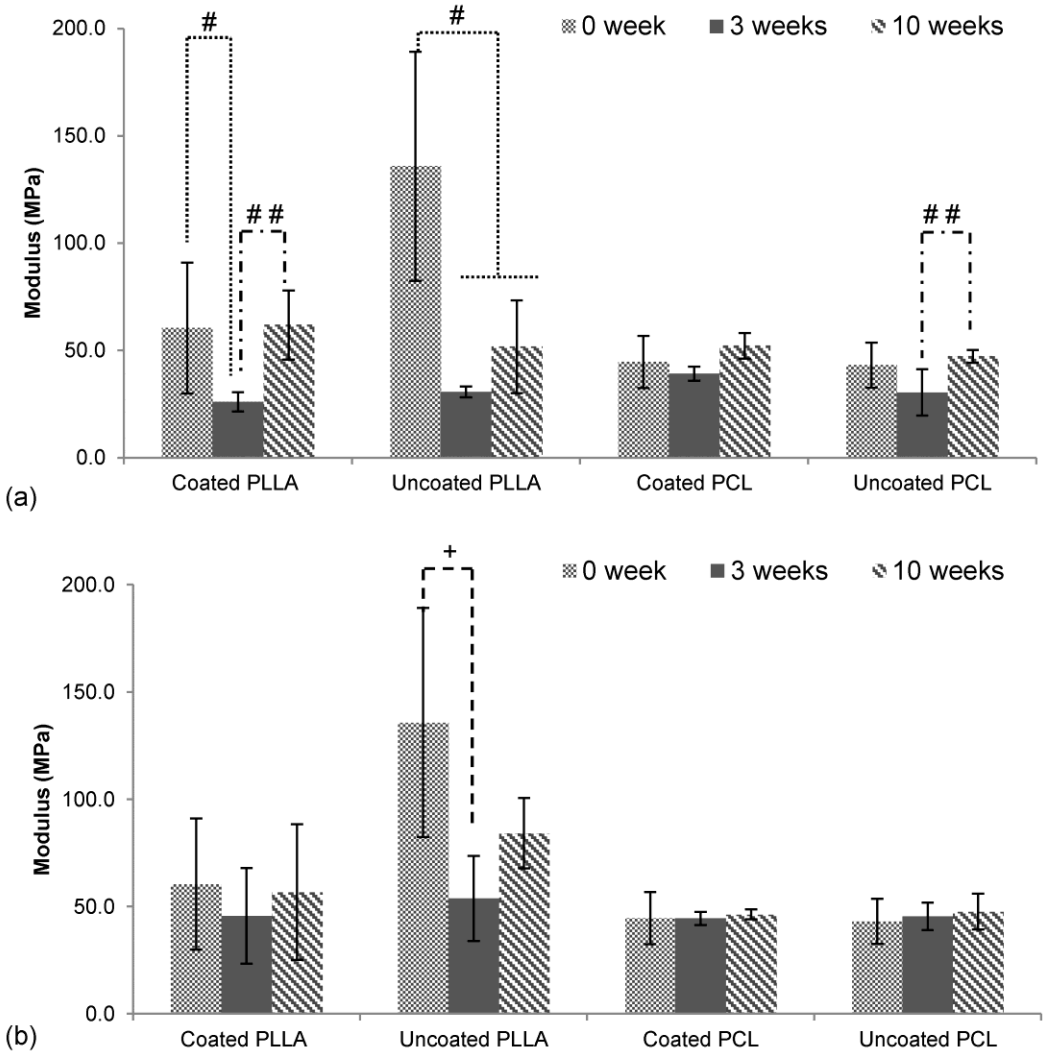

Fig 6.11 Elastic moduli of the scaffolds with generated bone tissues (a) and non-bone tissues (b). The coated and uncoated PLLA scaffolds lost their mechanical properties from 0 to 3 weeks due to the degradation of polymers. And the mechanical properties of the coated PLLA scaffolds increased significantly from 3 to 10 weeks, while the uncoated PLLA did not have significant increase (a). Both coated and uncoated PCL scaffolds showed significant or close to significant increase of mechanical properties (a).

6.5 Discussions

Computer aided tissue engineering has been developed to fabricate scaffolds with precisely controlled architectures to match anatomical shapes and achieve desired properties for clinical applications. Many SFF techniques enable fabrication of designed scaffolds using biodegradable materials, including PLLA, PLGA and PCL. However,

their hydrophobicity and poor osteoconductivity needed to be overcome to enhance bone ingrowth. In addition, although some research showed biomineral coatings on PLLA and PCL scaffolds [37,38], no study has performed coating SFF PLLA and PCL scaffolds with the same architecture. To achieve fully developed bone ingrowth in porous scaffolds, we developed the combination of SFF scaffolds and mSBF techniques using two different polymers, PLLA and PCL, fabricated using identical process.

To test our hypothesis, PLLA and PCL scaffolds need to have the identical structures and the mineral coating should cover the entire scaffold surfaces. μ-CT data demonstrated that the fabricated PLLA and PCL scaffolds had the identical structure and orthogonally interconnected pores or channels, which agreed with our previous SFF scaffold studies including PLLA, 50:50PLGA, and PCL scaffolds [7,39]. The μ-CT was also used to confirm that entire surface of the porous scaffolds were successfully coated with mineral layers [40]. These fully designed interconnected channels also allowed infiltrating mSBF solution into the center of the scaffolds to allow biomineral layers to cover the center of scaffolds. This is an advantage of SFF scaffolds compared to salt leaching scaffold which tend to have less open pore structures terminating effectively coat at the center of the scaffolds [35].

mSBF has been studied to grow mineral layers on biodegradable materials [33,41,42], and SFF scaffolds [43]. The coated mineral layers have plate-like morphology which is similar to human bone tissues. EDS data shows calcium and phosphate peaks on the coated mineral which indicated both coated PLLA and PCL scaffolds had nucleated mineral, similar Ca/P ratios to each other which is near that of hydroxyapatite [21,41].

Both coated scaffolds showed crystal peaks of mineral at 26 º and 32º which correspond to the (002) plane and (211) (112) planes of apatite [44]. Coated PLLA showed a wider peak at 32º where crystal peaks of PLLA also exists, and many peaks besides crystal peaks due to crystal structure of PLLA polymer, which was confirmed from the XRD data of uncoated PLLA scaffolds [45]. In contrast, coated PCL showed two peaks from the PCL polymer around 21º and 24º, similar to a previous study [46].

To generate bone tissue in an ectopic site, *ex vivo* gene therapy with adenovirus BMP-7 was used. *In vitro* BMP-7 secretion results showed that secretion decreased at longer time points, which is different than the consistent secretion of BMP-2 from adenovirus transduced HGFs up to 2 weeks *in vitro* [47]. As similar to our previous scaffolds studies, bone shells formed surrounding the scaffolds [39,48,49]. qPCR data show signals of early osteoblast differentiation with Runx2 and late tissue mineralization with OCN, which support the fact that the bone shells contain osteogenic factors [50,51]. In contrast, the control groups with GFP transduced HGFs showed very little bone gene expression and did not generate bone shells. The groups with BMP-7 transdueced HGFs only contributed the bone formation.

In the μ-CT images, generated bone tissues have similar density to initially coated mineral layers, and it is difficult to separate generated bone tissues from original mineral coating. Since most of mineral layers have lower threshold value than 1100, we chose the threshold value (1100) to determine bone tissues in the scaffolds.

From the μ-CT data, no significant difference in bone ingrowth in the coated scaffolds was observed at 3 weeks compared to the uncoated scaffolds. The mineral coated scaffolds showed significantly greater bone ingrowth at 10 weeks which agrees with

some previous studies. Mineralized porous PLGA scaffolds showed higher bone formation than the non-mineralized scaffolds in rat cranium critical defects [33]. Improvements of bone formation were also found using mineralized PLGA microspheres implanted into mice subcutaneous sites [34]. A significant advantage of combining SFF with biomineralization is the completely connected growth bone, something difficult with salt leached scaffolds [35]. Thus, SFF scaffolds have designed fully connected channels which would allow to body fluid infiltration into the center of the scaffolds to support tissue ingrowth [6,8-10].

In *ex vivo* gene therapy, large bony shells tend to form outside of the scaffolds, and the layers of tissues may prevent diffusion of nutrients into the center of the scaffolds [52]. This may also cause accumulation of acidic by-product inside of the implants, which could prohibit cell migration and tissue ingrowth. However, histological images shows the coated scaffolds had more blood vessel-like tissue containing bone marrow compared with the uncoated scaffolds at 3 weeks. This may enhance bone cells in the marrow like space to lead advanced bone ingrowth at 10 weeks since invasion of blood vessel helps tissue ingrowth.

The mechanisms of mineral coating on advanced bone formation have not been fully understood. Biomineral coating increase hydrophilicity PLLA and PCL scaffolds, which may help cell adhesion, migration and proliferation [53-55]. Calcium phosphate mineral has been reported their capability of protein adsorption for cell adhesion and other bone specific proteins [56,57]. The proteins, especially fibronectin and vitronectin, are critical for osteoblasts to attach on biomaterials and produce extracellular matrices. In addition, BMP-7 proteins secreted from the HGFs may be attached on mineral coating to help

progression of osteogenesis. Existence of calcium ion from soluble calcium phosphate coating is reported to induce cell proliferation and differentiation [58].

Our result also differs from some of the previous studies using biodegradable scaffolds. For example, SFF PCL scaffolds implanted in subcutaneous sites did not show significant bone formation on biomineral coated scaffolds [27]. Another study showed that improved bone contact on starch-based biodegradable scaffolds at 3weeks but not 6 weeks [59]. These controversial results may be due to quality of biomineral layers, such as crystalinity of minerals [60].

Dissolution or absorption of biomineral layers has been discussed effect of cells, such as osteoclasts and macrophages, or effect of media *in vitro* or *in vivo* [61,62]. The scaffolds seeded with GFP transduced HGFs did not generate any bone shells and showed the presence of the biomineral layers of the scaffolds over the study period. This agrees with the fact that apatite layers were observed in the soft tissue after 30 weeks [32]. The μ-CT data in GFP seeded scaffolds demonstrated an increasing mineral layer accumulation on the scaffold, similar to previously seen carbonate apatite absorption in rat ectopic sites [62]. In contrast, mineral coating in orthotopic sites decreased their thickness although it existed at 24 weeks [24]. This can be explained by absence of osteoclasts in the ectopic sites which contribute resorption of mineral layers [24,32].

Although both PLLA and PCL scaffolds were treated with NaOH in the same manner to functionalize their surfaces for biomineral coating, only PLLA scaffold had significantly reduced mechanical properties. This indicates that only PLLA degrades due to NaOH treatment which has been used to test hydrolytic degradation of PLLA *in vitro* [63]. Implanted PLLA scaffolds also lost their mechanical properties from 0 to 3 weeks

due to degradation of polymer which is similar to our previous studies. Comparing mechanical properties of PLLA with and without bone tissues, PLLA scaffolds with bone tissue show lower mechanical properties which indicate that formed bone tissues inhibited acid by-products from PLLA and accelerated degradation.

Mechanical properties of implanted scaffolds in this study tend to increase as longer implantation time due to increase of tissue mineral densities. Advanced bone ingrowth increased mechanical properties of the coated PLLA compared with the uncoated PLLA. This results agree with the previous studies showing biomineral coated titanium implants showed less fibrous tissue and more bone contact on the surface, and had greater mechanical properties than uncoated implants [32,64]. In contrast, there is not much difference between the p values of the coated and uncoated PCL scaffolds. This data indicates that the coated and uncoated PLLA scaffolds lost their mechanical properties in the animal due to their degradation, and then advanced bone ingrowth support the mechanical properties of the coated PLLA scaffolds. PCL scaffolds with slower degradation may maintain their mechanical properties over this study time period, and the mechanical properties of bone tissues in the scaffolds may not sufficient to influence PCL scaffolds moduli.

The combination of SFF scaffolds and biomineral coating using mSBF presents further advantages for porous scaffolds for clinical applications. Although ceramic scaffolds, such as tricalcium phosphate or HA have been used as bone scaffolds due to their good osteoconductivity, their brittle mechanical properties as well as their resorption rates are still problems. For example, tricalcium phosphate with Ca:P ratio of 1.5 dissolves too fast, while hydroxyapatite with a Ca:P raito of 1.67 does not dissolve [65].

Some studies suggested that fabrication of polymer and TCP composite scaffolds using SFF techniques improved bone formation *in vivo* [48,66,67]. Compared with the previous techniques, the combination of SFF scaffolds and biomineral coating has significant advantages. This approach would improve and control scaffold properties since SFF scaffolds have proven control of mechanical properties and degradation based on their architectures and biomineral coatings have proven osteoconductivity. Furthermore, these techniques allow incorporation and controlled release of multiple proteins or DNAs to improve further bone formation [68,69].

Although we have shown the importance of biomineral coatings on bone formation, the bone tissue were generated in ectopic sites without any loadings. Examining biomineral coated scaffolds in orthotopic sites is necessary. Another advantage of mineral coatings is that degradation ratio of the coated scaffolds may be different than that of uncoated scaffolds. The degradation of PLLA creates acidic environments which causes autocatalysis of PLLA and accelerate its degradation. However, ionic calcium creates an alkali condition which may buffer the acidic environment and slow the degradation speed [34].

6.6 Conclusions

This study examined the combination of computer aided engineered scaffolds and biomineral coatings. SFF scaffolds made of PLLA and PCL were successfully coated with biomineral layers using the same mSBF procedures. The biomineral coated scaffold showed improved *in vivo* bone formation, and the bone tissues were fully connected and follow the scaffold architectures. PLLA scaffolds demonstrated increased mechanical

properties due to the increased bone ingrowth compensating for the loss of mechanical properties due to polymer degradation. Mineral coatings on the scaffolds were present *in vivo* over this study. In future research, dissolution and precipitation of mineral coating on bone formation needs to be further examined. In addition, biomineral coatings need to be fine-tuned depending on scaffold materials to improve further bone formation as well as control scaffold degradation.

References

[1] Hutmacher DW. Scaffold design and fabrication technologies for engineering tissues--state of the art and future perspectives. J Biomater Sci Polym Ed 2001;12:107-124.

[2] Sun W, Starly B, Darling A, Gomez C. Computer-aided tissue engineering: application to biomimetic modelling and design of tissue scaffolds. Biotechnol Appl Biochem 2004;39:49-58.

[3] Hutmacher DW, Sittinger M, Risbud MV. Scaffold-based tissue engineering: rationale for computer-aided design and solid free-form fabrication systems. Trends Biotechnol 2004;22:354-362.

[4] Hollister SJ. Porous scaffold design for tissue engineering. Nat Mater 2005;4:518-524.

[5] Martins A, Chung S, Pedro AJ, Sousa RA, Marques AP, Reis RL, et al. Hierarchical starch-based fibrous scaffold for bone tissue engineering applications. J Tissue Eng Regen Med 2009;3:37-42.

[6] Melchels FP, Barradas AM, van Blitterswijk CA, de Boer J, Feijen J, Grijpma DW. Effects of the architecture of tissue engineering scaffolds on cell seeding and culturing. Acta Biomater 2010;6:4208-4217.

[7] Saito E, Kang H, Taboas JM, Diggs A, Flanagan CL, Hollister SJ. Experimental and computational characterization of designed and fabricated 50:50 PLGA porous scaffolds for human trabecular bone applications. J Mater Sci Mater Med 2010;21:2371-2383.

[8] Choi SW, Zhang Y, Xia Y. Three-dimensional scaffolds for tissue engineering: the importance of uniformity in pore size and structure. Langmuir 2010;26:19001-19006.

[9] Lee KW, Wang S, Dadsetan M, Yaszemski MJ, Lu L. Enhanced cell ingrowth and proliferation through three-dimensional nanocomposite scaffolds with controlled pore structures. Biomacromolecules 2010;11:682-689.

[10] Kim K, Dean D, Wallace J, Breithaupt R, Mikos AG, Fisher JP. The influence of stereolithographic scaffold architecture and composition on osteogenic signal expression with rat bone marrow stromal cells. Biomaterials 2011;32:3750-3763.

[11] Middleton JC, Tipton AJ. Synthetic biodegradable polymers as orthopedic devices. Biomaterials 2000;21:2335-2346.

[12] Morent R, De Geyter N, Desmet T, Dubruel P, Leys C. Plasma Surface Modification of Biodegradable Polymers: A Review. Plasma Process Polym 2011;8:171-190.

[13] Hutmacher D, Hurzeler MB, Schliephake H. A review of material properties of biodegradable and bioresorbable polymers and devices for GTR and GBR applications. Int J Oral Maxillofac Implants 1996;11:667-678.

[14] Pierucci A, Duek EA, de Oliveira AL. Expression of basal lamina components by Schwann cells cultured on poly(lactic acid) (PLLA) and poly(caprolactone) (PCL) membranes. J Mater Sci Mater Med 2009;20:489-495.

[15] Rezwan K, Chen QZ, Blaker JJ, Boccaccini AR. Biodegradable and bioactive porous polymer/inorganic composite scaffolds for bone tissue engineering. Biomaterials 2006;27:3413-3431.

[16] Smith MH, Flanagan CL, Kemppainen JM, Sack JA, Chung H, Das S, et al. Computed tomography-based tissue-engineered scaffolds in craniomaxillofacial surgery. Int J Med Robot 2007;3:207-216.

[17] Hutmacher DW, Cool S. Concepts of scaffold-based tissue engineering--the rationale to use solid free-form fabrication techniques. J Cell Mol Med 2007;11:654-669.
[18] Chou YF, Huang W, Dunn JC, Miller TA, Wu BM. The effect of biomimetic apatite structure on osteoblast viability, proliferation, and gene expression. Biomaterials 2005;26:285-295.
[19] Kretlow JD, Mikos AG. Review: mineralization of synthetic polymer scaffolds for bone tissue engineering. Tissue Eng 2007;13:927-938.
[20] Liu Y, Wu G, de Groot K. Biomimetic coatings for bone tissue engineering of critical-sized defects. J R Soc Interface 2010;7 Suppl 5:S631-47.
[21] Murphy WL, Mooney DJ. Bioinspired growth of crystalline carbonate apatite on biodegradable polymer substrata. J Am Chem Soc 2002;124:1910-1917.
[22] Suarez-Gonzalez D, Barnhart K, Saito E, Vanderby R,Jr, Hollister SJ, Murphy WL. Controlled nucleation of hydroxyapatite on alginate scaffolds for stem cell-based bone tissue engineering. J Biomed Mater Res A 2010;95:222-234.
[23] Barrere F, van der Valk CM, Dalmeijer RA, Meijer G, van Blitterswijk CA, de Groot K, et al. Osteogenecity of octacalcium phosphate coatings applied on porous metal implants. J Biomed Mater Res A 2003;66:779-788.
[24] Barrere F, van der Valk CM, Meijer G, Dalmeijer RA, de Groot K, Layrolle P. Osteointegration of biomimetic apatite coating applied onto dense and porous metal implants in femurs of goats. J Biomed Mater Res B Appl Biomater 2003;67:655-665.
[25] Li P. Biomimetic nano-apatite coating capable of promoting bone ingrowth. J Biomed Mater Res A 2003;66:79-85.
[26] Murphy WL, Kohn DH, Mooney DJ. Growth of continuous bonelike mineral within porous poly(lactide-co-glycolide) scaffolds in vitro. J Biomed Mater Res 2000;50:50-58.
[27] Chim H, Hutmacher DW, Chou AM, Oliveira AL, Reis RL, Lim TC, et al. A comparative analysis of scaffold material modifications for load-bearing applications in bone tissue engineering. Int J Oral Maxillofac Surg 2006;35:928-934.
[28] Holmbom J, Sodergard A, Ekholm E, Martson M, Kuusilehto A, Saukko P, et al. Long-term evaluation of porous poly(epsilon-caprolactone-co-L-lactide) as a bone-filling material. J Biomed Mater Res A 2005;75:308-315.
[29] Gorna K, Gogolewski S. Preparation, degradation, and calcification of biodegradable polyurethane foams for bone graft substitutes. J Biomed Mater Res A 2003;67:813-827.
[30] Kim SS, Park MS, Gwak SJ, Choi CY, Kim BS. Accelerated bonelike apatite growth on porous polymer/ceramic composite scaffolds in vitro. Tissue Eng 2006;12:2997-3006.
[31] Lickorish D, Guan L, Davies JE. A three-phase, fully resorbable, polyester/calcium phosphate scaffold for bone tissue engineering: Evolution of scaffold design. Biomaterials 2007;28:1495-1502.
[32] Nagano M, Kitsugi T, Nakamura T, Kokubo T, Tanahashi M. Bone bonding ability of an apatite-coated polymer produced using a biomimetic method: a mechanical and histological study in vivo. J Biomed Mater Res 1996;31:487-494.
[33] Murphy WL, Simmons CA, Kaigler D, Mooney DJ. Bone regeneration via a mineral substrate and induced angiogenesis. J Dent Res 2004;83:204-210.

[34] Kang SW, Yang HS, Seo SW, Han DK, Kim BS. Apatite-coated poly(lactic-co-glycolic acid) microspheres as an injectable scaffold for bone tissue engineering. J Biomed Mater Res A 2008;85:747-756.
[35] Du C, Meijer GJ, van de Valk C, Haan RE, Bezemer JM, Hesseling SC, et al. Bone growth in biomimetic apatite coated porous Polyactive 1000PEGT70PBT30 implants. Biomaterials 2002;23:4649-4656.
[36] Lopez-Heredia MA, Sohier J, Gaillard C, Quillard S, Dorget M, Layrolle P. Rapid prototyped porous titanium coated with calcium phosphate as a scaffold for bone tissue engineering. Biomaterials 2008;29:2608-2615.
[37] Chen J, Chu B, Hsiao BS. Mineralization of hydroxyapatite in electrospun nanofibrous poly(L-lactic acid) scaffolds. J Biomed Mater Res A 2006;79:307-317.
[38] Araujo JV, Martins A, Leonor IB, Pinho ED, Reis RL, Neves NM. Surface controlled biomimetic coating of polycaprolactone nanofiber meshes to be used as bone extracellular matrix analogues. J Biomater Sci Polym Ed 2008;19:1261-1278.
[39] Roosa SM, Kemppainen JM, Moffitt EN, Krebsbach PH, Hollister SJ. The pore size of polycaprolactone scaffolds has limited influence on bone regeneration in an in vivo model. J Biomed Mater Res A 2010;92:359-368.
[40] Oliveira AL, Malafaya PB, Costa SA, Sousa RA, Reis RL. Micro-computed tomography (micro-CT) as a potential tool to assess the effect of dynamic coating routes on the formation of biomimetic apatite layers on 3D-plotted biodegradable polymeric scaffolds. J Mater Sci Mater Med 2007;18:211-223.
[41] Jongpaiboonkit L, Franklin-Ford T, Murphy WL. Growth of hydroxyapatite coatings on biodegradable polymer microspheres. ACS Appl Mater Interfaces 2009;1:1504-1511.
[42] Murphy WL, Hsiong S, Richardson TP, Simmons CA, Mooney DJ. Effects of a bone-like mineral film on phenotype of adult human mesenchymal stem cells in vitro. Biomaterials 2005;26:303-310.
[43] Arafat MT, Lam CX, Ekaputra AK, Wong SY, Li X, Gibson I. Biomimetic composite coating on rapid prototyped scaffolds for bone tissue engineering. Acta Biomater 2011;7:809-820.
[44] Chen Y, Mak AF, Li J, Wang M, Shum AW. Formation of apatite on poly(alpha-hydroxy acid) in an accelerated biomimetic process. J Biomed Mater Res B Appl Biomater 2005;73:68-76.
[45] Yokoyama Y, Oyane A, Ito A. Biomimetic coating of an apatite layer on poly(L-lactic acid); improvement of adhesive strength of the coating. J Mater Sci Mater Med 2007;18:1727-1734.
[46] Kim HW, Knowles JC, Kim HE. Development of hydroxyapatite bone scaffold for controlled drug release via poly(epsilon-caprolactone) and hydroxyapatite hybrid coatings. J Biomed Mater Res B Appl Biomater 2004;70:240-249.
[47] Shin JH, Kim KH, Kim SH, Koo KT, Kim TI, Seol YJ, et al. Ex vivo bone morphogenetic protein-2 gene delivery using gingival fibroblasts promotes bone regeneration in rats. J Clin Periodontol 2010;37:305-311.
[48] Lin CY, Schek RM, Mistry AS, Shi X, Mikos AG, Krebsbach PH, et al. Functional bone engineering using ex vivo gene therapy and topology-optimized, biodegradable polymer composite scaffolds. Tissue Eng 2005;11:1589-1598.

[49] Williams JM, Adewunmi A, Schek RM, Flanagan CL, Krebsbach PH, Feinberg SE, et al. Bone tissue engineering using polycaprolactone scaffolds fabricated via selective laser sintering. Biomaterials 2005;26:4817-4827.
[50] Franceschi RT. The developmental control of osteoblast-specific gene expression: role of specific transcription factors and the extracellular matrix environment. Crit Rev Oral Biol Med 1999;10:40-57.
[51] Marie PJ. Transcription factors controlling osteoblastogenesis. Arch Biochem Biophys 2008;473:98-105.
[52] Kruyt MC, Dhert WJ, Oner FC, van Blitterswijk CA, Verbout AJ, de Bruijn JD. Analysis of ectopic and orthotopic bone formation in cell-based tissue-engineered constructs in goats. Biomaterials 2007;28:1798-1805.
[53] Araujo JV, Cunha-Reis C, Rada T, da Silva MA, Gomes ME, Yang Y, et al. Dynamic culture of osteogenic cells in biomimetically coated poly(caprolactone) nanofibre mesh constructs. Tissue Eng Part A 2010;16:557-563.
[54] Chen Y, Mak AF, Wang M, Li JS, Wong MS. In vitro behavior of osteoblast-like cells on PLLA films with a biomimetic apatite or apatite/collagen composite coating. J Mater Sci Mater Med 2008;19:2261-2268.
[55] Ngiam M, Liao S, Patil AJ, Cheng Z, Yang F, Gubler MJ, et al. Fabrication of mineralized polymeric nanofibrous composites for bone graft materials. Tissue Eng Part A 2009;15:535-546.
[56] Barrere F, van Blitterswijk CA, de Groot K. Bone regeneration: molecular and cellular interactions with calcium phosphate ceramics. Int J Nanomedicine 2006;1:317-332.
[57] Yu HS, Jang JH, Kim TI, Lee HH, Kim HW. Apatite-mineralized polycaprolactone nanofibrous web as a bone tissue regeneration substrate. J Biomed Mater Res A 2009;88:747-754.
[58] Wang J, de Boer J, de Groot K. Proliferation and differentiation of osteoblast-like MC3T3-E1 cells on biomimetically and electrolytically deposited calcium phosphate coatings. J Biomed Mater Res A 2009;90:664-670.
[59] Salgado AJ, Coutinho OP, Reis RL, Davies JE. In vivo response to starch-based scaffolds designed for bone tissue engineering applications. J Biomed Mater Res A 2007;80:983-989.
[60] Dekker RJ, de Bruijn JD, Stigter M, Barrere F, Layrolle P, van Blitterswijk CA. Bone tissue engineering on amorphous carbonated apatite and crystalline octacalcium phosphate-coated titanium discs. Biomaterials 2005;26:5231-5239.
[61] Leeuwenburgh S, Layrolle P, Barrere F, de Bruijn J, Schoonman J, van Blitterswijk CA, et al. Osteoclastic resorption of biomimetic calcium phosphate coatings in vitro. J Biomed Mater Res 2001;56:208-215.
[62] Barrere F, van der Valk CM, Dalmeijer RA, van Blitterswijk CA, de Groot K, Layrolle P. In vitro and in vivo degradation of biomimetic octacalcium phosphate and carbonate apatite coatings on titanium implants. J Biomed Mater Res A 2003;64:378-387.
[63] Cam D, Hyon SH, Ikada Y. Degradation of high molecular weight poly(L-lactide) in alkaline medium. Biomaterials 1995;16:833-843.

[64] Yan WQ, Nakamura T, Kawanabe K, Nishigochi S, Oka M, Kokubo T. Apatite layer-coated titanium for use as bone bonding implants. Biomaterials 1997;18:1185-1190.
[65] Chau AM, Mobbs RJ. Bone graft substitutes in anterior cervical discectomy and fusion. Eur Spine J 2009;18:449-464.
[66] Rai B, Oest ME, Dupont KM, Ho KH, Teoh SH, Guldberg RE. Combination of platelet-rich plasma with polycaprolactone-tricalcium phosphate scaffolds for segmental bone defect repair. J Biomed Mater Res A 2007;81:888-899.
[67] Yu D, Li Q, Mu X, Chang T, Xiong Z. Bone regeneration of critical calvarial defect in goat model by PLGA/TCP/rhBMP-2 scaffolds prepared by low-temperature rapid-prototyping technology. Int J Oral Maxillofac Surg 2008;37:929-934.
[68] Choi S, Murphy WL. Sustained plasmid DNA release from dissolving mineral coatings. Acta Biomater 2010;6:3426-3435.
[69] Luong LN, Hong SI, Patel RJ, Outslay ME, Kohn DH. Spatial control of protein within biomimetically nucleated mineral. Biomaterials 2006;27:1175-1186.

CHAPTER 7

Summary and Future Work

7.1 Summary

Engineered porous scaffolds for bone application have been studied over a few decades, and many researchers have been examining and discussing ideal scaffolds to support bone generation. The overall goal of this thesis was to fabricate scaffolds with the capability of supporting mechanical loads in bone defects, bone formation, and the gradual transfer of load bearing from the scaffold to the forming bone tissues as proposed by Hutmacher et al. (Fig 7.1 (a)) [1]. We have utilized computer aided design, solid freeform fabrication (SFF), and biomineral coating to develop porous scaffolds with targeted characteristics, including controlled architectures, mechanical properties and surface properties. PLLA and PLGA, which are FDA approved and currently used as orthopaedic and spine products, were mainly used to fabricate scaffolds. In the last part of the thesis, PCL was also used because of its slower degradation compared with PLLA and PLGA.

In chapter three, porous scaffolds with designed architectures and mechanical properties were fabricated for load bearing application, essentially having linear elastic moduli within the low to middle range of human trabecular bone. Although there are a large number of studies characterizing the mechanical properties of PLGA scaffolds,

these scaffolds typically had mechanical properties much less than trabecular bone. The combination of μ-CT and the voxel based finite element method were further used to analyze the fabricated scaffolds and showed successful prediction of scaffolds mechanical properties, both compressive moduli and yield strength. Chapter three demonstrated the capability of designing and fabricating scaffolds with desired architecture and mechanical properties (both linear elastic moduli and yield strength) within the range of human trabecular bone. It was also shown that non-destructive techniques combining micro-CT scanning with voxel finite element method could accurately predict scaffold mechanical properties, thus providing a method for not only design of new scaffolds, but also quality control of fabricated scaffolds.

In chapter four, the effects of scaffold architectures and materials on bone formation were examined using mice ectopic models and *ex vivo* gene therapy. 50:50PLGA and PLLA scaffolds with identical porous architectures were fabricated and implanted for 4 and 8 weeks. The 50:50PLGA scaffolds mostly lost their architecture and mechanical properties at 4 weeks due to their short degradation time. In contrast, the PLLA scaffolds maintained their architectures over the study period, while losing their mechanical properties. The mechanical properties of scaffold and tissue complex were either maintained or improved over scaffold degradation due to some bone ingrowth and higher mineralization. This study concluded that material (in this case, mainly due to degradation speed and loss of architecture) had a significant influence while pore size had no effect on bone formation. It was demonstrated that some mechanical properties transfer from PLLA scaffolds to composites of scaffold and newly generated tissues, while 50:50PLGA completely lost their architectural structure at an early time point (Fig

7.1(b)). This study indicates that PLLA is a more favorable scaffold material for load bearing application than 50:50PLGA.

In chapter five, effects of PLLA scaffold initial architectures on degradation profiles were investigated using an ectopic model up to 21 weeks. The results successfully demonstrated that scaffold architecture had a significant effect on degradation (Fig 7.1 (c)). Specifically, a scaffold surface areas and strut size, but not pore size and porosity, were critical for scaffold design to control degradation. It was hypothesized that fully interconnected porous architectures help to easily remove by-products from the center of the scaffolds and avoid acidic concentration, which leads to autocatalysis. The mechanical properties changed depending on the scaffold architectures, specifically, there is a complex interaction between material, strut size (large struts perhaps undergoing faster degradation but still able to carry load due to larger area), and surface area. The major finding in this chapter is the significant influence of scaffold design, particularly strut size and surface area, on scaffolds degradation.

Through chapters three to five, designed SFF scaffolds showed mechanical properties within the range of trabecular bone, and the controlled architecture provided insight into how pore size, strut size, porosity and surface area affected bone formation and scaffolds degradation. In chapter six, we combined SFF scaffolds with biomineral coatings to achieve further bone ingrowth into scaffolds. SFF PLLA and PCL scaffolds with the same architecture were fabricated and coated with biomineral layer using modified SBF. The orthogonally interconnected pore architectures of the SFF scaffolds facilitated successful coating of the scaffold internal with biomineral layers. *In vivo* results showed that both biomineral coated PLLA and PCL scaffolds had fully connected ingrowth (Fig

7.2 (b)), while non-coated PLLA and PCL scaffolds had a little bone ingrowth (Fig 7.2 (a)). This result demonstrated that biomineral coating successfully improved bone formation on biodegradable scaffolds. Furthermore, fully interconnected pore channels of SFF scaffolds allowed tissue ingrowth into the center of the scaffolds. The advanced bone ingrowth also compensated for mechanical properties loss of the coated PLLA scaffolds due to degradation. This study indicated that improved bone ingrowth transferred some mechanical load from the scaffold to newly generated tissues (Fig 7.1 (d)).

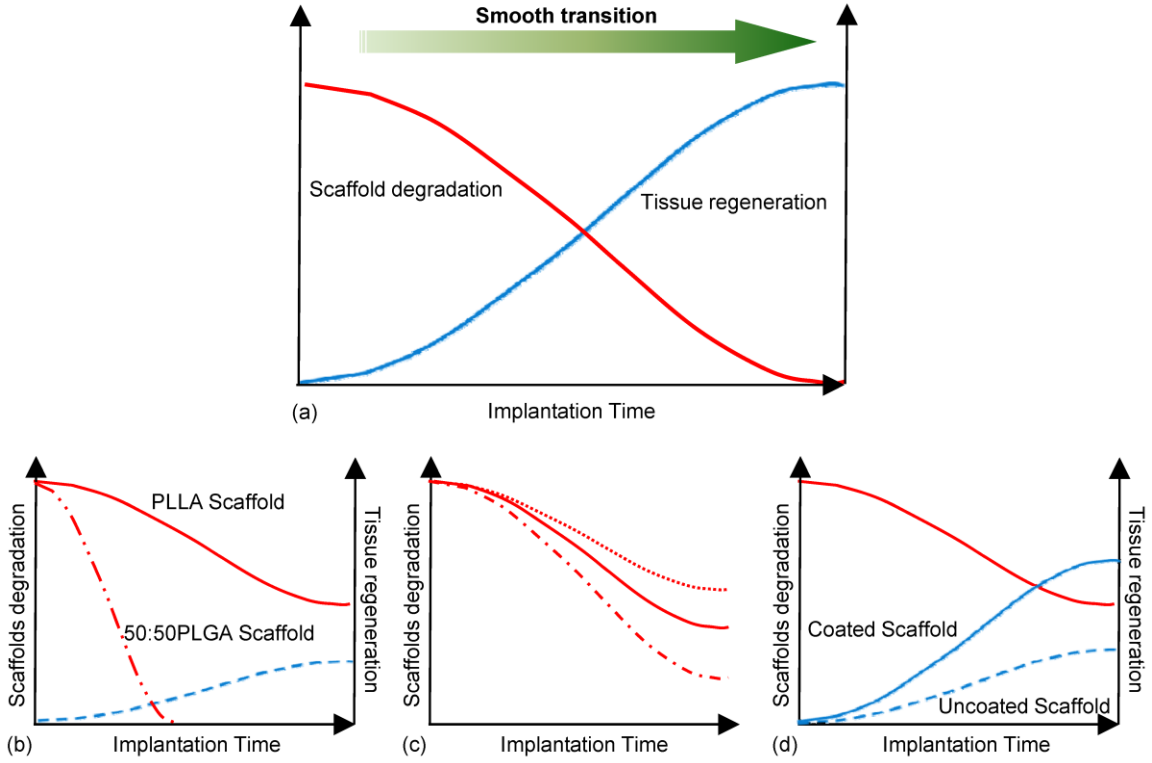

Fig 7.1 The relation between scaffolds (Red) and tissue regeneration (Blue). (a): Ideal scaffolds should degrade in concert with new bone regeneration. (b): Chapter three showed the relation between scaffold degradations and bone generation. 50:50PLGA scaffolds degrade in short time; in contrast, PLLA scaffolds degraded longer time. Small bone in growth was observed, but not fully connected. (c): Chapter four revealed the scaffold architectures can control their degradation. Scaffolds with smaller strut size and larger surface area help to slow their degradation. (d): Chapter six proved that SFF scaffolds with biomineral coating improve bone ingrowth, and the advanced bone ingrowth improved mechanical properties.

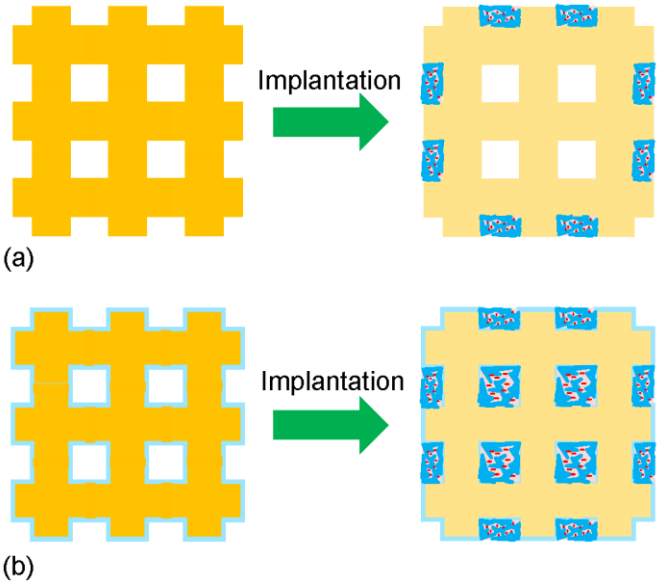

Fig 7.2 The schematic images of the relation biodegradable SFF scaffolds and bone ingrowth. The color change of scaffolds indicates degradation of scaffolds after implantation. (a): Uncoated PLLA and PCL scaffolds only have bone tissue formation outside of the scaffolds. (b): Biomineral coated PLLA and PLC scaffolds successfully had bone ingrowth and filled with trabecular like tissues.

7.2 Future Direction

This thesis demonstrated that SFF polymer and polymer/CaP coated scaffolds are a promising alternative to current metal and calcium implants for bone reconstruction as well as the conventional engineered scaffolds. As for future directions, SFF scaffolds with and without coating need to be tested in larger and more clinically relevant orthotopic defects instead of small size scaffolds implanted in mice subcutaneous sites. Scaffolds in orthotopic sites will be exposed to bone cells, including osteoblasts, osteocytes, and osteoclasts, as well as mechanical loadings. All these factors will affect the rate of bone generation and scaffold degradation.

We have shown SFF scaffold degradation can be controlled by scaffold initial architectures using PLLA. Further correlation of degradation between the scaffold architectures and their materials need to be tested. Moreover, simulation of mechanical

properties of scaffolds, during their *in vivo* degradation, will be another challenge. Other polymers and their compositions, such as PGA and 85:25PLGA, can be examined to determine scaffold architecture effects on each polymer. It is also important to examine larger scaffolds with further complicated architectures, and the local degradation differences inside of the scaffolds.

The scaffolds in this study had homogeneous architectures. In larger scaffolds, composite scaffolds with various architectures and materials can be developed. For example, scaffolds for femur application can have small porous architectures outside and large porous architectures at the center for bone marrow space as shown in Fig 7.3. The scaffold with large porous architectures could be made of a fast degrading material, such as PLGA and low molecular weight of PLLA, to create space for generating tissues as well as allowing easy removal of by-products. Conversely, the scaffold regions with small pore architectures made of slow degradation materials, such as PCL and high molecular weight of PLLA, would support long term mechanical loading. The scaffolds can further be incorporated with proteins, DNAs, and genes for local delivery to enhance bone formation and reduce inflammation [2-5].

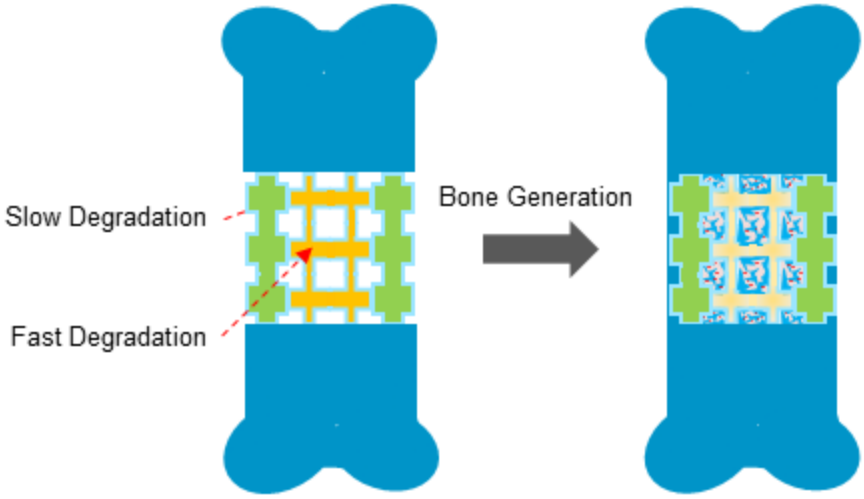

Fig 7.3 Example of a composite scaffold with different degradation rate materials and architectures. The internal part has large pore size and fast degradation to support tissue generation. This part also can be incorporated with some growth factor, virus etc to enhance tissue formation and reduce inflammatory response. The outer part is made of smaller pore size and slow degradation material to support long term mechanical loading at the defect sites.

Lastly, future scaffolds should globally support tissue defects as well as locally enhance bone generation. It has been well documented that mechanical force or stimuli effects and regulate stem cells, bone cells and bone formation [6-8]. It also has been demonstrated computational model of local and global architectures on bone formation [9-12]. And, we have been demonstrated effects of scaffold architectures, such as pore size and permeability, on bone formation *in vivo* as shown in the chapter four and our previous papers [13,14]. However, it has not been examined to control of deformation of fabricated scaffold pores which cause local strain, pressure and fluid shear stress for the sake of bone generation along with global deformation of scaffolds. Combining the information, scaffolds can be computationally designed and fabricated to control independent local and global strain to support loads of body and stimulate bone formation (Fig 7.4). Under physiological loadings, the pore designs can be control local strains and fluid flow to stimulate cell activities and bone formation.

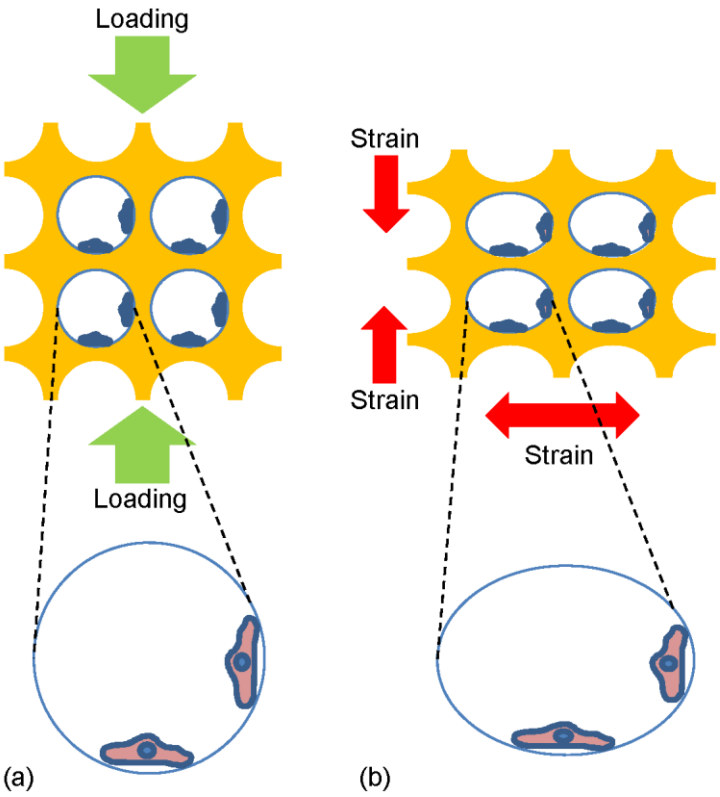

Fig 7.4 Example of control scaffold local and global mechanical properties, before (a) and after (b) deformation. Deformation of local pore should induce local strain as well as fluid shear stress to enhance and ostogenesis during loadings. The architectures of the local pore can determine profiles of local strain and fluid shear stress.

References

[1] Hutmacher DW. Scaffold design and fabrication technologies for engineering tissues--state of the art and future perspectives. J Biomater Sci Polym Ed 2001;12:107-124.

[2] Choi S, Murphy WL. Sustained plasmid DNA release from dissolving mineral coatings. Acta Biomater 2010;6:3426-3435.

[3] Luong LN, Hong SI, Patel RJ, Outslay ME, Kohn DH. Spatial control of protein within biomimetically nucleated mineral. Biomaterials 2006;27:1175-1186.

[4] Hu WW, Elkasabi Y, Chen HY, Zhang Y, Lahann J, Hollister SJ, et al. The use of reactive polymer coatings to facilitate gene delivery from poly (epsilon-caprolactone) scaffolds. Biomaterials 2009;30:5785-5792.

[5] Zhang H, Migneco F, Lin CY, Hollister SJ. Chemically-conjugated bone morphogenetic protein-2 on three-dimensional polycaprolactone scaffolds stimulates osteogenic activity in bone marrow stromal cells. Tissue Eng Part A 2010;16:3441-3448.

[6] Kelly DJ, Jacobs CR. The role of mechanical signals in regulating chondrogenesis and osteogenesis of mesenchymal stem cells. Birth Defects Res C Embryo Today 2010;90:75-85.

[7] Castillo AB, Jacobs CR. Mesenchymal stem cell mechanobiology. Curr Osteoporos Rep 2010;8:98-104.

[8] Thompson MS, Epari DR, Bieler F, Duda GN. In vitro models for bone mechanobiology: applications in bone regeneration and tissue engineering. Proc Inst Mech Eng H 2010;224:1533-1541.

[9] Claes LE, Heigele CA. Magnitudes of local stress and strain along bony surfaces predict the course and type of fracture healing. J Biomech 1999;32:255-266.

[10] Prendergast PJ, Huiskes R, Soballe K. ESB Research Award 1996. Biophysical stimuli on cells during tissue differentiation at implant interfaces. J Biomech 1997;30:539-548.

[11] Boccaccio A, Ballini A, Pappalettere C, Tullo D, Cantore S, Desiate A. Finite element method (FEM), mechanobiology and biomimetic scaffolds in bone tissue engineering. Int J Biol Sci 2011;7:112-132.

[12] Prendergast PJ, Huiskes R. The biomechanics of Wolff's law: recent advances. Ir J Med Sci 1995;164:152-154.

[13] Mitsak AG, Kemppainen JM, Harris MT, Hollister SJ. Effect of polycaprolactone scaffold permeability on bone regeneration in vivo. Tissue Eng Part A 2011;17:1831-1839.

[14] Roosa SM, Kemppainen JM, Moffitt EN, Krebsbach PH, Hollister SJ. The pore size of polycaprolactone scaffolds has limited influence on bone regeneration in an in vivo model. J Biomed Mater Res A 2010;92:359-368.

APPENDICES

A. Effect of Computer Designed PLLA Scaffold Permeability on Bone Ingrowth *In Vivo* (TERMIS-NA abstract, 2011)

Introduction: Ideal engineered bone scaffolds should enhance bone ingrowth to support defects and degrade in concert with generating bone tissue. Many studies have reported that scaffold architecture parameters, such as permeability, are important factors affecting nutrient infiltration and bone ingrowth into porous scaffolds. The previously reported scaffolds, however, were made by conventional techniques, such as salt-leaching, which did not rigorously control architectures [1,2]. We have developed designed poly (L-lactic acid) (PLLA) porous scaffolds using computer aided design and solid freeform fabrication (SFF) techniques. The goal of this study is to determine the effect of designed scaffold permeability on bone formation *in vivo*.

Methods: Two types of porous PLLA scaffolds (Diameter 6.4mm, Height 3.8mm) with different permeability, 0.688 and 3.991 10-7m^4/N-s, and porosities, 53 and 73 %, were computationally designed, and denoted as Low_Perm and, High_Perm, respectively (Fig A.1, Top view (a,e), Isometric view (b,f)). Low_Perm has spherical and necking structures of pore connections, while High_Perm has cylindrical and open channels. The designed scaffolds were made of PLLA using an indirect SFF technique. The sterilized scaffolds were seeded with fibrin gel containing adenovirus BMP-7 transduced human gingival fibroblasts, and were subcutaneously implanted into immuno-compromised mice

for 4, 8 and 12 weeks. The scaffolds were scanned using a high resolution Micro-CT Scanner before and after implantation. To determine bone ingrowth, the region of interest (ROI) (6.25mm diameter, 2.39mm height) was chosen at the middle of a scaffold. Bone volume (BV) and tissue mineral density (TMD) within the ROI were calculated. Following Micro-CT analysis, compression tests and histological evaluation with H&E were performed. One-way ANOVA or Student t-test was performed to determine significance ($p<0.05$) (N=6-8).

Results: Fabricated Low_Perm and High_Perm scaffolds had similar architectures and porosities, 55.6±4.2 and 73.2±2.1 (%), to the original designs (Fig A.1, pictures (c, g), Micro-CT rendering images (d, h)). The scaffold surface areas were similar to each other, 362.3±22.2 (Low_Perm) and 341.2±20.4 (High_Perm) (mm^2). High_Perm showed advanced bone ingrowth all time points, while Low_Perm had advanced bone ingrowth at 8 and 12 weeks (Fig A.2, indicated by #). High_Perm had significantly higher bone ingrowth than Low_Perm at 8 and 12 weeks, but not at 4 weeks (Fig A.2, indicated by *). Compressive moduli showed an initial decrease due to significant scaffold degradation, followed by a slight increase because of bone ingrowth (Fig A.3). Similar to micro-CT data, H&E images show that small bone ingrowth at 4 weeks, and advanced bone ingrowth containing trabecular structures and bone marrow-like tissues at 8 and 12 weeks (Fig A.4).

Discussion and Conclusions: Both Micro-CT data and histology proved that the scaffolds had bone ingrowth after implantation in this study. Clearly, the highly permeable scaffolds supported more bone ingrowth *in vivo*. Open channels of High_Perm may allow more efficient body fluid infiltration into the scaffolds which

helped cell migration and bone tissue ingrowth compared with Low_Perm with necking pore connections. In addition, decrease of the differences of bone ingrowth at 12 weeks indicates that higher permeability may be more effective during active bone formation. Advanced bone ingrowth supported mechanical properties while both PLLA scaffolds degraded and lost their mechanical properties. This study suggests that permeability is an important scaffold design factor significantly affecting the rate of bone ingrowth, which is favoured by higher permeability.

Acknowledgement: NIH R01 AR 053379, Micro-CT machine for the ORL at University of Michigan

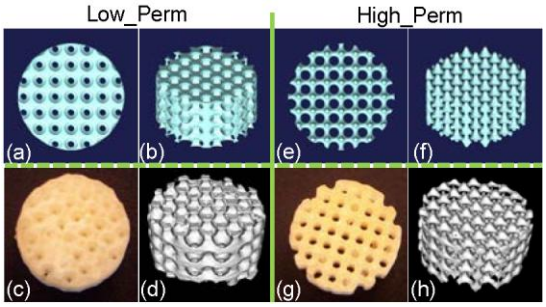

Fig A.1 Designed (a,b,e,f) and fabricated (c,d,g,h) scaffolds

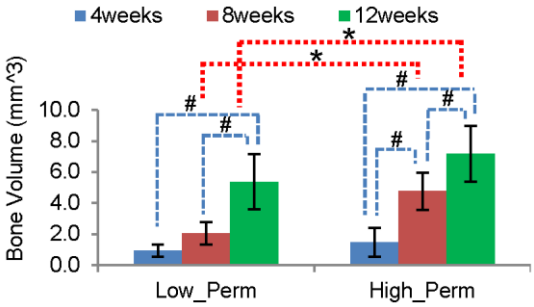

Fig A.2 Bone ingrowth after implantation

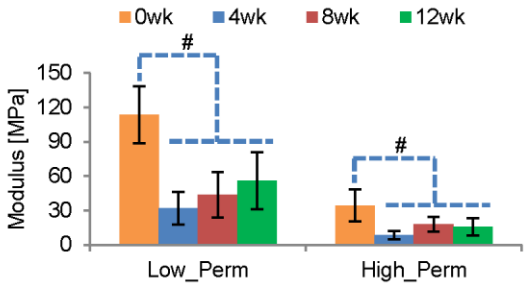

Fig A.3 Compressive moduli at each time point

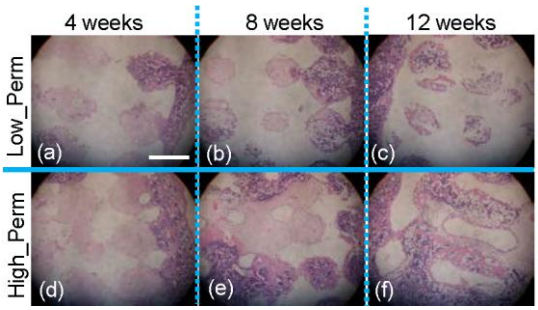

Fig A.4 H&E images of implanted scaffolds

B. Engineered Wavy Fibered Porous Polycaprolactone Soft Tissue Scaffolds: Design, Fabrication and Mechanical Properties (ORS abstract, 2005)

Introduction:

Skeletal soft tissues including meniscal and intervertebral fibrocartilaginous disks, cartilage, ligaments, and tendons exhibit a wide range of moduli typically ranging from slightly less than 1 MPa to over 100 MPa. Common scaffolds used to engineer soft tissues are typically hydrogels or knit polymers. These materials cannot withstand the extreme range of soft tissue mechanical forces, nor can their design/fabrication be controlled to match anisotropic tissue properties.

To address the need for soft tissue scaffolds with controlled porosity and mechanical properties, we have developed a wavy fiber scaffold design. We also fabricated these complex scaffold architectures from the biodegradable polymer Polycaprolactone (PCL) using a Selective Laser Sintering (SLS) technique. We demonstrate that these scaffolds have tightly controlled porosity, yet exhibit a controlled range of moduli and yield strains that fall within reported values for many soft tissues. We also show that computational simulations reliably predict experimental results, allowing control of scaffold design variables including pitch and fiber diameter to match desired anisotropic soft tissue properties.

Methods:

Curvy Scaffold Design and Fabrication:

5 types (n=6) of wavy shape scaffolds were designed using image-based techniques. These image-based techniques create wavy fibers based on sine functions ($Y = P \times Sin(\alpha\theta)$, P is pitch, α is const.) for orthogonal interconnecting fibers. Pitch and fiber diameter can be rigorously controlled. Pitch heights for tested designs were 0, 0.1, 0.3, 0.5, and 0.7mm (denoted as P0, P1, P3, P5 and P7). Interconnecting pores were generated as a unit cell and replicated to fill the cubic volume. The resulting image design was converted automatically to STL format.

Scaffold Fabrication:

PCL powder (CAPA® 6501, Mn ≈ 50,000, particle size ≤ 100μm) was purchased from Solvay Coprolactones (Warrington, UK). Scaffolds were built on a Sinterstation® 2000 SLS machine (3D Systems Inc., Valencia, CA) using a low power CO_2 laser (λ = 10.6μm, CW power < 10W, 450μm spot) to sinter the PCL powder in the desired 3D scaffold architecture.

Micro-Computed Tomography:

Porous cube scaffolds were scanned using a MS-130 Micro-CT Scanner (GE Medical Systems, Toronto, CAN) at 28 μm resolution. Scaffold volume fraction was calculated using Microview software.

Mechanical Testing:

The specimens were uniaxially tested to failure at a rate of 1mm/min after a preload of 1 lbs. was applied using a MTS Alliance RT30 Electromechanical test frame (MTS Systems Corp., MN). The Modulus was calculated at the first linear portion of the stress

strain curve and ultimate strain was taken at peak load before onset of plastic deformation.

Voxel Homogenization:

Designed images were input to a voxel-based homogenization software VOXELCON-HG (Quint Corp, Tokyo, Japan) to create voxel finite element models. Complete anisotropic effective stiffness constants were computed assuming a base PCL modulus of 120 MPa from previous tests.

Results and Conclusions

Example designed unit cell, designed scaffold, μCT of actual fabricated scaffold and actual fabricated scaffold are shown in Fig B.1. The unit cell dimension and scaffold dimensions were 2.4 × 2.4 × 2.4 (mm) and 12.0 × 12.0 × 24.0 (mm), respectively. The overall mechanical properties and FEM analysis results are shown in Table B.1. The average modulus decreased from 17MPa to 4MPa as the pitch height increased in the range from 0.1 to 0.7mm, demonstrating a tightly controlled dependence on fiber wave pitch for the same volume fraction. The average moduli of the design P1 through P7 were within the range of toe and linear region of soft tissues including the supraspinatus tendon (17.3 ± 8.9 MPa) [3], human forearm interosseous ligament toe-region modulus (roughly estimated at 4MPa from [4]) and annulus fibrosus of the intervertebral disc (0.2~2.5MPa for Toe-region and 0.45 ~ 17.4MPa for linear region) [5]. Strains before yield ranged from 9 to 32%, also within the failure strains reported for many soft tissues, and the highest pitch design exhibited a nonlinear stress-strain curve similar to typical soft tissues (Fig B.3). These ranges were obtained for scaffolds with the same volume fraction, demonstrating that scaffolds with designed microstructure can be tailored for different soft tissue loading environments, yet have the same porosity for delivering

biologic factors. In the future, we will perform tensile and cyclic loading tests on the same designed scaffolds to examine pitch effects on those properties.

Acknowledgments: NIH R01 DE13608 (BRP), NIH R21 DE014736

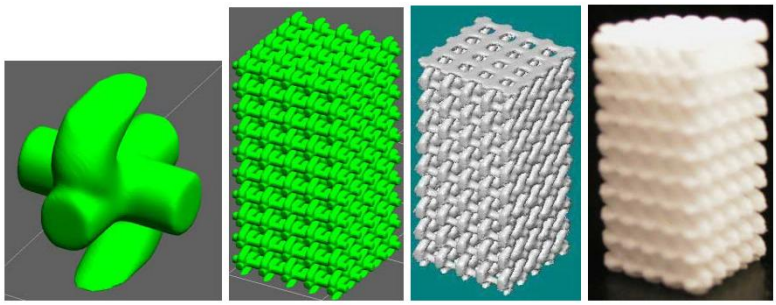

Fig B.1 Example unit cell design (left), scaffold design (2nd from the left), μ-CT rendering (2nd from the right) and fabricated scaffold picture (right)

Table B.1 Mechanical properties of scaffolds, FEM (Voxelcon-HG) analysis results and Volume Fraction from micro-CT data

Type of Wave Design	P0	P1	P3	P5	P7
Hight of Pitch (mm)	0.0	0.1	0.3	0.5	0.7
Modulus (MPa)	17.23 ± 0.29	17.41 ± 0.18	10.07 ± 0.32	6.30 ± 0.27	4.45 ± 0.12
Voxelcon HG (MPa)	12.93	11.56	5.91	3.02	1.64
Ultimate Strain (%)	8.55 ± 0.42	10.79 ± 0.79	15.81 ± 0.60	15.17 ± 4.47	32.43 ± 1.18
Volume Fraction (%)	29.82 ± 0.38	30.12 ± 0.31	31.91 ± 0.27	32.65 ± 0.30	32.43 ± 0.25

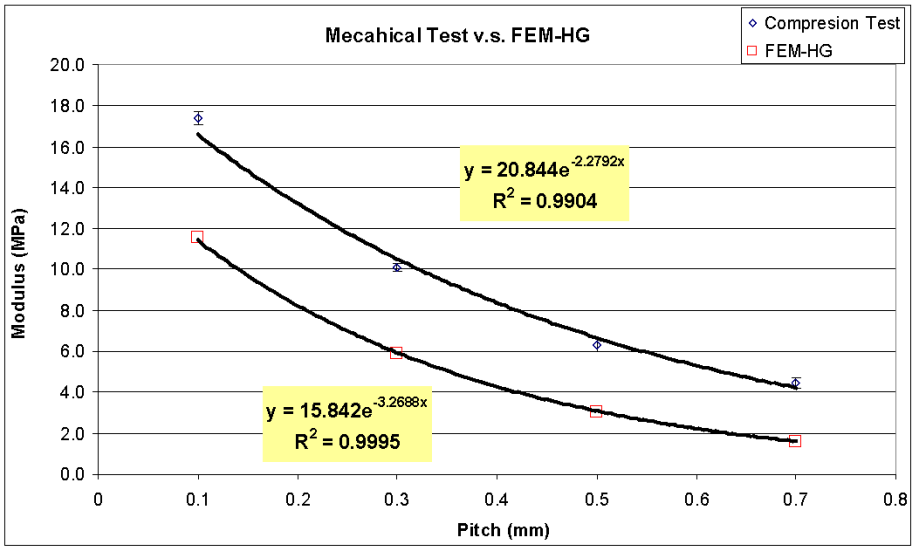

Fig B.2 Dependence of compressive moduli on pitch height for both mechanical tests and Voxelcon-HG (FEM) analysis.

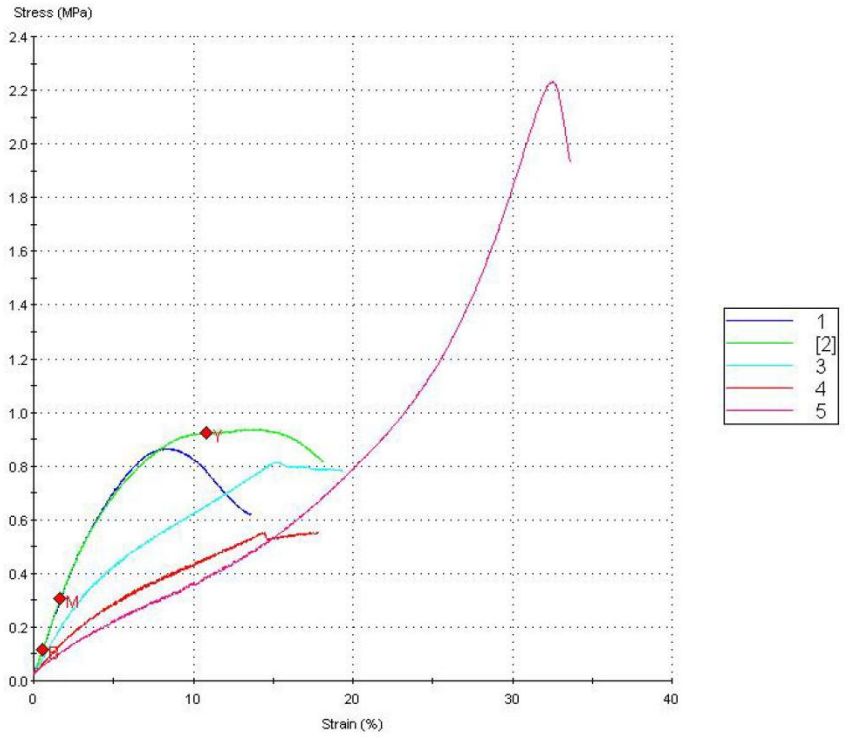

Fig B.3 Stress-Strain Curves from different designs of scaffolds (Line 1: P0, 2: P1, 2: P3, 3: P5, 5: P7)

References

[1] Kim K, Dean D, Wallace J, Breithaupt R, Mikos AG, Fisher JP. The influence of stereolithographic scaffold architecture and composition on osteogenic signal expression with rat bone marrow stromal cells. Biomaterials 2011;32:3750-3763.
[2] Lee KW, Wang S, Dadsetan M, Yaszemski MJ, Lu L. Enhanced cell ingrowth and proliferation through three-dimensional nanocomposite scaffolds with controlled pore structures. Biomacromolecules 2010;11:682-689.
[3] Nightingale EJ, Allen CP, Sonnabend DH, Goldberg J, Walsh WR. Mechanical properties of the rotator cuff: response to cyclic loading at varying abduction angles. Knee Surg Sports Traumatol Arthrosc 2003;11:389-392.
[4] Stabile KJ, Pfaeffle J, Weiss JA, Fischer K, Tomaino MM. Bi-directional mechanical properties of the human forearm interosseous ligament. J Orthop Res 2004;22:607-612.
[5] Elliott DM, Setton LA. Anisotropic and inhomogeneous tensile behavior of the human anulus fibrosus: experimental measurement and material model predictions. J Biomech Eng 2001;123:256-263.